STUDIES ON GAMMA RAY INTERACTION PARAMETERS OF SELECTED THERMOPLASTIC, BIOPOLYMER AND RARE EARTH OXIDE SAMPLES

Thesis submitted to the University of Calicut
in partial fulfillment of the requirements
for the award of the degree of

DOCTOR OF PHILOSOPHY
in
PHYSICS

By

THULASI P. V.

Under the guidance of

Prof.(Dr.) ANTONY JOSEPH

Department of Physics
University of Calicut
Kerala, India

January 2023

Dedicated to my Family

CERTIFICATE

This is to certify that the thesis entitled "**Studies on gamma ray interaction parameters of selected thermoplastic, biopolymer and rare earth oxide samples**", submitted by **Mrs. Thulasi P. V.** to the University of Calicut in partial fulfilment of the requirements for the award of the degree of Doctor of Philosophy is a bonafide record of the research work carried out by her under my supervision and guidance at the Department of Physics, University of Calicut. The content of the thesis in full or parts has not been submitted to any other Institute or University by her for the award of any other degree, diploma etc. The thesis has been checked for plagiarisn, using OURIGINAL software, at the CHMK library, University of Calicut and the similarity index is found within the permissible limit. Also, the corrections/suggestions recommended by the adjudicators have been incorporated in the thesis and that the contents in the thesis and the soft copy are one and the same.

University of Calicut

Date :08/06/2023

Dr. Antony Joseph
Senior Professor (Retd.)
(Supervising Guide)
Department of Physics
University of Calicut
Calicut University PO
Kerala - 673 635

DECLARATION

I hereby declare that the thesis entitled "**Studies on gamma ray interaction parameters of selected thermoplastic, biopolymer and rare earth oxide samples**" is based on the original work done by me at the Department of Physics, University of Calicut, under the supervision of Dr. Antony Joseph. This thesis has not been submitted by me for the award of any other degree, diploma etc. of any university or institute.

University of Calicut **Thulasi P V**

Date : 13/01/2023

Acknowledgement

First and foremost, I thank the God almighty, for the blessings offered.

I take this opportunity to place on record my profound sense of gratitude to my research guide Dr. Antony Joseph, former Head and Retired. Senior Professor, Dept. of Physics, University of Calicut, for his invaluable guidance, untiring supervision and constant encouragement given throughout the course of this investigation. Words are inadequate to acknowledge my indebtedness to him.

I express my sincere gratitude to Dr. K.M.Varier, former Head and Retired. Professor, Dept. of Physics, University of Calicut, for providing me valuable suggestions in various stages of the work. I recollect with overwhelming gratitude that the discussions with him provided many insights into the research work carried out.

I am extremely grateful to Professor H. M. Somashekarappa, Former Head, University Science Instrumentation Centre (USIC) and Centre-in-Charge, Centre for Application of Radioisotopes and Radiation Technology (CARRT), Mangalore University, Mangalagangothri, for providing all the necessary fa-

cilities for conducting the experiments.

I also take this opportunity to express my sincere gratitude to Dr. Karunakara N., Professor, USIC, Mangalore University for his help and encouragement.

A special thanks to Dr. Vinayak Anand Kamat, Department of Physics, Anjuman Arts, Science and Commerce College, for his help in conducting experiments at CARRT, Mangalore University and his moral support and encouragement.

I express my deep sense of gratitude to Prof. (Dr.) Ravikumar C.D, Head, Dept. of Physics, University of Calicut, for his whole-hearted help and for providing all the necessary facilities in the department throughout the work. I am thankful to former HoDs, Prof. (Dr.) P.P.Pradyumnan, Prof. (Dr.) A.M VinodKumar and Prof. (Dr.) M.M.Musthafa for their valuable suggestions and for the facilities offered during the research period. I also express my gratitude to all other teaching and nonteaching staff in the department.

I would also like to thank the Principal and the faculty members of the Department of Physics, M.P.M.M.S.N. Trusts College, Shoranur and SNG College, Chelannur, for their constant encouragement throughout the work.

I am glad to express my sincere gratitude to my research colleagues. Each of them gave valuable support and motivation throughout the research tenure and memorable days.

It gives me great pleasure to acknowledge the help and moral encouragement of my mother Vanaja, my father Narayanan (Late) and my brother Jayaraj throughout the period of this work, without which I would not have

succeeded in accomplishing this work.

I express my immense gratitude to my husband Mr. Abhilash, daughter Parvathy and my son Pranav for their tolerance and unflinching support extended to me throughout this study.

Finally, I thank all my friends and well-wishers for their encouragement throughout all stages of the research work.

Contents

List of Tables

List of Figures

List of Publications

1. **P V Thulasi**, Antony Joseph and K M Varier
   "Studies on partial and total photon interaction parameters in the energy range 1 keV – 100 GeV of some synthetic polymers having medical applications ", *Radiation Physics and Chemistry*, **180**, 109252, 2021.

2. **P V Thulasi**, Antony Joseph, K M Varier, Somashekarappa H M, Vinayak Anand Kamat and Vishnu C V
   "Coherent scattering cross sections of some rare earth compounds at small angles below 10^0 for 59.54 keV gamma rays", *Radiation Physics and Chemistry*, **202**, 110539, 2023.

List of Presentations

1. **P V Thulasi**, Antony Joseph, Somashekarappa H M and Vinayak Anand Kamat
   "Coherent scattering cross sections of some rare earth compounds at small angles below 10^o for 662 keV gamma rays", *Proceedings of DAE Symposium on Nuclear Physics*, **65**, 812, 2021.

2. **P V Thulasi**, Antony Joseph and K M Varier
   "Effective atomic number studies in coconut oil samples using 662 keV gamma rays ", *AIP Conference Proceedings*, **2379**, 020002, 2021.

Abstract

The extensive use of radiation in various fields such as medical physics, industry, space research, radiation shielding, dosimetry etc. necessitates the knowledge of the parameters associated with the interaction of radiation with materials. As part of the present work, we have determined theoretically, the mass attenuation coefficient, effective atomic number and electron density of selected thermoplastic and biopolymer samples, having medical applications, for total as well as partial gamma ray interaction processes in the wide range of energies 1 keV to 100 GeV. The mass energy-absorption coefficient, the effective atomic number corresponding to gamma ray energy absorption in these media and the kerma relative to air of these polymers were also estimated for the energy range of 1 keV–20 MeV. Variation of these parameters with photon energy and chemical composition of polymers has been studied. The estimated values were compared with experimental data, wherever available, and these show good agreement. The effective atomic numbers of these polymers obtained by different methods have been compared in various energy regions and possible conclusions were drawn.

We have also estimated the radiation interaction parameters of selected chemotherapy drugs administered concurrently with radiation therapy in the energy range 1 keV to 100 GeV by using the EpiXS program. The radiation response of the selected drugs have been compared at different energy regions.

Except at absorption edges, the selected drugs have shown similar interaction parameter variations with photon energy.

We have also determined the angle integrated total scattering cross sections of some rare earth oxides experimentally for 59.54 keV and 662 keV gamma rays in the angular ranges of 0–4^0, 0–6^0, 0–8^0 and 0–10^0 . From the experimental total scattering cross sections, the corresponding angle integrated incoherent scattering cross sections obtained from ENDF library (based on the non-relativistic Hartree – Fock form factor method) was subtracted to obtain the angle integrated coherent scattering cross sections. The angle integrated coherent scattering cross sections show good agreement with that determined from ENDF data. The effective atomic numbers of the selected rare earth oxides were extracted by applying the ratio of cross section method. The variation of angle integrated coherent scattering cross section with the effective atomic number of the selected compounds have been studied.

In addition, some attenuation measurements have been carried out on edible oil samples using 662 keV gamma rays. Here, we have determined the mass attenuation coefficients, from which the effective atomic numbers were deduced. The variation of interaction parameters with the composition of the food samples were also studied.

Chapter 1

Introduction

The term radiation refers to the emission or propagation of energy through space or material medium in the form of waves or particles. Radiations are broadly classified into charged radiations and uncharged radiations. Charged radiations consist of fast moving electrons and heavy charged particles like protons, alpha particles, fission fragments and the products of many nuclear reactions. Uncharged radiations include electromagnetic radiations and neutrons. Electromagnetic radiations consist of a stream of photons, which are zero mass, zero charge particles having a velocity that is equal to the speed of light. Each photon carries a quantum of energy which can be expressed as $E = h\nu$, where h is the Plank's constant and ν is the frequency of the radiation. Different electromagnetic radiations differ in the energy carried by the photons in them. Gamma rays and X-rays are electromagnetic radiations which differ only in their mode of origin. Gamma rays are emitted during nuclear transitions, while the characteristic X-rays are produced during the electronic transitions between K, L, M ... shells in the atoms. But continuous X-rays are the result of the acceleration or deceleration of free electrons and other charged particles. The interaction of these radiations with matter does

not depend upon the mode of origin, but depends on the nature of radiations, the energy of the radiations and on the properties of the material medium with which it interacts (Varier, 2009).

The study of interaction of gamma rays and X-rays with matter have diverse applications in various fields like medicine, industrial radiography, agriculture, radiation shielding, biology, radiation transport etc. Linear attenuation coefficient, mass attenuation coefficient, effective atomic number, effective electron density etc. are the basic parameters which measure the probability of interaction of gamma rays with materials. X-rays and gamma rays interact with materials by different processes in which a partial or total transfer of photon energy to the interacting material takes place. Any one of the following processes can happen depending on the energy of the radiation and the nature of the interacting medium.

- The incident photon may penetrate through the medium without interaction.
- It may interact with the medium and may get completely absorbed by depositing its full energy in the medium.
- It may interact with the medium and get scattered off from its original direction by depositing a part of its energy in the medium.

Also, while passing through a medium, the photon may interact either with the orbital electrons of the atoms in the medium or with the nuclei of the atoms in the absorbing medium. Fano (Fano, 1953) classified all the possible interactions of photons with matter into twelve different categories.

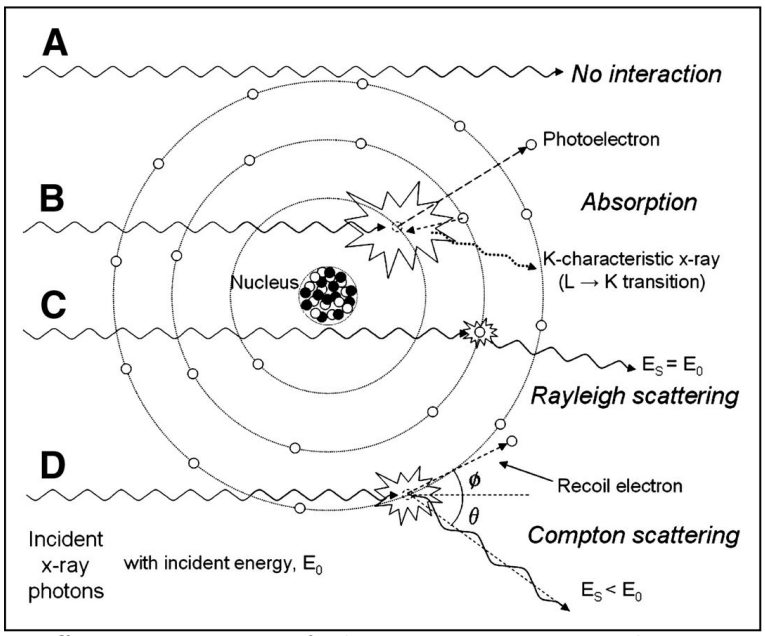

Figure 1.1: Different processes of photon interaction with matter (Seibert & Boone, 2005).

Kinds of interaction

- Interaction with atomic electrons
- Interaction with nucleons
- Interaction with the electric field surrounding nuclei or electrons
- Interaction with the meson field surrounding the nucleons

Effects of Interaction

- Complete absorption
- Elastic scattering (coherent)
- Inelastic scattering (incoherent)

We can combine column 1 and column 2 in 12 different ways, which corresponds to the twelve different processes of interactions. These twelve interaction processes generally come under two categories - Scattering and Absorption. The different gamma ray interaction processes with matter are summarised in Figure 1.1 (Seibert & Boone, 2005).

1.1 Scattering

A physical process in which a beam of radiation is forced to deviate from a straight trajectory by one or more localized non-uniformities in the medium through which it passes, is generally referred to as scattering. It is mainly classified into two, elastic scattering and inelastic scattering.

1.1.1 Elastic Scattering

In elastic scattering, the gamma ray energy is unchanged except for a negligible amount, due to the recoil of the scattering nucleus required for the momentum conservation. Since there is no internal excitation of the scatterer here, no energy is deposited by the photon in the medium. This approximation is true, when the incident gamma ray energy is much less than the rest mass energy of the scatterer. Elastic scattering can take place from free electrons, bound electrons or from nuclei of the atoms. Elastic scattering from free electrons or nuclei is called Thomson scattering. If it occurs from bound electrons, it is referred to as Rayleigh scattering. Nuclear resonance scattering also contributes to nuclear scattering. The interaction of the incident photon with the Coulomb field of a nucleus results in Delbruck scattering.

Thomson scattering

In free electron Thomson scattering, the electromagnetic field of the incident photon makes the electron to oscillate in the direction of its electric vector, with the same frequency as that of the incident wave. As a result, the oscillating electron emits electromagnetic radiations of the same frequency as that of the incident photon as shown in Figure 1.2 (Latha, 2012). The differential scattering cross section for the interaction was first estimated by Thomson

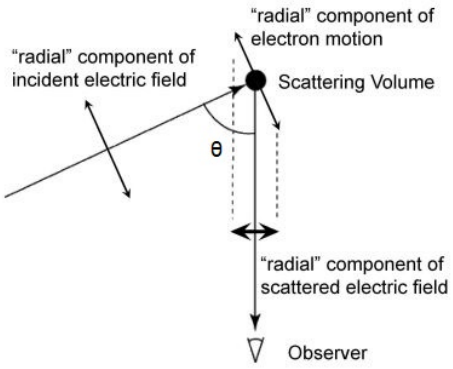

Figure 1.2: Thomson scattering of gamma rays by an electron (Latha, 2012)

.

using classical electrodynamics, which is given as,

$$\frac{d\sigma_T}{d\Omega} = \frac{1}{2} r_o^2 (1 + \cos^2\theta) \tag{1.1}$$

where r_o is the classical electron radius that is given by $r_o = \frac{e^2}{m_0 c^2}$, θ is the scattering angle, which is the angle between the incident photon and the scattered photon. $\frac{d\sigma_T}{d\Omega}$ is the differential scattering cross section per unit solid angle.

In nuclear Thomson scattering, the incident photon interacts with the nucleus as a whole and gets scattered without any change in energy. Since the nucleus is very heavy, its rest mass energy is much larger, compared with the energy of the incident photon. As a result, the recoil momentum of the nucleus is very small. Differential nuclear Thomson scattering cross section is given as

$$\frac{d\sigma_{NT}}{d\Omega} = \frac{Z^4}{2} r_o^2 (1 + \cos^2\theta) \tag{1.2}$$

where Z is the charge of the nucleus. In Thomson scattering, the finite distribution of the charge is neglected and the scattering centre is considered as a point charge.

Rayleigh scattering

The Rayleigh scattering is often referred to as coherent scattering. In this scattering, the incident photon is scattered from a bound electron and in this process the atom is neither excited nor ionised. The atom is left in the ground state after the scattering process. The scattering from different parts of the atomic clouds of electrons combine in phase to give the coherent scattering (Kissel, 2000). Here, the scattered intensity is proportional to the fourth power of the reciprocal of the wavelength of the incident photon. This process mainly occurs at low energies and for large Z values, where the electron binding energies influence the Compton effect. At high photon energies the Rayleigh scattering is confined to small angles for all the absorbers. For high atomic number absorbers at low energies, the angular distribution of scattered photons is much broader.

In form factor approximation, the Rayleigh scattering is treated as Thomson scattering from a finite charge distribution and the corresponding formula for differential scattering cross section is given as (Chatterjee & Roy, 1998),

$$\frac{d\sigma_R}{d\Omega} = (\frac{d\sigma_T}{d\Omega}) f^2(x, Z) \tag{1.3}$$

where f(x,Z) is the atomic form factor and $x = (\frac{1}{\lambda})sin(\frac{\theta}{2})$, is the corresponding momentum transfer when photon is scattered through an angle θ. Here, the wavelength λ is taken in Angstrom. Atomic form factor can be approximated as the effective charge that scatters the photon and can be expressed as the integral,

$$f(x, Z) = 4\pi \int \rho(r) sin(xr) r^2 dr \tag{1.4}$$

where $\rho(r)$ is the electron number distribution of the atom, assumed spherically

symmetric and normalized to Z.

Based on the ground state wave function used to derive the charge distribution of the atoms, two approaches are there, the relativistic form factor (RFF) and the non-relativistic form factor (NRFF). Later, Brown and Mayer (Brown, G. E and Mayers, D. F, 1956) proposed the relativistic modified form factor approach based on the suggestions of Franz (Franz, 1936). In this form factor calculations, the electron binding energy effects are neglected. A fully relativistic approach, taking into account the electron binding energy effects is the S - matrix formulation of Brown, Peierls and Woodward (Brown, G. E and Peierls, R. E, 1955).

Nuclear resonance scattering

In nuclear resonance scattering, when the incident gamma ray energy comes closer to one of the energy levels of a nucleus, the incident photon excites the nucleus to that excited levels and the subsequent de-excitation will result in the emission of the excitation energy in the form of gamma rays. Here, the energy of the incident photons remains the same except for a negligible loss due to the recoil of the nucleus. It has a clear resonance behaviour with full width at half maximum (FWHM) characterized by the energy width of the nuclear level of energy E_0 involved in the process. The cross section in this case is given as,

$$\sigma_{NR} = \frac{\lambda^2 \Gamma \Gamma_\gamma}{4\pi[(E_0 - E_\gamma)^2 + (\frac{\Gamma}{2})^2]} \tag{1.5}$$

where λ is the wavelength of the incident photon, Γ is the total width of the nuclear level, Γ_γ is the partial width for gamma decay of the excited state of energy E_0 and E_γ is the photon energy. At low energies, due to the narrow width of nuclear levels, the chance of overlap of the incident photon energy

with the excitation energy of the target nuclear level is very rare and hence the probability of occurrence of nuclear resonance scattering in the elastic scattering of photons is negligible.

Besides the above mentioned nuclear resonance scattering, a strong photon absorption is observed in many nuclei near the gamma ray energies given by,

$$E_0 = \epsilon A^{-\frac{1}{3}} \tag{1.6}$$

where ϵ varies between 70 MeV and 80 MeV and A is the mass number of the scatterer. This scattering process is known as Giant Dipole Resonance Scattering (GDR) and this process is appreciable only when the incident photon energy exceeds 10 MeV.

Delbruck scattering

Delbruck scattering or elastic nuclear potential scattering is due to the virtual electron pair formation in the nuclear Coulomb field. The actual process involves the absorption of an incident photon by an electron in the negative energy state, followed by the creation of an electron - positron pair and the subsequent annihilation of the pair to give a scattered photon of exactly the same energy as that of the incident photon. At gamma ray energies below 1 MeV, the cross section of this process is negligibly small. The cross section has a Z^4 dependence on the atomic number of the scatterer. The real and imaginary part of the scattering amplitude corresponds to virtual and real pair production in the intermediate state. But real pair production is possible only when the energy of the incident photon reaches the pair production threshold of 1.022 MeV.

1.1.2 Inelastic scattering

In inelastic scattering, the incident photon either gains energy or loses its energy, so that the kinetic energy of the incident photon is not conserved. Inelastic scattering is often referred to as Compton scattering, in which a high energy photon collides with a free electron and transfers a part of its energy. When an electron with relativistic energy collides with an infrared or visible photon, the electron gives energy to the photon and this process is called inverse-Compton scattering.

Compton scattering

In Compton scattering (also called incoherent scattering), a photon of energy E_γ hits on a loosely bound orbital electron and gets scattered at an angle θ with respect the initial direction, with a reduced energy E'_γ. Here, the photon transfers a part of its energy to an orbital electron and as a result the electron gets emitted at an angle ϕ with respect to the direction of incident photon as shown in Figure 1.3 (Latha, 2012). The relation between E_γ and E'_γ is given as,

$$E'_\gamma = \frac{E_\gamma}{1 + \alpha(1 - cos\theta)} \tag{1.7}$$

where $\alpha = \frac{E_\gamma}{m_0 c^2}$ is the gamma ray energy expressed in terms of the rest mass of the electron. The cross section for the Compton scattering from a free electron has been derived by Klein and Nishina (Klein & Nishina, 1929), based on Dirac's relativistic theory of the electron, which is given as,

$$\frac{d\sigma_{KN}}{d\Omega} = (\frac{{r_0}^2}{2})\frac{1 + cos^2\theta + \frac{\alpha^2(1-cos\theta)^2}{(1+\alpha(1-cos\theta))}}{[1 + \alpha(1 - cos\theta)]^2} \tag{1.8}$$

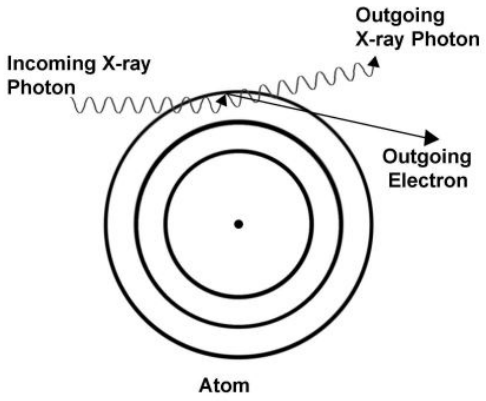

Figure 1.3: Compton scattering of gamma rays from a loosely bound electron of the target atom (Latha, 2012)

.

Here, r_0 is the classical electron radius and the differential solid angle $d\Omega = 2\pi sin\theta d\theta$. When the effect of electron binding is taken into account, the differential incoherent Compton scattering cross section $\frac{d\sigma_C}{d\Omega}$ is given as,

$$\frac{d\sigma_c}{d\Omega} = \frac{d\sigma_{KN}}{d\Omega} S(x, Z) \tag{1.9}$$

where S(x,Z) is the the incoherent scattering function with x being the momentum transfer in inverse Angstrom units, which is given as $x = \frac{sin\frac{\theta}{2}}{\lambda}$. Here, λ is the wavelength of the photon in Angstrom. If the momentum transferred is small, the value of S(x,Z) approaches zero and when it is large, S(x,Z) approaches the value Z.

1.1.3 Absorption

In the process of absorption, the incident radiation substantially or completely deposits its energy in the interacting medium. Some times, the absorption is treated as the extreme form of inelastic scattering. In classical physics, absorption and scattering are treated as different processes, but in quantum

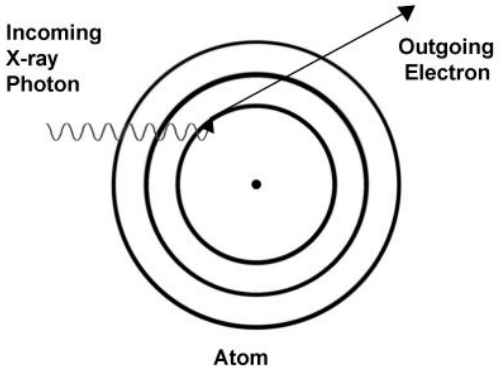

Figure 1.4: Schematic representation of photoelectric absorption of an incident gamma ray by an atomic electron and the subsequent ejection of the electron out of the atom (Latha, 2012).

mechanics, in S - matrix analysis , the absorption is treated as a form of scattering. There are several processes in which the absorption of gamma rays take place, in which photoelectric effect and pair production are the important processes.

Photoelectric effect

In photoelectric absorption, the incident gamma ray interacts with an atomic electron and transfers its entire energy to the electron. If the incident gamma ray energy E_γ is greater than the binding energy E_B of the electron, the electron will be ejected from the atom with a kinetic energy KE_e, which is given as,

$$KE_e = E_\gamma - E_B \tag{1.10}$$

The photoelectric absorption is illustrated in Figure 1.4 (Latha, 2012). Here, the small recoil energy taken by the atom to conserve the momentum is neglected. When the electron is ejected from the atom, a vacancy is created in

that particular shell and then the atom will be in the excited state. This vacancy is filled up by an electron from the outer shell and during the subsequent decay of the excited atom, a characteristic X-ray will be emitted. The energy of the characteristic X-ray photon will be the difference in energy between the initial and final states of the electron. For gamma rays of sufficient energy, the most probable origin of photoelectron is the most tightly bound K shell of the atom. The probability of this process increases with increase in the atomic number of the absorber. No single formula is available for photoelectric cross section for all ranges of photon energy E_γ and atomic number Z of the absorber. But, a rough approximation of the cross section of photoelectric effect σ_{PH} is given as,

$$\sigma_{PH} = constant \times \frac{Z^n}{E_\gamma^3} \tag{1.11}$$

where n varies between 4 and 5. For high Z materials, photoelectric effect is the prominent mode of interaction at low gamma ray energies. In the plot of the photoelectric cross section versus gamma ray energy shown in Figure 1.5 (Varier, 2009), the discontinuities in the curve or "absorption edges" appear at energies which correspond to the binding energies of the electrons in the various shells of the absorber atom. The edge lying highest in energy therefore corresponds to the binding energy of the K shell electron. For gamma ray energies slightly above the edge, the photon energy is just sufficient to undergo a photoelectric interaction in which the K-electron is ejected from the atom. For gamma ray energies slightly below the edge, this process is no longer possible and therefore the interaction probability drops abruptly. Similar absorption edges occur at lower energies for the L, M,... electron shells of the atom also.

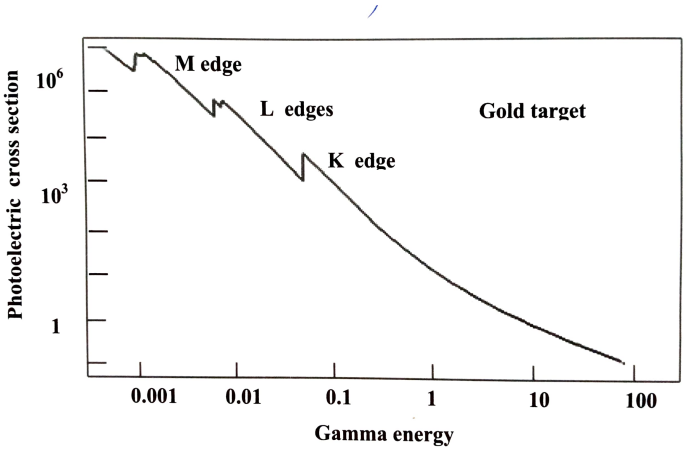

Figure 1.5: Energy dependence of photoelectric absorption for gold (Varier, 2009)

.

Pair production

In pair production, the entire energy of the incident gamma ray is deposited in the medium and is used for the production of the electron - positron pair. The process can be represented as,

$$\gamma \rightarrow e^- + e^+ \tag{1.12}$$

The energy change in this process can be written as,

$$E_\gamma = 2m_e c^2 + KE_{e^-} + KE_{e^+} \tag{1.13}$$

where m_e is the rest mass of electron, KE_{e^-} and KE_{e^+} are the kinetic energies of electron and positron, respectively. This process is possible only for gamma ray energies above 1.022 MeV (Oppenheimer & Plesset, 1933). Above this threshold energy, the cross section of the pair production process increases with energy and at higher energies it becomes the prominent interaction mode. If the atom is neither excited nor ionised during the pair production, then the

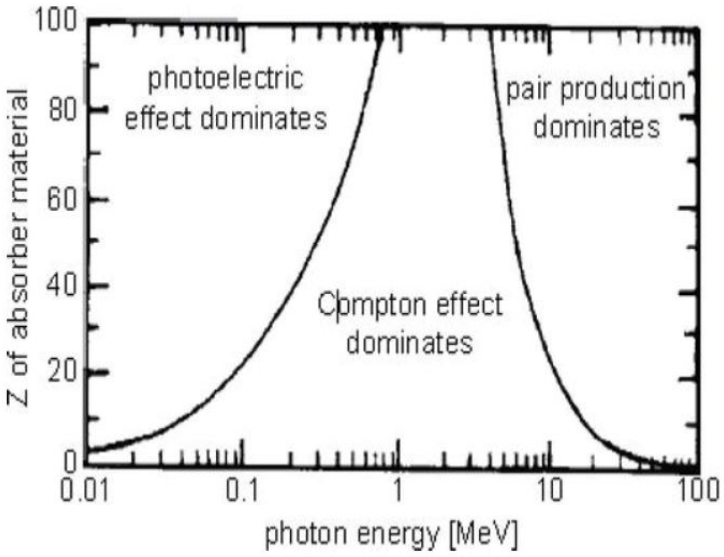

Figure 1.6: The relative importance of three major types of gamma ray interactions. The lines show the values of Z and photon energy for which two neighbouring effects are equal (Knoll, Glenn F, 1970).

process is called elastic pair production. If the atomic electrons are excited, then the process is called inelastic pair production. If the atom is ionized, then it is called triplet pair production. This process takes place either in the field of a nucleus or in the field of an electron. The threshold energy for pair production in electronic field is 2.044 MeV. In the case of high Z elements, at low photon energies the cross section of pair production in electronic field is negligible compared to that in nuclear field.

The relative importance of the major gamma ray interaction processes - photoelectric effect, Compton scattering and pair production for different gamma ray energies and for absorbers which varies in their Z values are shown in Figure 1.6. Three areas are defined in the plot where the photoelectric effect, Compton scattering and pair production dominate (Knoll, Glenn F, 1970).

1.1.4 General aspects of attenuation

Beer-Lambert law

When X-rays or gamma rays pass through matter, its intensity gets reduced either by absorption or by scattering and this process is called attenuation. The attenuation of gamma rays through matter is characterized by the parameter linear attenuation coefficient (μ) or mass attenuation coefficient (μ_m). The linear attenuation coefficient μ gives the probability of interaction of a photon with the absorber per unit path length. It depends upon the the energy (E_γ) of the incident photon and the atomic number of the absorber. The exponential decay of the intensity of gamma rays is given as,

$$I = I_o e^{-\mu x} \tag{1.14}$$

where I_o is the intensity of the incident radiation, I is that of the transmitted radiation and x is the thickness of the absorber. Here, the linear attenuation coefficient (μ) is expressed in cm^{-1} and it depends on the density of the medium. Since it changes with the physical state of the absorber, another parameter - the mass attenuation coefficient, expressed as $\frac{\mu}{\rho}$, which is independent of the density of the medium, is introduced. Then the absorption law can be written as,

$$I = I_o e^{-\frac{\mu}{\rho} t} \tag{1.15}$$

where $t = x\rho$ is the mass thickness of the absorber, with ρ being the density of the medium. This is known as Beer-Lambert law. This exponential decay of gamma ray intensity while passing through a medium depends on the nature of the prominent interaction processes. When gamma radiations of intensity I

pass through a medium having thickness dx, let dI be the number of photons getting removed from the direct beam due to interaction with the medium. Then,

$$\frac{dI}{I} = \frac{N_A \rho \sigma dx}{A} \tag{1.16}$$

where N_A is the Avogadro number and σ is the total cross section for the attenuation of gamma rays. The total cross section σ can be expressed as,

$$\sigma = \sigma_\tau + \sigma_C + \sigma_{pair} \tag{1.17}$$

Here, σ_τ, σ_C and σ_{pair} are the cross sections due to photoelectric effect, Compton scattering and pair production, respectively. If N is the total number of atoms per unit volume of the absorber, then the linear attenuation coefficient (μ) can be written as,

$$\mu = N\sigma \tag{1.18}$$

Integrating equation 1.16, we get back the Beer-Lambert law.

The gamma ray interaction can also be characterised by the parameter mean free path (λ). It is the average distance travelled by the gamma radiation through matter before an interaction takes place. The mean free path can be obtained as,

$$\lambda = \frac{\int_o^\infty x e^{-\mu x} dx}{\int_o^\infty e^{-\mu x} dx} \tag{1.19}$$

1.1.5 Half-Value Layer (HVL)

The Half-Value Layer (HVL) is the thickness of the absorber which reduces the intensity of the photon beam to half of the original value. It can be obtained

as,

$$HVL = \frac{0.693}{\mu} \tag{1.20}$$

Mixture rule

The mass attenuation coefficient is independent of the density and physical state of the interacting medium. So, to find the mass attenuation coefficient of a mixture or a compound containing different elements, we can apply the Mixture rule (Jackson & Hawkes, 1981). According to this rule, the mass attenuation coefficient of a mixture or compound $\left(\frac{\mu}{\rho}\right)_c$ can be expressed as,

$$\left(\frac{\mu}{\rho}\right)_c = \sum_i \omega_i \left(\frac{\mu}{\rho}\right)_i \tag{1.21}$$

where $\left(\frac{\mu}{\rho}\right)_i$ and ω_i are respectively the mass attenuation coefficient and the weight fraction of the ith constituent element present in the compound.

Narrow beam and broad beam geometries

In gamma ray attenuation coefficient measurements using Beer-Lambert law, I_0 represents the incident photon beam intensity and I represents the intensity of the transmitted photons which reach the detector without any interactions with the target. But, in a practical experimental setup, a good collimation is not always possible. Then, in such cases, besides the pure transmitted radiations, the scattered radiations and X-rays emitted by the absorber may also reach the detector. But the detector cannot distinguish between these photons. Such a geometry is known as a broad beam geometry or a poor geometry. When gamma rays are well collimated, and the transmitted gamma rays which escapes without interaction with the absorber only reaches the detector, then such a geometry is known as narrow beam geometry. In narrow beam geom-

etry, the inscattering angle is always set less than 0.5^0, which prevents the coherently and incoherently scattered radiations from reaching the detector.

Effective atomic number

The cross section of different gamma ray interaction processes depends on the energy of the incident photons and on the atomic number of the constituent element of the absorber (if the absorber is made up of a single element) (Perumallu et al., 1985). In the case of composite materials, a single atomic number cannot be used for determining the photon interaction cross section in the entire energy range, as in the case of pure elements. The importance of the effective atomic number (Z_{eff}) comes in this situation and this concept was first introduced by Hine (Hine, 1952). Here, it is assumed that for photon interactions, a composite material containing different elements in different proportions behaves in the same way, when it is replaced by an equal number of identical atoms, each having Z_{eff} number of electrons (Manohara et al., 2008b). The effective atomic number is used to calculate the energy absorption in the medium. There are different methods for estimating the effective atomic number of composite materials, which is discussed in detail in chapter 3.

Effective electron density

The number of electrons per unit mass of the material is known as the effective electron density (N_{eff}). It is related to the effective atomic number as (Niranjan et al., 2012),

$$N_{eff} = N_A Z_{eff} / < A > \tag{1.22}$$

where N_A is the Avogadro number and $< A >$ is the average mass number of the constituent elements. N_{eff} also varies in the same way as Z_{eff}, with the incident photon energy. It is also a very useful parameter in calculating the absorbed dose in the medium.

Mass energy-absorption coefficient

The Mass energy-absorption coefficient $\left(\frac{\mu_{en}}{\rho}\right)$ is used for determining the energy deposited by the incident photon beam per unit mass of the absorber (Hubbell & Seltzer, 1995). It is something different from the mass attenuation coefficient, which is a measure of how strongly a substance absorbs or scatters radiation at a given wavelength per unit mass.

Mass energy-transfer coefficient

The Mass energy-transfer coefficient $\left(\frac{\mu_{tr}}{\rho}\right)$ is used for determining the energy trasferred by the incident photon beam per unit mass of the absorber (Hubbell & Seltzer, 1995).

Kerma

Kerma (K) is the kinetic energy released per unit mass, which can be defined as the sum of the kinetic energies of all those primary charged particles released by photons per unit mass at the point of interest (McNair, 1981).

If μ_{tr} is the linear energy-transfer coefficient and ψ is the energy fluence of monoenergetic photons passing normally through an area A of the absorber, the energy transferred to the charged particles in a volume over a short distance dx behind the area is then $A\mu_{tr}dx$. Since the mass in the volume with density

ρ is $\rho A dx$, the kerma is

$$K = \frac{\psi A \mu_{tr} dx}{\rho A dx} = \psi \left(\frac{\mu_{tr}}{\rho} \right) \tag{1.23}$$

This is the relation between kerma (K) and the mass energy- transfer coefficient $\left(\frac{\mu_{tr}}{\rho}\right)$ (Attix, 1986). But, the mass energy-absorption coefficient $\left(\frac{\mu_{en}}{\rho}\right)$ is related to the mass energy-transfer coefficient $\left(\frac{\mu_{tr}}{\rho}\right)$ by,

$$\left(\frac{\mu_{en}}{\rho} \right) = \left(\frac{\mu_{tr}}{\rho} \right) (1 - g) \tag{1.24}$$

in which g represents the average fraction of secondary electron energy that is lost in radiactive interactions. For low energy incident photons and for low Z materials, g approaches zero and $\left(\frac{\mu_{en}}{\rho}\right) = \left(\frac{\mu_{tr}}{\rho}\right)$ (Attix, 1986). So, in such cases, kerma(K) can be written in terms of the mass energy-absorption coefficient as (Manohara et al., 2008a),

$$K = \psi \left(\frac{\mu_{en}}{\rho} \right) \tag{1.25}$$

1.2 XCOM

XCOM is a web database developed by Berger and Hubbell in 1987 (Berger & Hubbell, 1987), which can be used to calculate the photon cross sections for scattering, photoelectric absorption and pair production, as well as the total attenuation coefficients, for any element, compound or mixture ($Z \leq 100$), at energies from 1 keV to 100 GeV. The XCOM program can generate cross sections on a standard energy grid, or on a grid selected by the user, or for a mix of both grids. Cross sections at energies immediately above and below all the absorption edges are automatically included. XCOM provides two forms

of output - data in tabular form and graphical display of the tabular data. The program provides total cross sections, attenuation coefficients and partial cross sections for incoherent scattering, coherent scattering, photoelectric absorption, and pair production in the field of the atomic nucleus and in the field of the atomic electrons. Total attenuation coefficients with and without the contribution from coherent scattering are also given. The interaction coefficients and total attenuation coefficients for compounds or mixtures are obtained as sum of the corresponding quantities for the atomic constituents. From the chemical formula entered by the user, the fractions by weight of the constituents are calculated by XCOM. For mixtures, the user should supply the fractions by weight of the various components.

1.3 ENDF

Evaluated Nuclear Data Format (ENDF) are used for encoding nuclear data evaluations for use in nuclear research and technology. ENDF format were originally developed for use in US national nuclear data files called ENDF/B. These files were gone through various upgradations to include new features. In this work, we have used the data from ENDF/B - VIII.0 library. The new ENDF/B-VIII.0 library (Brown et al., 2018), released in 2018, fully incorporates the new IAEA standard data and results from across the US and the international nuclear science community, over the last six years. The values of the atomic cross sections included in this library have been modified in recent updates of the nuclear data files (Midhun et al., 2019).

1.4 EpiXS program

EpiXS is a Microsoft Windows based software used for studying photon attenuation, dosimetry and shielding. It uses the data from EPICS2017 data library of ENDF/B-VIII and EPDL97 of ENDF/B-VI.8. The software performs data library interpolation between 1 keV and 100 GeV and calculates partial and total cross sections, mass attenuation coefficients, linear attenuation coefficients, mean free paths, half-value layers, effective atomic numbers, electron densities, and the auxiliary parameters and build-up factors for energy-absorption and exposure via Geometric Progression, for any user-defined material (Hila et al., 2021).

The contents of the subsequent chapters in this thesis are as follows.

In Chapter 2, we are presenting the review of literature relevant to the present work. It also contains the motivation for selecting this problem and the objectives of the present study.

Chapter 3 contains the details of the gamma ray interaction studies on the selected thermoplastic and biopolymer samples in the wide range of energy from 1 keV to 100 GeV.

Chapter 4 covers the details of the studies on radiation interaction parameters of the selected chemotherapy drugs administered concurrently with radiation therapy, in the energy range 1 keV to 100 GeV.

Chapter 5 contains the details of the coherent scattering studies of rare earth oxides using 59.54 keV and 662 keV gamma ray energies.

In chapter 6, the gamma ray attenuation studies carried out on edible oil samples is presented.

Chapter 7 contains the summary and the scope for the future of the present work.

Bibliography

Attix, F. H. 1986, Introduction to Radiological Physics and Radiation Dosimetry (Wiley, Newyork)

Berger, M. J., & Hubbell, J. H. 1987, XCOM photon cross sections on a personal computer. NBSIR 87-3597. National Bureau of Standards (former name of NIST). Gaithersburg, MD

Brown, D., Chadwick, M., Capote, R., et al. 2018, Nuclear Data Sheets, 148, 1

Brown, G. E and Mayers, D. F. 1956, Proceedings of the Royal Society of London. Series A. Mathematical and Physical Sciences, 234, 387

Brown, G. E and Peierls, R. E. 1955, in Roy. Soc. London, Vol. 227, 51

Chatterjee, B. K., & Roy, S. C. 1998, J. Phys. Chem. Ref. Data, 27, 1011

Fano, U. 1953, Nucleonics (U.S.) Ceased publication, 11

Franz, W. 1936, Z. Phys., 98, 314

Hila, F. C., Asuncion-Astronomo, A., Dingle, C. A. M., et al. 2021, Radiation Physics and Chemistry, 182, 109331

Hine, G. J. 1952, Phys. Rev., 85, 725

Hubbell, J. H., & Seltzer, S. M. 1995, NISTIR-5632

Jackson, D. F., & Hawkes, D. J. 1981, Phys. Rep., 70, 169

Kissel, L. 2000, Radiation Physics and Chemistry, 59, 185

Klein, O., & Nishina, Y. 1929, Z. Phys, 52, 853

Knoll, Glenn F. 1970, Radiation detection and measurement (John Wiley & Sons)

Latha, P. 2012, PhD thesis, Department of Physics, University of Calicut

Manohara, S., Hanagodimath, S., & Gerward, L. 2008a, Physics in Medicine & Biology, 53, N377

Manohara, S. R., Hanagodimath, S. M., Thind, K. S., & Gerward, L. 2008b, Nucl. Instrum. Methods in Phys. Res.B, 266, 3906

McNair, A. 1981, J. Labelled Compd. Radiopharm., 18, 1398

Midhun, C. V., Musthafa, M. M., Akbar, S., et al. 2019, Nuclear Science and Engineering., 194, 207

Niranjan, R. S., Rudraswamy, B., & Dhananjaya, N. 2012, Pramana – J. Phys., 78, 451

Oppenheimer, J. R., & Plesset, M. S. 1933, Physical Review, 44, 53

Perumallu, A., NageshwaraRao, A., & Krishna Rao, G. 1985, Physica, 132C, 388

Seibert, J. A., & Boone, J. M. 2005, Journal of Nuclear Medicine Technology, 33, 3

Varier, K. M. 2009, Nuclear radiation detection, measurement and analysis (Narosa publishing house, NewDelhi)

Chapter 2

Review of literature

2.1 Introduction

Data on the interaction of low energy gamma rays with matter are required for many scientific, industrial, agricultural, engineering and medical applications. Many experimental and theoretical studies have reported to be carried out to determine the gamma ray interaction parameters such as attenuation coefficients, effective atomic numbers, effective electron densities, scattering cross sections etc., by different methods. In experimental studies, the basic components involved are the gamma ray source, absorber and detector. Even though the basic components are the same, wide range of experimental setups with different geometries, incorporating additional components could be seen in the literature. Theoretically, there are different methods for finding the effective atomic number of composite materials. In the present chapter, we have made an attempt to review the studies on gamma ray attenuation, effective atomic number, effective electron density, kerma and scattering cross sections.

2.2 Gamma ray attenuation measurements - General

Experimental determination of the attenuation coefficients of gamma rays have been reported right from the early days of nuclear physics. Concurrently, there were developments in the theoretical aspects of these also. The agreement of the measured values with the theoretical predictions had given firm basis for the theoretical models and the experimental observations (Storm & Israel, 1970; Hubbell, 1982; Henke et al., 1982; Saloman et al., 1988).

Jackson and Hawkes (Jackson & Hawkes, 1981) in 1981 reported the X-ray attenuation coefficients of elements and mixtures of elements in the energy range 30 - 150 keV. Based on their studies, more accurate formula for the photoelectric cross section and for the sum of the coherent and incoherent cross sections, were put forward.

Varier et al. (Varier et al., 1986) studied the effect of finite absorber dimensions in gamma ray attenuation, using copper and mercury absorbers. A correlated effect was observed in their measurements due to the absorber thickness and its dimensions in transverse directions.

The National Bureau of Standards (NBS) database (Aoman & Hubbell, 1986) provides experimental X-ray attenuation coefficients (total absorption cross sections) and cross sections calculated using relativistic Hartree-Slater model, in the case of photoelectric cross section for all elements of atomic number Z = 1- 92, for the energy range 0.1-100 keV.

Berger and Hubbell (Berger & Hubbell, 1987) developed a computer program, named XCOM, for finding the total attenuation coefficients and photon cross sections for photoelectric absorption, pair production and total attenu-

ation coefficients for elements, compounds and mixtures ($Z \leq 100$) for 1 keV to 100 GeV.

Elkateb and Abdul Hameed in 1991 (El-Kateb & Abdul-Hamid, 1991) reported mass attenuation coefficients of gamma rays in materials containing hydrogen, carbon, and oxygen, in the energy range 0.05 to 1.333 MeV. The experimental results obtained were analyzed in terms of the total cross sections, effective atomic numbers and electron densities.

Results of many other measurements of linear and mass attenuation coefficients of gamma rays are also available in literature (Budak et al., 1999; Teli et al., 2000; Appaji Gowda et al., 2003; Midgley, 2005; Appaji Gowda, S. B., Mallikarjuna,M .L , Gowda, R and Umesh, T . K, 2006).

Angelone et al. in 2001 (Angelone et al., 2001) measured the mass attenuation coefficients for elemental materials (C, Al, Ti, V, Mn, Fe, Co, Ni, Cu, Zn, Zr, Nb, Mo, Rh, Pd, Ag, Cd, In, Ta, Pt, Au, Pb) in the range $6 \leq Z \leq 82$, using a high purity germanium detector with X-rays of energy 13 - 50 keV. The measured values were compared with theoretical values obtained from XCOM.

Later, XCOM was modified and transformed to Microsoft Windows platform by Gerward et al. (Gerward et al., 2004). The Windows version known as WinXCom can generate cross sections or attenuation coefficients on a standard energy grid or on a grid specified by the user, or for a mix of both grids. The program provides total cross sections and attenuation coefficients as well as partial cross sections for incoherent and coherent scattering, photoelectric absorption and pair production.

Kulwant Singh et al. (Singh et al., 2005) in 2005 analysed the shielding

properties of CaO–SrO–B_2O_3 glasses by measuring the mass attenuation coefficients, effective atomic numbers and effective electron densities for photon energies 511, 662, 1173, and 1332 keV. The results obtained were compared with theoretical calculations. From density measurements, the molar volume of the glasses had been derived, and the excess volume had been determined as a function of composition.

Midgley in 2005 (Midgley, 2005) measured the X-ray linear attenuation coefficient for low atomic number materials at energies 32 – 66 keV and 140 keV. The obtained results have an uncertainty of less than 2%. He (Midgley, S, 2006) also investigated the maximum angular width of a narrow beam for X-ray linear attenuation coefficient measurements, by studying the angular distributions of photons scattered by elements with Z ranging from 1 to 20 at energies 6 keV to 100 MeV, using tabulated atomic form factors and incoherent scattering functions.

Chikkappa in 2013 (Chikkappa, 2013) and Kumar and Kerur in 2006 (Kumar & Kerur, 2016) used the technique of gamma ray attenuation for measuring the water content of natural and dried leaves, soil samples and wood samples etc.

Recently, Kacal et al. (Kaçal et al., 2021) analysed the radiation attenuation properties for Li_2WO_4 doped polyester composites using HPGe detector with the help of the transmission geometry between 59.5 and 1408.0 keV photon energies. The results were compared with the results obtained by WinXCOM computer program which showed good agreement. The study showed that the radiation protection performance of unsaturated polyester increases when Li_2WO_4 is added as filler.

2.3 Theoretical studies on the effective atomic number and the effective electron density - General

In 1952, Hine (Hine, 1952) introduced the concept of effective atomic number. Theoretically, there are different methods to estimate the effective atomic numbers of composite materials (Singh et al., 2014b).

In 1965 Murthy (Murty, 1965) suggested some theoretical expressions for the effective atomic number of heterogeneous materials and he had suggested that for heterogenous materials, different effective atomic numbers may be required for different photon interaction processes.

In 1985, Perumallu et al. (Perumallu et al., 1985) studied the atomic number dependence of photon interactions in multielemental materials. Based on this study, they had suggested an empirical relation for the mass attenuation coefficient to characterize a phantom material.

Parthasaradhi et al. (Parthasaradhi et al., 1989) computed the effective atomic number of biological materials in the energy range of 1 to 50 MeV for photons, electrons and He ions. From their study, it was found that the effective atomic number for photons and electrons increases with energy and it remains constant for He ions.

Mudahar et al. (Mudahar et al., 1991) studied the energy dependence of the effective atomic number of alloys for photons in the energy range of 10 keV to 100 GeV. They reported that for the total photon interaction, the effective atomic number initially increases to the maximum value with increase in energy and then decreases to the minimum value with further increase in

energy. After that, the effective atomic number again increases with increase in energy for all the selected alloys.

Singh et al. (Singh et al., 2002) in 2002 reported the effective atomic number and the effective electron densities of some body tissues and amino acids in the wide photon energy range of 10^{-3} to 10^{5} MeV. They observed significant variations in effective atomic number due to composition of the material and domination of different interaction processes in different energy regions. Gowda et al. (Gowda et al., 2005) in 2005 reported the effective atomic number and electron density in amino acids and sugar samples in the energy range 30 to 1333 keV.

Manohara et al. (Manohara & Hanagodimath, 2007) calculated the effective atomic numbers and electron densities of some essential amino acids like histidine, leucine, lysine, methionine, phenylalanine, threonine and tryptophan for total and partial photon interactions by the direct method in the energy range of 1 keV to 100 GeV, using WinXCOM. Also, they had reported the same in the case of fatty acids and cysteine (Manohara et al., 2010). These parameters were found to vary with photon energies and with the chemical composition of the amino acids.

In another study, Manohara et al. (Manohara et al., 2008b) suggested a set of comprehensive formulas for calculating the effective atomic number and electron densities of various materials. The formulas were derived from first principles using photon interaction cross sections of the constituent atoms.

In 2009, a comparative study of two methods to determine the effective atomic numbers of biomolecules had been conducted by Manohara et al. (Manohara et al., 2009) in the energy range of 1 keV–20 MeV. They concluded that in the medium energies, the effective atomic number obtained by

the direct and interpolation methods are the same and it is equal to the mean atomic number of the constituent atoms in the material.

Kurudirek et al (Kurudirek et al., 2010) in 2010 reported the effective atomic numbers of various alloys by using a direct method for total photon interaction in the energy region of 1 keV to 100 GeV. They observed that the effective atomic number varies with the composition of alloys.

Medhat et al. (Medhat, 2011) in 2011 reported the total mass attenuation coefficients, effective atomic numbers and electron densities of different types of solid state nuclear track detectors for the total and partial photon interactions in the energy range of 1 keV to 100 GeV, using the WinXCom program. The values of these parameters have been found to vary with photon energy and chemical composition of the detectors.

Using WinXCOM, Manjunatha et al. (Manjunatha & Rudraswamy, 2013) computed the effective atomic numbers and the effective electron densities of human organs and tissues in the energy region of 1 keV to 100 GeV. The effective atomic numbers of human organs and tissues were found to vary with both photon energy and chemical composition.

Asok Kumar (Kumar, 2016) calculated various parameters of dosimetric importance such as effective atomic numbers and electron densities of nucleobases in DNA for the total and partial photon interaction processes in the energy range of 1 keV to 100 GeV. He concluded that these parameters are found to vary with energy and chemical compositions of the interacting media.

2.4 Experimental studies on the effective atomic number and electron density - General

Many reports on the experimental studies for measuring the effective atomic number and effective electron densities of composite materials are available in literature (Özdemir & Kurudirek, 2009; Elmahroug et al., 2015).

Bhandal et al. (Bhandal et al., 1992) in 1992 measured the total photon mass attenuation coefficients of seven fatty acids in the energy range 356 to 1116 keV and from the measured mass attenuation coefficients, they had extracted the effective atomic numbers and electron densities.

Mass attenuation coefficients, effective atomic numbers and electron densities of some thermoluminescent dosimetric compounds were determined by Gowda et al. (Gowda et al., 2004) in 2004 at 279.2, 320.07, 514.0, 661.6, 1115.5, 1173.2 and 1332.5 keV gamma ray energies using a hyper pure germanium detector.

Manjunathaguru et al. (Manjunathaguru & Umesh, 2006) in 2006 measured the effective atomic numbers and electron densities of some biologically important compounds containing H, C, N and O, in the energy range 145 to 1330 keV using a high purity germanium detector and derived a semi-empirical relation for the total attenuation coefficients of the investigated samples.

Cevic et al. (Cevik et al., 2008) in 2008 reported the effective atomic number and effective electron densities of semiconductors at different energies from 9.7 to 87.3 keV, by using the secondary excitation method. Experimental values are compared with theoretical values obtained by using XCOM.

The mass attenuation coefficients, effective atomic numbers and effec-

tive electron densities of Cu/Zn alloys were determined by Kaewkhao et al. (Kaewkhao et al., 2008) in 2008 on the basis of the mixture rule at 356, 511, 662, 835 and 1275 keV gamma ray energies, using NaI(Tl) scintillation detector. They observed that the effective atomic number and electron densities are almost independent of energy.

Akkurt et al. (Akkurt, 2009) calculated the mass attenuation coefficients for the photon energy in the range 1 keV to 1 GeV and also measured the mass attenuation coefficients at the photon energies of 662, 1173 and 1332 keV, using NaI(Tl) detector and hence estimated the effective atomic number and electron densities of different steel samples.

Demir et al. (Demir & Han, 2009) measured the total mass attenuation coefficients for GaAs, GaAs (semi-insulating; S-I) GaAs:Si (N^+), GaAs:Zn, InP:Fe, InP:Fe–As, InP:S and InP:Zn crystals at 22.1, 25.0, 59.5 and 88.0 keV photon energies, irradiated with ^{109}Cd and ^{241}Am radioactive point sources using transmission arrangement with a Si(Li) detector. The effective atomic number and the effective electron densities of the investigated crystals were also determined.

Limkitjaroenporn et al. (Limkitjaroenporn et al., 2013) measured the mass attenuation coefficient of Inconel 738 superalloy at different gamma ray energies by using the Compton scattering technique and the effective atomic number and electron density were also calculated. He also compared the experimental data with theoretical values calculated using the WinXCom program.

Water-equivalence study of some phantoms, based on the effective atomic numbers and electron densities for clinical MV X-ray and Co-60 gamma ray beams were conducted by Kurudirek et al. (Kurudirek, 2013).

Pravina et al. (Pawar & Bichile, 2013) reported mass attenuation coefficients, effective atomic number and effective electron densities of some amino acids at 122, 356, 511, 662, 1170, 1275 and 1330 keV photon energies using NaI (Tl) scintillation detector.

Kore et al. (Kore et al., 2014) in 2014 measured the mass attenuation coefficient, effective atomic number and electron density of some amino acids at 122, 356, 511, 662, 1170, 1275 and 1330 keV photon energies using NaI(Tl) scintillation detector.

In 2014, Kurudirek et al. (Kurudirek, M., 2014) also measured the effective atomic number and electron density of some human tissues and dosimetric materials for different photon energies relevant to radiotherapy and medical applications.

Akman et al. (Akman et al., 2015) reported the effective atomic number and electron density of some samarium compounds using the experimental total mass attenuation coefficient values near the K-edge in the X-ray energy range from 36.847 up to 57.142 keV. Here, the secondary X- rays from different sources, excited by 59.54 keV gamma rays of Am source, was used. They found that the measured values are in good agreement with theoretically estimated values.

In 2016 More et al. (More et al., 2016) measured the effective atomic number and electron density of amino acids within the energy range of 0.122–1.330 MeV, using a NaI(Tl) scintillation detection system. They observed that the effective atomic numbers and electron densities are almost constant.

Gamma ray attenuation parameters of composite filler, zirconium and acrylic coating materials used in dental treatment were determined for nine dif-

ferent gamma energies emitting from Ra-226 and Eu-152 radioactive sources, with NaI(Tl) detector by Nigar Abbasova et al. (Abbasova et al., 2019). The results obtained were compared with the NIST database and EGSnrc Monte Carlo (MC) code. It was found that general trends of these parameters are consistent with the literature.

The gamma ray shielding parameters of Zn-Cd-Sn-Pb quaternary alloy were measured by Kaur et al. (Kaur et al., 2019) for 511 keV and 662 keV gamma rays in transmission beam geometry by using NaI(Tl) scintillation detector.

2.5 Effective atomic number studies on polymers

The effective atomic number studies on polymers and plastics are significant because they are often used as tissue-equivalent and phantom materials (Kaçal et al., 2019).

Using NaI(Tl) scintillation detector, Nayak et al. (Nayak et al., 2001) measured the effective atomic number of some polymers and other materials for photoelectric process at 59.54 keV. They observed that at lower gamma energies the measured photoelectric cross sections agree with the theoretical values, for polymers composed of low Z constituent elements.

Icelli et al. (İçelli et al., 2008) determined the effective atomic number of polypyrrole for the characteristic K X-rays of Zr, Mo, Ag, In, Sb, Ba and Pr for total photon interactions in the energy range 15.74 to 40.93 keV from the measured total attenuation coefficients. The obtained experimental values were compared with theoretical XCOM values.

Kucuk et al. (Kucuk et al., 2013) determined the mass attenuation coefficients, effective atomic number and effective electron density of some polymers - polyamide-6, poly-methyl methacrylate, low-density polyethylene, polypropylene and polystyrene at 59.5, 511, 661.6, 1173.2, 1274.5 and 1332.5 keV photon energies using NaI (Tl) scintillation detector.

Singh et al. (Singh et al., 2014a) computed the effective atomic numbers of some low Z materials like, polyethylene (PE), polystyrene (PS), polypropylene (PP), Perspex (PX), polycarbonate (PC), nylon 6-6 (PA-6), plaster of Paris (POP), and TH/L2 in a wide range of energies. It was found that PE, PS, PX, and PA-6 were equivalent to adipose and muscle, POP was equivalent to cortical bone and TH/L2 was equivalent to thyroid tissue.

Kacal et al. (Kaçal et al., 2019) determined the gamma ray attenuation parameters of eight different polymers (Polyamide (Nylon 6) (PA-6), polyacrylonitrile (PAN), polyvinylidenechloride (PVDC), polyaniline (PANI), polyethyleneterephthalate (PET), polyphenylenesulfide (PPS), polypyrrole (PPy) and polytetrafluoroethylene (PTFE), using a high resolution HPGe detector and different radioactive sources in the energy range 81 to 1333 keV. They found that the effective atomic number of PVDC and PTFE are comparatively higher than that of the remaining polymers and PA-6 possesses the lowest effective atomic number.

2.6 Studies on kerma (K)

Kerma measures the amount of energy that is transferred from photons to electrons per unit mass at a certain position. It is related to the absorbed dose.

In 2008, Manohara et al. (Manohara et al., 2008a) calculated the effective atomic number, the effective electron density and kerma of some fatty acids and carbohydrates for photon interaction in the extended energy range from 1 keV to 100 GeV, using an accurate database of photon interaction cross sections and the WinXCom program. They observed that carbohydrates have a larger kerma than fatty acids in the low energy region, while fatty acids have a larger kerma than carbohydrates in the medium energy range, where Compton scattering is the dominant interaction process.

Demir et al. (Demir & Turşucu, 2012) in 2012 reported the mass attenuation coefficient, mass energy-absorption coefficient and kerma of some vitamins at 356.61, 661.66, 1250 and 1408.01 keV photon energies, by using a NaI(Tl) scintillation detector.

Yilmas et al. (Yilmaz et al., 2015) in 2015 determined the mass attenuation coefficient, mass energy-absorption coefficient and kerma for Fe alloys at photon energies of 17.44 to 51.70 keV, using a high resolution HPGe detector. They observed that kerma relative to air were different in Fe-Ce and Fe-Ni alloys, which is due to the dependence of the photoelectric cross section on the atomic numbers of the material.

Arslan et al. (Arslan, 2019) in 2019 investigated the mass attenuation coefficients, effective atomic numbers, effective electron densities and kerma relative to air for adipose, muscle and bone tissues in the photon energy region from 20 keV up to 50 MeV with Geant4 simulation package. They reported that kerma of tissues under study relative to air were dependent on the absorption edges of constituent elements of the tissue

Taylor et al. (Taylor et al., 2012) introduced the Auto-Zeff software for calculating the effective atomic numbers. This software facilitates easy com-

putation of the effective atomic numbers as a function of energy, as well as the average and spectral-weighted means.

Niranjan et al. (Niranjan et al., 2012) in 2012 computed the effective atomic number, electron density and kerma of oxides of lanthanides for a wide range of gamma ray energies and they reported that these parameters were found to vary with photon energies.

2.7 Studies on gamma ray interaction parameters of chemotherapy drugs

Ferdi Akman et al. (Akman et al., 2015) computed the gamma ray attenuation parameters of some chemotheraphy drugs (Lomustine, Cisplatin, Carmustine, Chlorambucil) in the energy range of 1 keV to 100 GeV. They reported that among the selected drugs, Cisplatin has the highest mass attenuation coefficient and the effective atomic number while, Chlorambucil has the highest mean free path and the half-value layer among the selected drugs.

Nergiz Yıldız Yorgun et al. (Yorgun & Kavaz, 2019) experimentally determined the mass attenuation coefficient, half-value layer and the effective atomic number of some cancer drugs (Tadocel, Fluro-5, Erbitux, Carboplatin, Temodal, Tamoxifen, Endoksan and Oxaliplatin) at 13.81 keV, 17.7 keV, 26.34 keV and 59.54 keV photon energies by using a Si(Li) detector . They reported that among the selected drugs, oxaliplatin, carboplatin and endoksan are more effective in the selected energy range.

Esra Kavaz et al. (Kavaz et al., 2015) computed gamma ray absorption and exposure of build-up factors of some chemotherapy drugs in the energy range 0.015 MeV to 15 MeV. They observed that the build-up of photons is

less in azathoprine and more in vinblastine among the selected drugs.

2.8 Studies on the coherent scattering cross section of photons

Studies on the coherent scattering cross section is important in diverse fields like radiation transport, attenuation, reactor shielding, industrial radiography and medical physics etc.

Kane et al. (Kane & Holzwarth, 1961) had investigated the dependence of the differential cross section for the coherent scattering of 1.17 MeV and 1.33 MeV gamma rays on atomic number and they found that coherent scattering cross section varies as Z^n where n is 3.07 ± 0.18.

Anand et al. (Anand & Sood, 1965) in 1965 investigated the atomic number dependence of the elastic scattering cross section of gamma rays below 1 MeV at different angles. The results indicate that the index to the power of atomic number on which the cross section depends increases with the momentum transfer involved in the scattering.

Roy et al. (Roy, 1978) also analysed the variation of Z dependence of elastic scattering with momentum transfer and reported the power law dependence at different regions of the momentum transfer.

With the help of a Ge(Li) detector, Basavaraju et al. (Basavaraju et al., 1979) in 1979 determined the elastic scattering cross sections of lead, tantalum and molybdenum for 1.17 and 1.33 MeV gamma rays between 30^o and 115^o. Subsequently, they (Basavaraju et al., 1994) had also determined the differential elastic scattering cross section of 81 keV gamma rays by aluminum, nickel,

tantalum, gold, and lead through angles of $60^o, 90^o, 120^o$ and 133^0, by using a HPGe detector. The experimentally obtained cross sections were compared with theoretical values calculated by modified relativistic form factors (MF's), a combination of MF's and angle-independent "anomalous" scattering factors (ASF's), and the relativistic second order S-matrix. The measured values showed good agreement with S-matrix values.

Govinda Nayak et al. (Nayak et al., 1992) reported the differential coherent scattering cross sections of some medium and heavy elements for 59.54 keV gamma rays scattered at 90^o by a reflection geometry setup. They suggested that the Relativistic Modified Form Factor theory is more appropriate in predicting the form factors in the intermediate photon momentum transfer region.

Gowda et al. (Gowda et al., 1995) in 1995 developed a new method to determine the total coherent scattering cross sections of elements for gamma rays. By this method, they determined the total coherent scattering cross sections of Bi, Pb, W and Ba at a gamma ray energy of 661.6 keV.

Latha et al. (Latha et al., 2012) in 2012 measured the coherent and incoherent scattering cross sections using a high purity germanium detector, on elements with atomic numbers ranging from 13 to 50, using ^{241}Am gamma rays and the experimental values were compared with theoretical results and it showed good agreement.

Simsek et al. (Simsek & Ertugrul, 2001) in 2001 experimentally determined the differential coherent scattering cross sections of 59.54 keV gamma rays in Ag, In, and Sn at different angles, ranging from 40^o to 135^o and the results obtained showed better agreement with Relativistic Modified Form Factor based calculations.

Shahi et al. (Shahi et al., 1997) measured the differential cross sections of the elastic scattering of 22.1 keV photons by thirty elements in the atomic region $12 \leq Z \leq 92$ at an angle 117^o. They reported that values based on the combination of Modified Form Factors and angle independent anomalous scattering factors show good agreement with S-matrix values and it can be used when the experimental data are not available.

2.9 Studies on small angle coherent scattering cross sections of photons

Most of the scattering studies at small angles are done by the shadow cone method. Roy et al. (Roy et al., 1975) in 1975 measured the coherent scattering cross sections of gamma rays for C, Al, Cu, Sn, Hg, Pb, Bi and Th at very low momentum transfers, using 145 keV photons obtained from ^{141}Ce source, by the shadow cone method.

By using the shadow cone method, Kane et al. (Kane et al., 1978) also studied the elastic and Compton scattering of 1.17 and 1.33 MeV gamma rays through angles between 4.5^o and 8^o using a Ge(Li) detector.

Ramanathan et al. (Ramanathan et al., 1979) in1979 determined the differential cross sections for elastic scattering on Cu, Cd, Ta, and Pb, at small angles and incident energies ranging from 244.7 keV to 1408.0 keV. They concluded that the deviation of the form factors may be due to the influence of the intermediate bound states on the scattering amplitude.

Puri et al. (Puri et al., 1996) in 1996 measured the differential cross sections for the elastic scattering of 59.5 keV photons by nineteen elements in the atomic region $13 \leq Z \leq 82$ at 130^o using annular source geometry. They

observed that for low Z elements, with K-shell threshold below 59.5 keV, the measured scattering differential cross sections agree well with the form factor approximations, but for high Z elements, a good agreement was observed with S-matrix calculations.

Puttaswamy et al. (Puttaswamy et al., 1984) suggested a new method, using a simple geometrical set-up, earlier used for gamma ray transmission studies. In 2011, using this method, Vinay Kumar et al. (Vinaykumar, L and Iliyas Khan and Umesh Gupta, 2011) reported the total scattering cross sections of some lead and sodium compounds at angles less than 10^o for 59.54 keV gamma rays. They suggested that in the low momentum transfer region, the non-relativistic theoretical total scattering cross sections computed by using the form factor and the scattering function (tabulated by non-relativistic HF) are quite adequate in explaining the measured total scattering cross sections. They also reported the coherent scattering cross sections of some lanthanides for low momentum transfer at small angles with 59.54 keV and 661.6 keV gamma rays (Vinaykumar & Umesh, 2014). Employing this technique, recently, Vinay Kumar and Umesh (Vinaykumar, L and Umesh, T K, 2016) have reported the angle integrated scattering cross section of 59.54 keV photons by elemental samples having atomic number in the region $13 \leq Z \leq 82$.

2.10 Gamma ray attenuation measurements in food samples.

Many investigators have reported the attenuation coefficient of different types of milk samples using gamma ray spectroscopic techniques (Chaudhari & Girase, 2013; Chaudhari, L. M. and Girase, S. B., 2013; Chaudhari, L. M. and

Girase, S. B, 2014).

Chaudhari and Rathod in 2013 (Chaudhari & Rathod, 2013) measured the gamma ray attenuation coefficients of glucose solutions. It was observed that as the concentration of glucose sample increases, linear and mass attenuation coefficient decreases.

Chikkappa et al. in 2014 (Chikkappa, Udgani and Ramesh, Thimmasandra Narayan, 2014) used the gamma ray spectroscopic technique for the detection of melamine contamination in solid milk powder. They observed that the linear attenuation coefficient increases with increase in the quantity of melamine contamination in milk powder. The results indicate that this technique can be used for the non-destructive qualitative and quantitative detection of melamine in adulterated milk powder.

Rajeswari et al. (Rajeshwari, T and Hanumantagouda, 2018) in 2018 reported the mass attenuation coefficient measurements in turmeric samples. This study showed that the mass attenuation coefficient depends on the energy of the radiation and the nature of the absorber.

Revathy et al. (Revathy et al., 2018) determined the effective atomic number in some food materials and medicines using ^{137}Cs source. Based on this study, it is suggested that the gamma attenuation technique can be used as an effective non-destructive method for finding adulteration of food materials.

2.11 Motivation for the present work

Materials composed with high atomic number elements are important in radiation protection and shielding purposes, but those containing low Z elements are used as tissue-equivalent substances or phantom materials. The effective

atomic number and effective electron density are the two decisive parameters in selecting a material as tissue substitute. In particular, polymers are suited as tissue-substitutes due to the ease of processing, flexibility, low cost, physical and chemical properties and stability in environment (Singh et al., 2014b). The detailed review of literature shows that only limited studies are reported in the gamma ray interaction parameters of polymers and also, those studies are confined to some selected photon energies or some specific energy ranges. So, we have carried out a detailed study on the gamma ray interaction parameters of eleven polymers having medical applications in the wide energy range of 1 keV to 100 GeV.

In chemoradiotherapy, the chemotherapy drugs are administered concurrently with radiotherapy, which is usually used to treat many cancer cases at later stages. So, the studies on the radiation interaction parameters of these drugs are useful in treatment planning. Even though the interaction parameters of different chemotherapy drugs with photons are available, here we have selected some drugs, whose photon interaction studies are not carried out so far.

Accurate values of coherent scattering cross section are significant in diverse fields. Rare earth oxide samples have many scientific, technological and industrial applications. So the studies on their behaviour in radiation environment is important. Also, from the detailed review of literature, it is found that, for small angles below 10^o and at low momentum transfers, the experimental scattering studies are scarce, due to the difficulty of resolving the coherent scattered peak from the main peak, even by using high resolution detectors. So, here, we have carried out some scattering studies at small angles below 10^o on some rare earth oxide samples by using the simple geometrical setup

suggested by Puttaswamy et al. (Puttaswamy et al., 1984).

Literature reports suggest that gamma ray attenuation can be used as a nondestructive technique for finding the adulteration in food samples (Revathy et al., 2018). So, we have performed a systematic study on gamma ray interaction parameters in edible oil samples, using 662 keV gamma rays.

2.12 Objectives of the present work

The objectives of the present work are four-fold :

- To study the partial and total photon interaction of gamma rays in the energy range 1 keV-100 GeV with the selected synthetic polymers having medical applications.

  The effective atomic numbers and effective electron densities of the polymers - Polylactic acid, Polycaprolactone, Polyglycolic acid, Polylactic-co-glycolic acid, Polyethylene terephthalate, Polybutyl methacrylate, Polymethyl methacrylate, Polymethyl pentene, Polyacrylonitrile, Polyvinylpyrollidone, Polydimethylsilicone are to be determined by the ratio of cross section method for total as well as partial gamma ray interaction processes in the wide range of energies 1 keV to 100 GeV. The mass energy-absorption coefficient and the effective atomic number corresponding to gamma ray energy absorption in these media are also to be estimated for the energy range of 1 keV to 20 MeV. The variation of these parameters with energy and chemical composition of the polymers are also to be studied. The kerma relative to air of these polymers are to be calculated for 1 keV to 20 MeV.

  Also, the effective atomic numbers and the effective electron densities

of the same polymers are to be estimated by different methods like direct, ratio of cross section and interpolation, in the extensive energy range of 1 keV to 100 GeV. The single value for effective atomic number of these polymers are to be determined by the method suggested by Murty (Murty, 1965), power law (Singh & Badiger, 2016) and XmuDat (Nowotny, R, 1998). The suitability of using various methods are to be validated in different energy regions.

- To study the gamma ray interaction parameters of selected chemotherapy drugs in the energy range of 1 keV to 100 GeV.

  The gamma ray interaction parameters such as linear attenuation coefficient, mass attenuation coefficient, Half-Value Layer (HVL), effective atomic number and electron density of the selected chemotherapy drugs (Hydroxyurea, Trifluridine, Temozolomide, Mitomycin C, Trabectedin) are to be estimated in the energy range of 1 keV to 100 GeV. Radiation response of these drugs at different energy regions are to be studied.

- To obtain the coherent scattering cross section of the selected rare earth compounds at small angles below 10^o using 661.6 keV and 59.54 keV gamma rays.

  The angle integrated total scattering cross sections of the selected rare earth oxides are to be determined experimentally for 661.6 keV and 59.54 keV gamma rays in the angular range of (0-4^o, 0-6^o, 0-8^o and 0-10^o). From the experimental total scattering cross sections, the corresponding angle integrated incoherent scattering cross sections obtained from ENDF library (based on the non-relativistic Hartree-Fock form factor method) has to be subtracted to obtain the angle integrated coherent scattering cross sections. The obtained angle integrated coherent scattering cross

sections are then to be compared with that determined from ENDF data. The effective atomic numbers of the selected rare earth oxides are also to be extracted by applying the ratio of cross section method. The variation of the angle integrated coherent scattering cross section with the effective atomic number of the selected compounds have then to be investigated.

- To measure the gamma ray attenuation coefficients in edible oil samples using 661.6 keV gamma rays.

  Gamma ray attenuation measurements have to be conducted in pure coconut oil, paraffin oil and a mixture of both in different proportions using 661.6 keV gamma rays. Here, ^{137}Cs source with activity 720 µC has to be used and the transmitted radiations are to be analysed using the Cadmium Zinc Telluride (CZT) detector. From the measured linear attenuation coefficients of the samples, the mass attenuation coefficients and the effective atomic numbers are to be deduced. Variation of these parameters with composition has to be studied.

Bibliography

Abbasova, N., Yüksel, Z., Abbasov, E., Gülbiçim, H., & Çağatay Tufan, M. 2019, Results in Physics, 12, 2202

Akkurt, I. 2009, Annals of Nuclear Energy, 36, 1702

Akman, F., Durak, R., Turhan, M., & Kaçal, M. 2015, Applied Radiation and Isotopes, 101, 107

Anand, S., & Sood, B. 1965, Nuclear Physics, 73, 368

Angelone, M., Bubba, T., & Esposito, A. 2001, Applied Radiation and Isotopes, 55, 505

Aoman, E., & Hubbell, J. H. 1986, NBSIR–86-3431

Appaji Gowda, S. B., Mallikarjuna, M. L., Gowda, R., & Umesh, T. . K. 2003, Pramana J.Phys., 61, 539

Appaji Gowda, S. B., Mallikarjuna,M .L , Gowda, R and Umesh, T . K. 2006, Nucl.Inst. and Methods in Phys. Res. B, 2, 243

Arslan, H. 2019, Nuclear Science and Techniques, 30, 1

Basavaraju, G., Kane, P., Kissel, L. D., & Pratt, R. 1994, Physical Review A, 49, 3664

Basavaraju, G., Kane, P., & Varier, K. 1979, Pramana, 12, 665

Berger, M. J., & Hubbell, J. 1987, XCOM: Photon cross sections on a personal computer, Tech. rep., National Bureau of Standards, Washington, DC (USA). Center for Radiation

Bhandal, G., Ahmed, I., & Singh, K. 1992, International Journal of Radiation Applications and Instrumentation. Part A. Applied Radiation and Isotopes, 43, 1185

Budak, G., Karabulut, A., & Ertrulb, M. 1999, Nucl. Inst. and Methods in Phys.Res. B, 149, 379

Cevik, U., Bacaksiz, E., Damla, N., & Çelik, A. 2008, Radiation Measurements, 43, 1437

Chaudhari, L., & Rathod, S. 2013, Journal of Chemical, Biological and Physical Sciences (JCBPS), 3, 2087

Chaudhari, L. M., & Girase, S. B. 2013, Advances in Applied Science Research, 4, 102

Chaudhari, L. M. and Girase, S. B. 2013, Journal of Chemical, Biological and Physical Sciences, 3, 1425

Chaudhari, L. M. and Girase, S. B. 2014, International Journal of Chemical and Physical Sciences, 3, 2319

Chikkappa, U. 2013, Int J Eng Sci Inv, 2, 35

Chikkappa, Udgani and Ramesh, Thimmasandra Narayan. 2014, International Journal of Research in Applied, Natural and Social Sciences, 2, 81

Demir, D., & Turşucu, A. 2012, Annals of Nuclear Energy, 48, 17

Demir, L., & Han, I. 2009, Annals of Nuclear Energy, 36, 869

El-Kateb, A., & Abdul-Hamid, A. 1991, International Journal of Radiation Applications and Instrumentation. Part A. Applied Radiation and Isotopes, 42, 303

Elmahroug, Y., Tellili, B., & Souga, C. 2015, Annals of Nuclear Energy, 75, 268

Gerward, L., Guilbert, N., Jensen, K. B., & Levring, H. 2004, Radiation physics and chemistry, 71, 653

Gowda, C., Umesh, T., & Gowda, R. 1995, Nuclear Instruments and Methods in Physics Research Section B: Beam Interactions with Materials and Atoms, 95, 127

Gowda, S., Krishnaveni, S., & Gowda, R. 2005, Nuclear Instruments and Methods in Physics Research Section B: Beam Interactions with Materials and Atoms, 239, 361

Gowda, S., Krishnaveni, S., Yashoda, T., Umesh, T. K., & Gowda, R. 2004, Pramana . J. Phys., 63, 529

Henke, B., Lee, P., Tanaka, T., Shimabukuro, R., & Fujikawa, B. 1982, Atomic Data and Nuclear Data Tables, 27, 1

Hine, G. 1952, Phys Rev, 85, 725

Hubbell, J. 1982, The International Journal of Applied Radiation and Isotopes, 33, 1269

İçelli, O., Erzeneoğlu, S., & Sağlam, M. 2008, Annals of Nuclear Energy, 35, 432

Jackson, D. F., & Hawkes, D. J. 1981, Phys. Rep., 70, 169

Kaçal, M. R., Akman, F., & Sayyed, M. I. 2019, Nucl. Eng. Technol., 51, 818

Kaewkhao, J., Laopaiboon, J., & Chewpraditkul, W. 2008, Journal of Quantitative Spectroscopy and Radiative Transfer, 109, 1260

Kane, P., Basavaraju, G., Mahajani, J., & Priyadarsini, A. 1978, Nuclear Instruments and Methods, 155, 467

Kane, P., & Holzwarth, G. 1961, Physical Review, 122, 1579

Kaur, T., Sharma, J., & Singh, T. 2019, Radiation Physics and Chemistry, 156, 193

Kavaz, E., Ahmadishadbad, N., & Özdemir, Y. 2015, Biomedicine & Pharmacotherapy, 69, 34

Kaçal, M., Dilsiz, K., Akman, F., & Polat, H. 2021, Radiation Physics and Chemistry, 179, 109257

Kore, Prashant, S., Pawar, & Pravina, P. 2014, Radiation Physics and Chemistry, 98, 86

Kucuk, N., Cakir, M., & Isitman, N. A. 2013, Radiat. Prot. Dosim., 153, 127

Kumar, A. 2016, Radiat. Phys. Chem., 127, 48

Kumar, R., & Kerur, B. 2016, J Chem Bio Phys Sci, 6, 135

Kurudirek, M. 2013, Nuclear Instruments and Methods in Physics Research, Section A: Accelerators, Spectrometers, Detectors and Associated Equipment, 701, 268

Kurudirek, M., Büyükyıldız, M., & Özdemir, Y. 2010, Nuclear Instruments and Methods in Physics Research Section A: Accelerators, Spectrometers, Detectors and Associated Equipment, 613, 251

Kurudirek, M. 2014, Radiation Physics and Chemistry, 102, 139

Latha, P., Abdullah, K. K., Unnikrishnan, M. P., Varier, K. M., & Babu, B. R. S. 2012, Phys. Scr, 85, 035303

Limkitjaroenporn, P., Kaewkhao, J., & Asavavisithchai, S. 2013, Annals of Nuclear Energy, 53, 64

Manjunatha, H., & Rudraswamy, B. 2013, Health physics, 104, 158

Manjunathaguru, V., & Umesh, T. 2006, Journal of Physics B: Atomic, Molecular and Optical Physics, 39, 3969

Manohara, S., & Hanagodimath, S. 2007, Nuclear Instruments and Methods in Physics Research Section B: Beam Interactions with Materials and Atoms, 258, 321

Manohara, S., Hanagodimath, S., & Gerward, L. 2008a, Physics in Medicine & Biology, 53, N377

Manohara, S., Hanagodimath, S., Thind, K., & Gerward, L. 2008b, Nuclear Instruments and Methods in Physics Research Section B: Beam Interactions with Materials and Atoms, 266, 3906

Manohara, S. R., Hanagodimath, S. M., & Gerward, L. 2009, Medical physics, 36, 137

Manohara, S. R., Hanagodimath, S. M., Thind, K. S., & Gerward, L. 2010, Applied Radiation and Isotopes, 68, 784

Medhat, M. 2011, Annals of Nuclear Energy, 38, 1252

Midgley, S. 2005, Radiation Physics and Chemistry, 72, 525

Midgley, S. 2006, Radiation Physics and Chemistry, 75, 945

More, C. V., Lokhande, R. M., & Pawar, P. P. 2016, Radiation Physics and Chemistry, 125, 14

Mudahar, G. S., Singh, M., & Singh, G. 1991, International journal of radiation applications and instrumentation. Part A. Applied radiation and isotopes, 42, 509

Murty, R. C. 1965, Nature, 207, 398

Nayak, N. G., Siddappa, K., Balakrishna, K., & Lingappa, N. 1992, Physical Review A, 45, 4490

Nayak, N. G., Vijaya, M., & Siddappa, K. 2001, Radiation Physics and Chemistry, 61, 559

Niranjan, R., Rudraswamy, B., & Dhananjaya, N. 2012, Pramana, 78, 451

Nowotny, R. 1998, "XMuDat: Photon attenuation data on PC " Tech.Rep. IAEA- NDS- 195, International atomic energy, Vienna, Tech. rep.

Parthasaradhi, K., Rao, B. M., & Prasad, S. G. 1989, Medical physics, 16, 653

Pawar, P. P., & Bichile, G. K. 2013, Radiation Physics and Chemistry, 92, 22

Perumallu, A., Rao, A. N., & Rao, G. K. 1985, Physica B+ C, 132, 388

Puri, S., Chand, B., Mehta, D., et al. 1996, Nuclear Instruments and Methods in Physics Research Section B: Beam Interactions with Materials and Atoms, 111, 209

Puttaswamy, K., Gowda, M., & Sanjeevaiah, B. 1984, Nuclear Instruments and Methods in Physics Research, 224, 461

Rajeshwari, T and Hanumantagouda. 2018, Ind J Pur Appl Phys, 56, 646

Ramanathan, N., Kennett, T., & Prestwich, W. 1979, Canadian Journal of Physics, 57, 343

Revathy, J. S., Anooja, J., Krishnaveni, R. B., Gangadathan, M. P., & Varier, K. M. 2018, Pramana J. Phys., 90, 1

Roy, S. 1978, Nuclear Instruments and Methods, 150, 283

Roy, S. C., Nath, A., & Ghose, A. M. 1975, Nucl. Instr. And Meth, 131, 163

Saloman, E., Hubbell, J., & Scofield, J. 1988, Atomic Data and Nuclear Data Tables, 38, 1

Shahi, J., Puri, S., Mehta, D., et al. 1997, Physical Review A, 55, 3557

Simsek, O., & Ertugrul, M. 2001, Instrumentation science and technology, 29, 404

Singh, K., Singh, H., Sharma, G., et al. 2005, Radiation Physics and Chemistry, 72, 225

Singh, K., et al. 2002, Indian journal of pure and applied Physics, 40, 442

Singh, V. P., Badiger, N., & Kucuk, N. 2014a, Journal of Nuclear Chemistry, 2014

Singh, V. P., & Badiger, N. M. 2016, Indian J. Pure Appl. Phys., 54, 333

Singh, V. P., Badiger, N. M., & Kucuk, N. 2014b, Radioprotection., 49, 115

Storm, L., & Israel, H. I. 1970, Atomic Data and Nuclear Data Tables, 7, 565

Taylor, M., Smith, R., Dossing, F., & Franich, R. 2012, Medical physics, 39, 1769

Teli, M. T., Nathuram, R., & Mahajana, C. 2000, Radiation Measurements, 32, 329

Varier, K. M., Kunju, S. N., & Madhusudanan, K. 1986, Physical Review A, 33, 2378

Vinaykumar, L., & Umesh, T. K. 2014, Eur. Phys. J. D, 68, 1

Vinaykumar, L and Iliyas Khan and Umesh Gupta. 2011, ISST J. Appl.Phys, 10, 4049

Vinaykumar, L and Umesh, T K. 2016, Journal of Radiation Research and Applied Sciences ., 9, 35

Yilmaz, D., ŞAHİN, Y., & DEMİR, L. 2015, Turkish Journal of Physics, 39, 81

Yorgun, N. Y., & Kavaz, E. 2019, Results in Physics, 13, 102150

Özdemir, Y., & Kurudirek, M. 2009, Annals of Nuclear Energy, 36, 1769

Chapter 3

Studies on partial and total gamma ray interaction parameters of some synthetic polymers having medical applications, in the energy range 1 keV to 100 GeV.

3.1 Introduction

The accurate values of the various parameters representing the interaction of radiation with materials, such as mass energy-absorption coefficient, effective atomic number, effective electron density and kerma are required in diverse fields, like radiation dosimetry, nuclear medicine, radiation protection, radiation therapy, medical diagnosis etc. Materials containing elements with high atomic number are important in radiation protection and shielding. But, materials made up of elements with low atomic number, like polymers and plastics

are used as tissue - equivalent substitutes and phantom materials (Kaçal et al., 2019). Tissue-equivalent materials are used for the simulation of radiation dose distribution in human organs (White, D. R., 1978). Generally, a material is treated as tissue-equivalent for photon interaction, if the radiation absorption and scattering exhibited by it are the same as that of the tissue under consideration. One can usually ensure this by estimating the mass attenuation coefficient, effective atomic number, mass energy-absorption coefficient etc. (Parthasaradhi, 1968; Weber & Van den Berge, 1969; White, 1977, 1978; Chandra Lingam et al., 1984; Rao et al., 1985; Parthasaradhi et al., 1989, 1992; Bhandal & Singh, 1993; Prasad et al., 1997; Kiran Kumar & Venkata Reddy, 1997). Polymers are often a choice for tissue substitutes due to the ease of processing, flexibility, low cost, physical and chemical properties and stability in the environment (Singh et al., 2014).

The total as well as partial interaction cross sections of gamma rays with materials have a profound dependence on the atomic number of the constituent elements. In the case of a composite material, containing different elements in different proportions, a single number cannot represent the effective atomic number uniquely in the entire energy region, as in the case of pure elements. The role of effective atomic number comes into play under such situations. The concept of effective atomic number (Z_{eff}) was first introduced by Hine (Hine, 1952). For a given energy, the Z_{eff} is useful in choosing a substitute composite material in the place of an element. The number of electrons per unit mass of the material will give the effective electron density. The energy absorption in a medium can be estimated in terms of the effective atomic number and the effective electron density values of the medium. So, the effective atomic number is practically used in radiotheraphy and medical imaging, in connection with the estimation of radiation dose. Also, Z_{eff} is a decisive factor in

determining the radiation response characteristics of materials in various other fields (Manohara, S. R and Hanagodimath, S. M and Gerward, L, 2009).

Many theoretical methods are there to evaluate the effective atomic number, such as direct (Manohara et al., 2008b), ratio of cross-section (Niranjan et al., 2012), logarithmic interpolation (Singh et al., 2007), power law (Singh & Badiger, 2016), XmuDat (Nowotny, 1998) and the method by Murty (Murty, 1965). Also, researchers have reported studies on effective atomic numbers of various composite materials such as dosimetric materials (Gowda et al., 2004; Singh & Badiger, 2013, 2016), biological compounds (Gowda et al., 2005; Manjunathaguru & Umesh, 2006; Manohara et al., 2008a, 2010), shielding materials (Elmahroug et al., 2015), semiconductors (Cevik et al., 2008), food samples (Revathy et al., 2018) etc. However, only limited studies had been reported in polymers (Govinda Nayak et al., 2001; Kucuk et al., 2013; Singh et al., 2014; Kaçal et al., 2019). So, in the present work, the effective atomic number and the effective electron density of some synthetic polymers, being used in clinical medicine, have been calculated by the ratio of cross section method for total and partial interaction processes, in the energy range of 1 keV to 100 GeV. The kerma relative to air has been reported for the energy range 1 keV to 20 MeV. The mass energy-absorption coefficient and the effective atomic number corresponding to the energy-absorption in the medium have been reported for the same energy range. Besides these, for total photon interaction, we have determined the Z_{eff} and N_{eff} of the selected polymers, by direct, ratio of cross section and interpolation methods, in the energy range 1 keV to 100 GeV. Also, the single effective atomic number was calculated by using XMuDat, power law and by the method suggested by Murty. The effective atomic numbers obtained by different methods were compared and the suitability of using different methods in various energy regions have been discussed. The results

are compared with the available experimental data. Also, We have compared the results obtained by direct method in the present approach with that from EpiXS program.

For the present work, the mass attenuation coefficients of the elements were taken from XCOM program (Berger & Hubbell, 1998) and the mass energy-absorption coefficient data were taken from the reports of Hubbell and Seltzer (Hubbell & Seltzer, 1995). The computations were done by using self-developed python codes. Python is a general purpose, high level programming language with an emphasis on the code readability. It is an open source software and its compiler is freely available. Here we have used the version 3.7.5 of the python software. In the present computations, we have inputed the mass attenuation coefficients and the mass energy-absorption coefficient of the elements.The Z_{eff} and N_{eff} were computed using the theoretical formulas given for different methods. The python codes were verified by reproducing the values reported by Manohara and Hanagodimath, (Manohara & Hanagodimath, 2007) by using the WinXCom program (Gerward et al., 2004).

3.2 Materials under study

The polymers selected for the present study are listed in Table 3.1 and their chemical compositions are displayed in Table 3.2. Weight fractions of the constituent elements were directly calculated from the chemical formula. Polylactic acid (PLA) is a degradable polyester of Levo(L)/Dextro(D)-lactic acid, which is used for making orthopedic fixation tools, ligament and vascular stents. It is also used for tendon repair. Polylactic-co-glycolic acid (PGLA) is a copolymer having the same application spectrum as that of PLA.

Table 3.1: Molecular formula and abbreviations of the synthetic polymers studied in the present work.

Sl. No	Sample	Abbre-viation	Chemical formula
1	Polylactic acid	PLA	$C_3H_4O_2$
2	Polycaprolactone	PCL	$C_6H_{10}O_2$
3	Polyglycolic acid	PGC	$C_2H_2O_2$
4	Polylactic-co-glycolic acid	PGLA	$C_5H_8O_5$
5	Polyethylene terephthalate	Mylar (PET)	$C_{10}H_8O_4$
6	Polybutyl methacrylate	PBMA	$C_8H_4O_2$
7	Polymethyl methacrylate	PMMA	$C_5H_8O_2$
8	Polymethylpentene	PMP	C_6H_{12}
9	Polyacrylonitrile	PAN	C_3H_3N
10	Polyvinylpyrollidone	PVP	C_6H_9NO
11	Polydimethylsilicone	PDMS	C_6H_6OSi

Biostable polyester Mylar is used as membranes, vascular grafts, surgical meshes, ligament and also for tendon repair. Polymethyl methacrylate (PMMA) and Polybutyl methacrylate (PBMA) are hard methacrylates being used as bone cement, as intraocular lens and as dialysis membranes. Polyvinylpyrollidone (PVP) is a hydrophilic, soluble polymer having applications in antifouling coating and as dialysis membranes. Polycaprolactone (PCL) is a diol used for polyurethane formation. Polyacrylonitrile (PAN) is used as dialysis membranes. Polydimethylsilicone (PDMS) is a highly inert elastomer, used for making catheters, nucleus pulposus substitutes, intraocular lenses, glaucoma drainage devices and also dialysis membranes. Besides these applications, some of the polymers are in use for packing medical implants. For the sterilisation of these medical implants, gamma ray irradiation method is used. The optimum dose to be delivered during sterilisation is to be

ensured, because in addition to killing bacterial cells, excess radiation may deteriorate the physical and chemical properties of the polymers. Uniform dose distribution is important during gamma sterilisation. To determine the exact sterilization dose of radiation and to calculate the build-up effect, the energy dependent Z_{eff} of polymer materials are required (Maitz, 2015).

Table 3.2: Elemental composition of the selected synthetic polymers.

Sample	Weight fraction				
	C	H	O	N	Si
PLA	0.5000	0.0559	0.4440		
PCL	0.6314	0.0883	0.2803		
PGC	0.4139	0.0347	0.5514		
PGLA	0.4055	0.0544	0.5401		-
Mylar	0.6250	0.0420	0.3330		
PBMA	0.7273	0.0305	0.2422		
PMMA	0.5998	0.0805	0.3196		
PMP	0.8563	0.1437			
PAN	0.6791	0.0570		0.2640	
PVP	0.6484	0.0816	0.1440	0.1260	
PDMS	0.5897	0.0495	0.1309		0.2298

3.3 Estimation of parameters

3.3.1 Mass attenuation coefficient

The intensity of gamma rays after passing through a layer of material of thickness x, with respect to the incident intensity I_o is given by Beer-Lambert law

$$I = I_0 e^{-\mu x} = I_0 e^{-(\frac{\mu}{\rho})t} \tag{3.1}$$

where t=xρ is the mass thickness (g/cm^2) and $(\frac{\mu}{\rho})$ is the mass attenuation coefficient (cm^2/g).

For a compound or a mixture, the mass attenuation coefficient, $\left(\frac{\mu}{\rho}\right)_c$ can be obtained by applying the mixture rule (Jackson & Hawkes, 1981),

$$\left(\frac{\mu}{\rho}\right)_c = \sum_i \omega_i \left(\frac{\mu}{\rho}\right)_i \tag{3.2}$$

where $\left(\frac{\mu}{\rho}\right)_i$ and ω_i are respectively the mass attenuation coefficient and weight fraction of the ith constituent element present in the compound.

The total photon interaction cross section σ can be expressed in terms of the partial interaction cross sections as given below.

$$\sigma = \sigma_{coherent} + \sigma_{incohrent} + \tau + \sigma_{pair,e} + \sigma_{pair,n} \tag{3.3}$$

Here, $\sigma_{coherent}$, $\sigma_{incohrent}$, τ, $\sigma_{pair,e}$ and $\sigma_{pair,n}$ are the coherent, incoherent, photoelectric, electronic pair production and nuclear pair production cross sections, respectively.

3.3.2 Calculation of the effective atomic number-different methods

Direct method (Manohara et al., 2008b)

The effective atomic numbers of polymers can be calculated by the direct method, using the following formula,

$$Z_{eff} = \frac{\sum_i \mathrm{f_i A_i} \left(\frac{\mu}{\rho}\right)_i}{\sum_i \mathrm{f_i} \frac{\mathrm{A_i}}{\mathrm{z_i}} \left(\frac{\mu}{\rho}\right)_i} \tag{3.4}$$

where f_i, A_i, $\left(\frac{\mu}{\rho}\right)_i$ and z_i are the fractional abundance, atomic mass, mass attenuation coefficient and atomic number of the i^{th} constituent element in the sample.

Ratio of cross section method (Niranjan et al., 2012)

In this method, first we deduce the atomic and electronic cross sections from the calculated mass attenuation coefficients of the compounds. The effective atomic number is then obtained from the ratio of the atomic cross section (σ_a) to the electronic cross section (σ_e).

$$\sigma_a = \frac{\left(\frac{\mu}{\rho}\right)_c}{N_o \sum_i \omega_i / A_i} \tag{3.5}$$

$$\sigma_e = \frac{1}{N_o} \sum_i \frac{\omega_i A_i \left(\frac{\mu}{\rho}\right)_i}{z_i} \tag{3.6}$$

In the above equations, $\left(\frac{\mu}{\rho}\right)_c$, N_o, ω_i and $\left(\frac{\mu}{\rho}\right)_i$ are the mass attenuation coefficient of the compound, the Avogadro number, weight fraction and mass attenuation coefficient of the i^{th} constituent element of the compound. Then,

$$Z_{eff} = \frac{\sigma_a}{\sigma_e} \tag{3.7}$$

Interpolation method (Singh et al., 2007)

Here, as the first step, the mass attenuation coefficients were estimated using the mixture rule. From this the effective atomic cross sections were deduced. The effective atomic cross sections so obtained for the polymers were then logarithmically interpolated at selected energies to extract the effective atomic

number, using the formula,

$$Z_{eff} = \frac{\mathrm{Z_1}(\log\sigma_2 - \log\sigma) - \mathrm{Z_2}(\log\sigma - \log\sigma_1)}{\log\sigma_2 - \log\sigma_1} \tag{3.8}$$

Here, σ_1 and σ_2 are the atomic cross sections of elements between which the atomic cross section σ of the polymer lies. $\mathrm{Z_1}$ and $\mathrm{Z_2}$ are the atomic number of the elements corresponding to σ_1 and σ_2, respectively.

Here, the two variables used are the atomic cross section of elements σ_a and their atomic number Z. Since the variation of σ_a with Z is not linear, we could not use linear interpolation. The variation of σ_a with Z shows exponential behaviour and hence, $\log(\sigma_a)$ shows a linear variation with Z. So here the effective atomic cross sections are logarithmically interpolated at selected energies to extract the effective atomic number.

Power law method (Singh & Badiger, 2016)

The effective atomic number using the power law is obtained by the following equation,

$$\mathrm{z_{eff}^{x}} = \sum_{\mathrm{i}} \mathrm{a_i z_i^{x}} \tag{3.9}$$

where 'x' values lies in the range 2.94-3.5 (Harold & Cunningham, 1985; Singh & Badiger, 2016) and $\mathrm{a_i}=\frac{\mathrm{s_i}}{\sum_{\mathrm{i}} \mathrm{s_i}}$ with $\mathrm{s_i}$ being the number of moles of i^{th} constituent element, which can be calculated by the equation,

$$\mathrm{s_i} = \frac{\mathrm{N_o \omega_i z_i}}{\mathrm{A_i}} \tag{3.10}$$

XmuDat Method (Nowotny, 1998)

XmuDat is a computer program for calculating the effective atomic number of elements, compounds and mixtures for photons of energy in the range 1 keV

to 50 MeV. It provides only a single value for the effective atomic number for all energies. The method uses the following equation,

$$Z_{eff} = \sum_{\mathrm{i}} (\alpha_{\mathrm{i}} \mathrm{z}_{\mathrm{i}}^{\mathrm{m}-1})^{\frac{1}{\mathrm{m}-1}} \tag{3.11}$$

where α_{i} are the fractional contents of electrons in the ith constituent element and m is a constant between 3 and 5.

Murty's method (Murty, 1965)

Murty suggested an empirical relation as given below, to calculate the effective atomic number of heterogeneous materials, consisting of a number of elements in varying proportions.

$$Z_{eff} = \frac{\sum_{\mathrm{i}} \omega_{\mathrm{i}} \mathrm{z}_{\mathrm{i}} \mathrm{A}_{\mathrm{i}}}{\sum_{\mathrm{i}} \omega_{\mathrm{i}} \mathrm{A}_{\mathrm{i}}} \tag{3.12}$$

where $\omega_{\mathrm{i}}, \mathrm{z}_{\mathrm{i}}$ and A_{i} are the weight fraction, atomic number and mass number of the ith constituent element in the compound.

3.3.3 The effective electron density (N_{eff})

The effective electron density of a compound can be expressed in terms of the effective atomic number by the formula (Manohara et al., 2008b),

$$N_{eff} = \frac{\mathrm{N_o n\, Z_{eff}}}{\sum_{\mathrm{i}} \mathrm{n_i A_i}} = \frac{\mathrm{N_o Z_{eff}}}{< \mathrm{A} >} \tag{3.13}$$

Here, <A>, n and n_i are the average atomic mass of the compound, total number of atoms present in the molecule and number of atoms of the ith constituent element in the molecule, respectively.

3.3.4 Kerma (K)

Kerma is the acronym for kinetic energy per unit mass. It can be defined as the sum of the initial kinetic energy of the secondary charged particles liberated per unit mass at the point of interest by the uncharged radiation (Attix, 1986).

Kerma (K) and mass energy-transfer coefficient $\left(\frac{\mu_{tr}}{\rho}\right)$ are related by the following expression,

$$K = \psi \left(\frac{\mu_{tr}}{\rho}\right) \tag{3.14}$$

where ψ is the energy fluence of photons passing normally through unit area of the absorber. But, the mass energy-absorption coefficient $\left(\frac{\mu_{en}}{\rho}\right)$ is related to the mass energy-transfer coefficient $\left(\frac{\mu_{tr}}{\rho}\right)$ by,

$$\left(\frac{\mu_{en}}{\rho}\right) = \left(\frac{\mu_{tr}}{\rho}\right)(1-g) \tag{3.15}$$

in which g represents the average fraction of secondary electron energy that is lost in radiactive interactions. For low energy incident photons and for low Z materials, g approaches zero and $\left(\frac{\mu_{en}}{\rho}\right) = \left(\frac{\mu_{tr}}{\rho}\right)$ (Attix, 1986). In the present study, the selected materials are polymers which are composed of low Z elements andthe energy range selected is from 1 keV to 20 MeV. So, here, kerma(K) can be written in terms of the mass energy-absorption coefficient as (Manohara et al., 2008a),

$$K = \psi \left(\frac{\mu_{en}}{\rho}\right) \tag{3.16}$$

Kerma of polymers relative to air is given by the expression (Manohara et al., 2008a; Niranjan et al., 2012; Singh & Badiger, 2016),

$$K_{poly,air} = \frac{(\mu_{en}/\rho)_{polymer}}{(\mu_{en}/\rho)_{air}} \tag{3.17}$$

where $(\mu_{en}/\rho)_{polymer}$ is obtained by the mixture rule applicable for the mass energy-absorption coefficient.

$$(\mu_{en}/\rho)_{polymer} = \sum_i \omega_i \left(\frac{\mu_{en}}{\rho}\right)_i \tag{3.18}$$

Here, ω_i and $\left(\frac{\mu_{en}}{\rho}\right)_i$ are respectively the weight fraction and mass energy-absorption coefficient of the ith constituent element in the polymer.

3.4 Results and discussion

3.4.1 Mass attenuation coefficient

Variation of the mass attenuation coefficient of polymers with energy of the gamma rays in the range 1 keV to 100 GeV is shown in Figure 3.1.

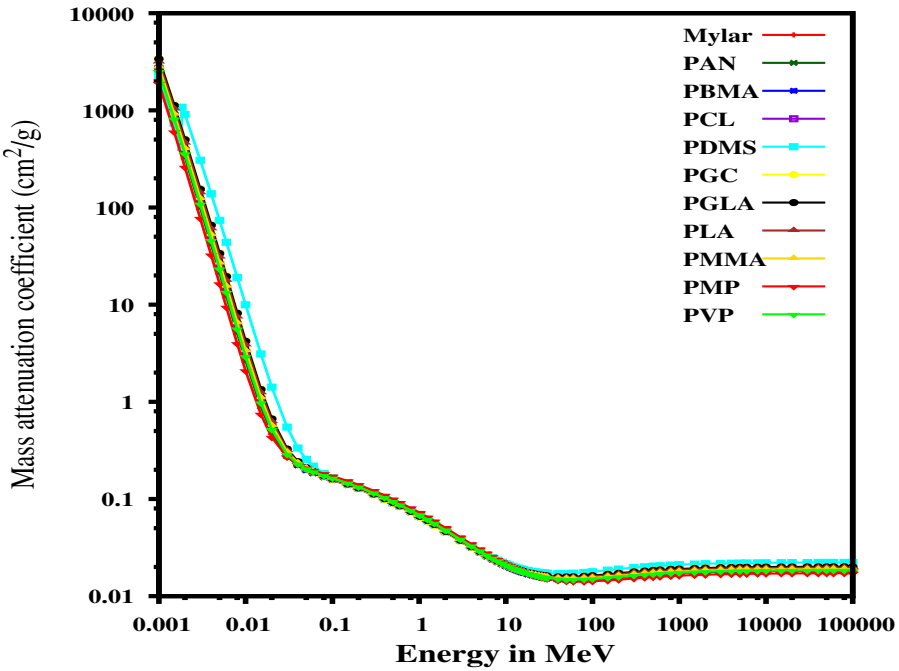

Figure 3.1: Variation of the mass attenuation coefficient $\left(\frac{\mu}{\rho}\right)_c$ of the selected polymers with incident photon energy, due to total photon interaction.

Mass attenuation coefficient varies with both photon energy and chemical composition of the polymers. The $\left(\frac{\mu}{\rho}\right)_c$ decreases rapidly with energy up to 50 keV and beyond that, it shows a linear decrease in the intermediate energy region. At high energy region, it increases slowly and becomes almost a constant. By observing the variation of $\left(\frac{\mu}{\rho}\right)_c$ among different polymer samples at specific energy values, it is evident from Figure 3.1, that, it is showing maximum variation up to 100 keV (note that the y-axis of Figure 3.1 is in the logarithmic scale). Then, for the energy range .1 MeV to 10 MeV, it is negligible and after that, up to 100 GeV, it is significant. These results support the earlier observation of Elmahroug et al. (Elmahroug et al., 2015) in some shielding materials. The variation of $\left(\frac{\mu}{\rho}\right)_c$ with energy of the incident photons and chemical composition of the polymers can be explained in terms of the partial photon interaction processes like photoelectric absorption, Compton scattering and pair production. At lower energy region, the photoelectric absorption is dominant and its cross section varies with the Z_{eff} of the interacting material as Z^{4-5} and inversely with the incident photon energy as $E^{3.5}$. In the intermediate energy region, Compton scattering is predominant and its cross section varies linearly with Z_{eff} and inversely with photon energy E. At high energy region, pair production is the dominant interaction mode and its cross section varies as Z^2 and $logE$ (Motz et al., 1969). In the case of PDMS, $\left(\frac{\mu}{\rho}\right)_c$ shows a sudden jump at 1.839 keV due to the silicon K absorption edge. $\left(\frac{\mu}{\rho}\right)_c$ has two values at 1.839 keV, $4.148 \times 10^2 g/cm^2$ and $1.078 \times 10^3 g/cm^2$.

3.4.2 Variation of Z_{eff} and N_{eff} with photon energy

Variation of Z_{eff} with incident photon energy in the range 1 keV to 100 GeV for the selected polymers, due to total and partial interaction processes, are displayed in Figures 3.2–3.7. It clearly points to the fact that Z_{eff} and N_{eff}varies

with energy, as mentioned earlier by Hine (Hine, 1952).

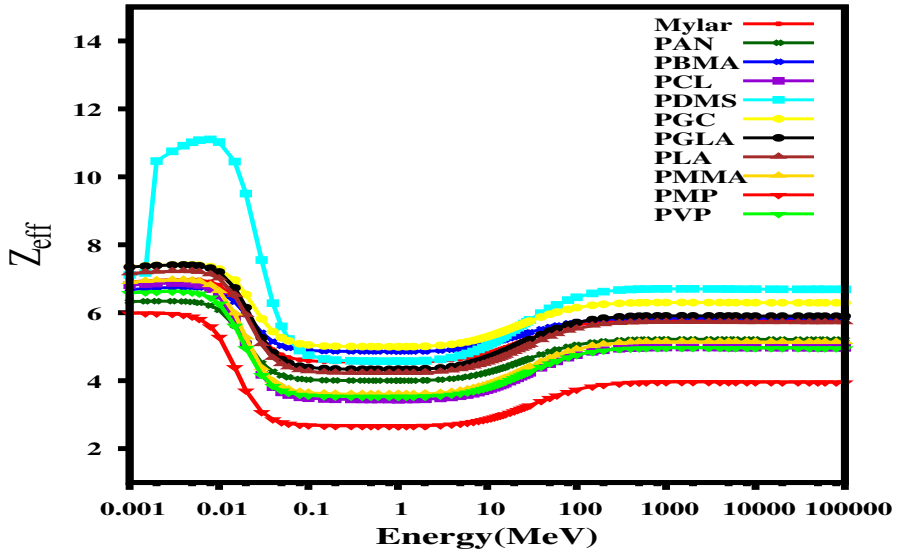

Figure 3.2: Variation of the effective atomic number of the selected polymers with photon energy, due to total photon interaction.

Total photon interaction

The variation of Z_{eff} with incident photon energy from 1 keV to 100 GeV, due to total photon interaction, in the case of all selected polymers are shown in Figure 3.2. Except PDMS, their behaviour are almost identical. Here, we can see three energy regions, 0 to 10 keV, 100 keV to 10 MeV and 100 MeV to 100 GeV, where respectively, the photoelectric absorption, Compton scattering and pair production are the dominant modes of interaction. In all these regions, the effective atomic number is almost independent of energy. Z_{eff} is maximum in the photoelectric dominant region and minimum in the Compton dominant region. It has an intermediate value, at the higher energy region, where the pair production is dominant. In the energy range 10 keV to 100 keV, the transition from photoelectric dominant region to Compton dominant region occurs and Z_{eff} shows a rapid decrease with energy.

Similarly, in the energy range 10 MeV to 100 MeV, the transition from Compton dominant region to pair production dominant region occurs and Z_{eff} increases sharply with energy. These findings are consistent with that of Manohara et al. (Manohara et al., 2008b) who had reported that Z_{eff} is maximum below 10 keV and minimum at the intermediate energy range.

Coherent scattering

The variation of Z_{eff} with photon energy, due to coherent scattering is displayed in Figure 3.3. For all the selected polymers, except PDMS, the Z_{eff} increases with increase in photon energy up to 200 keV and for PDMS it increases with energy up to 1 MeV. Thereafter, it becomes independent of energy. These results are similar as that of El-Kateb and Abdul Hamid (El-Kateb & Abdul-Hamid, 1991), who had shown that in materials containing carbon, hydrogen and oxygen, the effective atomic number tends to be constant with energy. For PDMS, the deviation may be due to the presence of silicon.

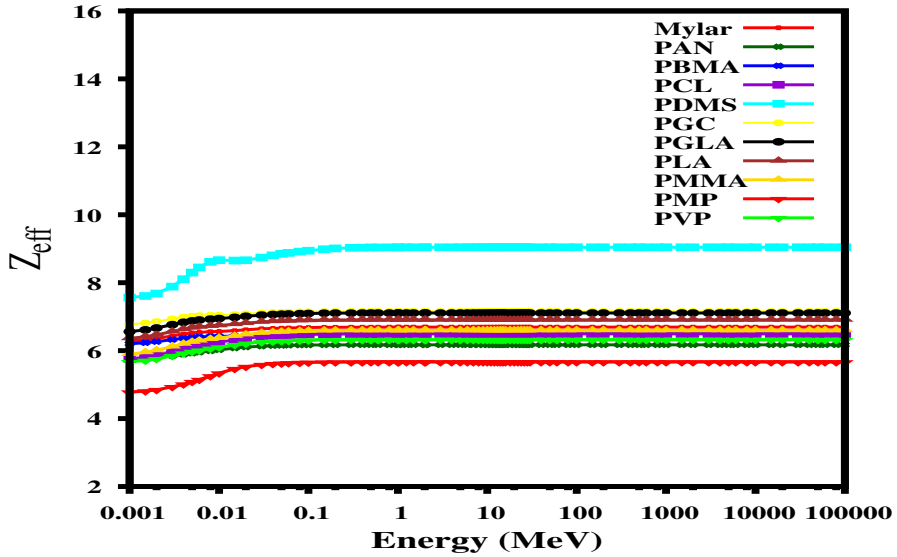

Figure 3.3: Variation of the effective atomic number of the selected polymers with photon energy, due to coherent scattering.

Incoherent scattering

For incoherent scattering, the variation of Z_{eff} with energy is displayed in Figure 3.4. The Z_{eff} varies sharply up to 100 keV and a slight variation was shown from 100 keV to 400 keV. After that, it remains constant with photon energy. The same kind of variation was reported for alloys by Mudahar and Singh (Mudahar et al., 1991). The present results are also in line with the reports of Ashok Kumar (Kumar, 2016) on nucleobases in DNA and that of Shantappa and Hanagodimath (Shantappa & Hanagodimath, 2014) on vitamins. The constant value of Z_{eff} for 400 keV-100 GeV photon energy, is the same as the mean atomic number of the polymers. These results are similar as that of Manohara et al., Olarinoye, Prasanna Kumar and Umesh (Manohara et al., 2008a; Olarinoye, 2011; Kumar & Umesh, 2011). This constant value of Z_{eff}, which is same as the mean atomic number of the polymers, may be due to the linear dependence of Compton atomic scattering cross section on atomic number Z (Attix, 1986). The mean atomic number of the selected polymers are in the order $PMP < PCL < PVP < PMMA < PAN < PLA < PGLA < PET < PDMS < PBMA < PGC$. The mean atomic number of a composite material depends on the atomic number as well as on the weight fraction of constituent elements. It is maximum for PGC and minimum for PMP among the selected polymers.

The Compton electronic cross section ($\sigma_{e,c}$) is independant of Z (Attix, 1986). Compton mass attenuation coefficient $\left(\frac{\mu}{\rho}\right)_{Compton}$, which is the cross section per unit mass, is related to the Compton electronic cross section as $\left(\frac{\mu}{\rho}\right)_{Compton} = \sigma_{e,c}\left(\frac{N_A Z}{A}\right)$, where N_A is the Avogadro's constant (Attix, 1986). Here, Z/A ranges between 0.4 and 0.5 for all elements except hydrogen. For hydrogen, $Z/A = 1$. So, Compton mass attenuation coefficient $\left(\frac{\mu}{\rho}\right)_{Compton}$

is approximately independent of Z, like the Compton electronic cross section with the exception of hydrogen (Attix, 1986). But, Compton atomic cross section($_a\sigma$) is related to electronic cross section as $\sigma_{a,c}$ = Z $\sigma_{e,c}$ (Attix, 1986). So, Compton atomic cross section has a linear dependance on Z. The variation of Z_{eff} at low energies depends on the weight fraction and the range of atomic numbers of the constituent elements in the polymers.

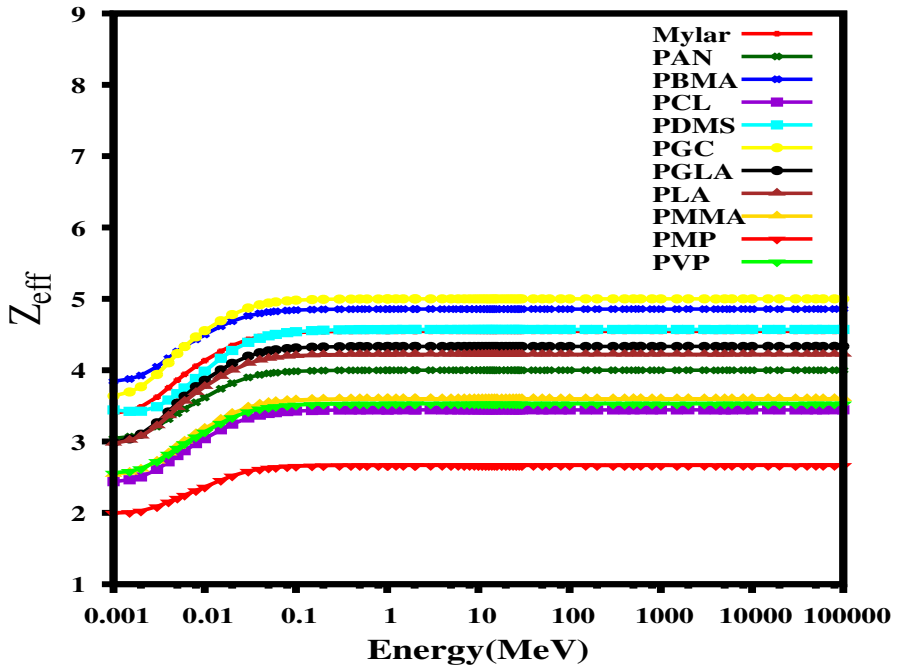

Figure 3.4: Variation of the effective atomic number of the selected polymers with photon energy, due to incoherent scattering.

Photoelectric absorption

For photoelectric absorption, the variation of Z_{eff} with energy is displayed in Figure 3.5. Except for PDMS, the effective atomic number is almost independent of the incident photon energy. For PDMS, a sharp jump occurs at 1.839 keV, which is at the K- absorption edge of silicon; then the Z_{eff} increases with photon energy up to 100 keV and after that it remains constant. This is

similar to the observations of Perumallu et al. (A.Perumallu & Rao, 1985) in multielemental materials. Photoelectric absorption is the predominant mode of interaction at low energies for high Z elements. The variation of Z_{eff} at low energies is maximum for PDMS and is minimum for PMP. This variation depends on the range of atomic numbers of the constituent elements and their weight fraction. The maximum variation in PDMS is due to the large difference in atomic number of the constituent elements from H(1) to Si(14). The minimum deviation in PMP is due to the fact that it contains only H (1) and C (6).

Pair production (electronic field)

Pair production is one of the significant energy loss mechanisms of relatively high energy photons on interacting with material media (Hubbell, J. H., 2004). The variation of Z_{eff} with photon energy due to pair production in the electric field of the electrons is shown in Figure 3.6. The Z_{eff} is almost independent of energy from 3 MeV to 30 MeV, then slightly decreases with energy from 30 keV to 50 GeV and after that it remains constant. This is the case for all the selected polymers. The atomic cross section of pair production in the field of electrons has a linear dependence on Z (Attix, 1986). In the case of pure elements it is directly proportional to the atomic number of elements. But, in the case of composite materials containing different elements in different proportions, the cross section depends on the atomic number of constituent elements and at the same time on the weight fraction of elements. Accordingly, the atomic number of each element is weighed differently in different compounds. Eventhough PDMS contains Silicon with high atomic number, the Z_{eff} of the polymer depends on the weight fraction of the constituent elements also.

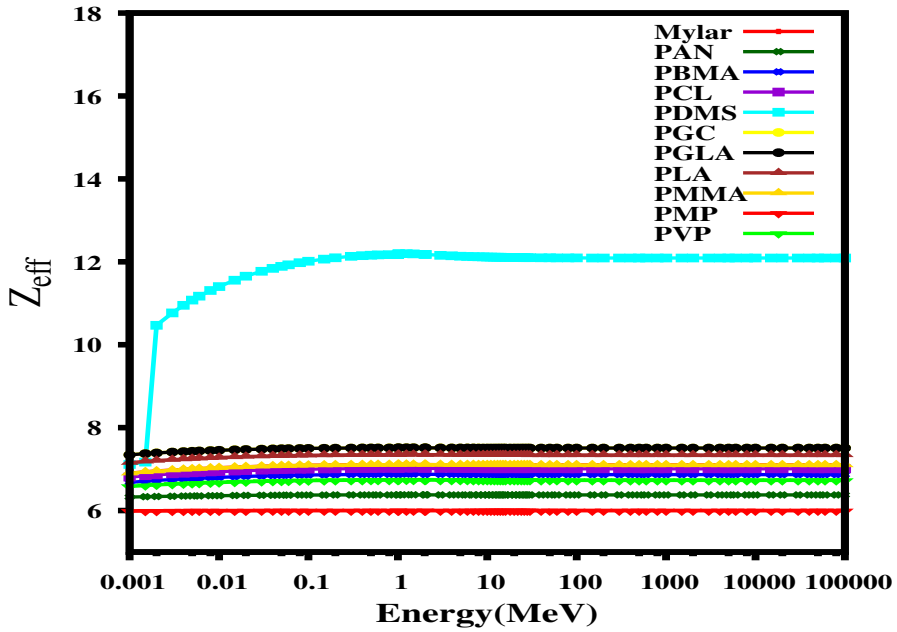

Figure 3.5: Variation of the effective atomic number of the selected polymers with photon energy, due to photoelectric absorption.

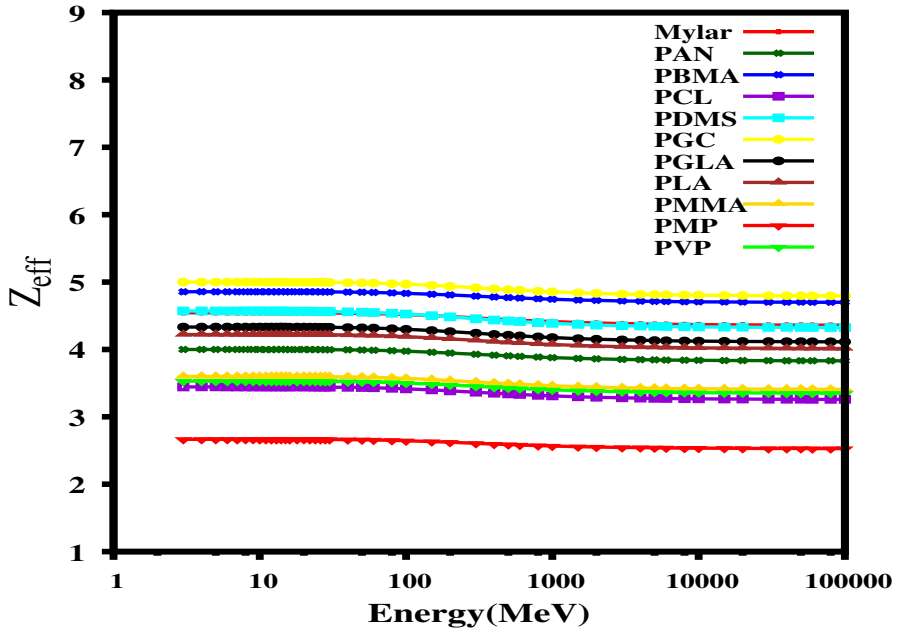

Figure 3.6: Variation of the effective atomic number of the selected polymers with photon energy, due to pair production in the field of electrons.

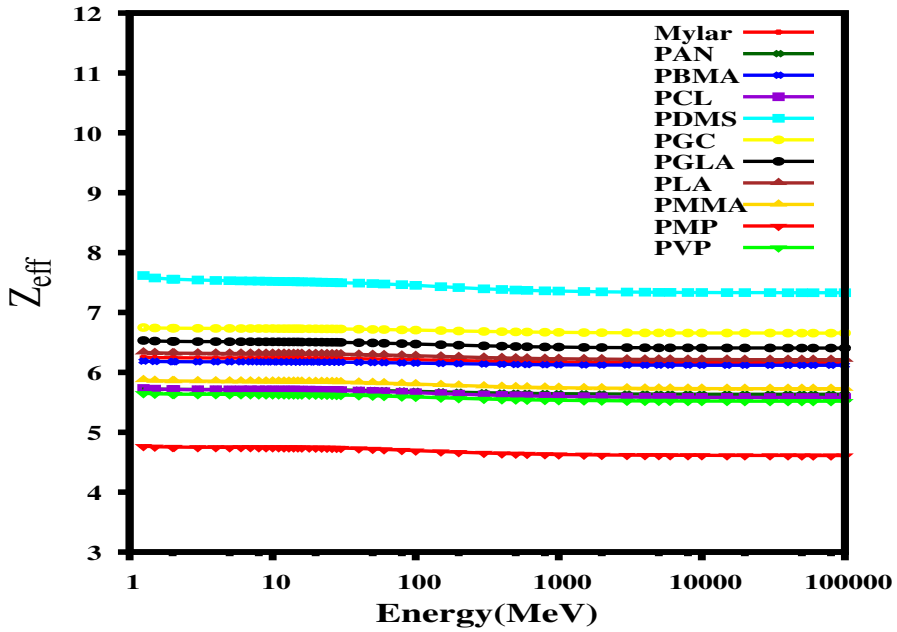

Figure 3.7: Variation of the effective atomic number of the selected polymers with photon energy, due to pair production in nuclear field.

Pair production (nuclear field)

The variation of Z_{eff} with photon energy due to pair production in the nuclear field is shown in Figure 3.7. The effective atomic number slightly decreases with photon energy from 1.25 MeV up to 3 GeV and thereafter it is independent of energy for all the selected polymers, except for PDMS. This is due to the fact that pair production in the nuclear field has a Z^2 dependence (Hubbell, 2006). In PDMS, the fall in Z_{eff} with energy is more because of the wide range of atomic numbers of its constituent elements.

The variation of N_{eff} with photon energy

The variation of N_{eff} with photon energy from 1 keV to100 GeV, for all the selected polymers, due to total and partial interaction processes, are shown in Figures 3.8–3.13. Since the two parameters Z_{eff} and N_{eff} are related, the

variation of N_{eff} with energy can be explained in the same way as that of Z_{eff}. N_{eff} and Z_{eff} are related by the expression $N_{eff} = \frac{N_o Z_{eff}}{<A>}$, where N_o is the Avogadro's constant and $< A >$ is the mean mass number of the polymer. Among the selected polymers, PMP contains hydrogen and carbon only and also, its mean mass number and mean atomic number, both are low compared with that of the other polymers. As discussed earlier, for incoherent scattering, the Z_{eff} is equal to the mean atomic number of polymers. So, as in Figure 3.4, PMP has the minimum value for Z_{eff} corresponding to incoherent scattering. But, as shown in Figure 3.10, N_{eff} of PMP has the highest value among the polymers since its mean mass number is very low. For each selected polymer, the $< A >$ is a constant for the entire energy range. So N_{eff} and Z_{eff} are linearly related. Accordingly, for a selected polymer, the variation of N_{eff} with energy can be explained in the same way as that of the Z_{eff}.

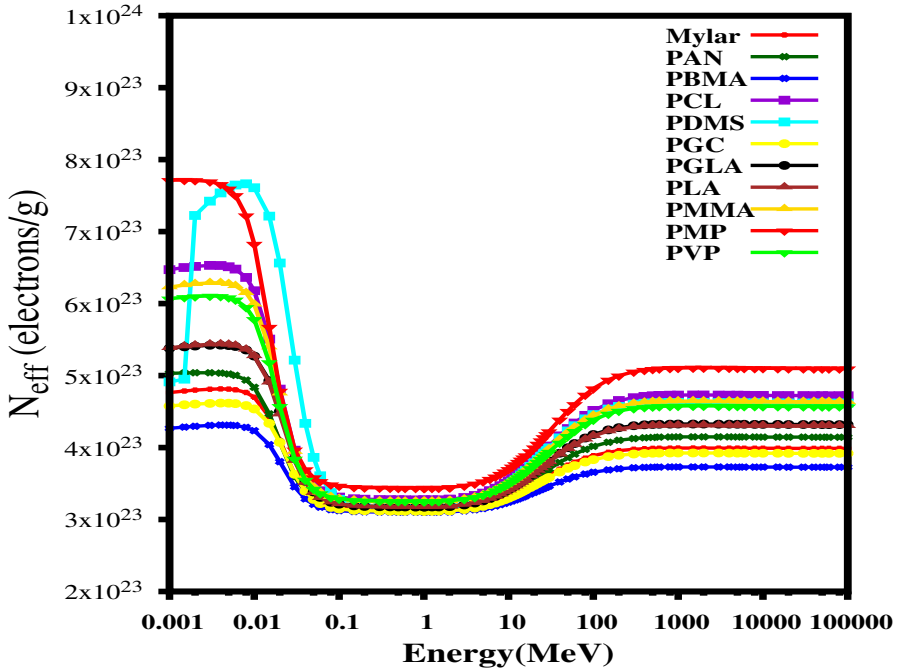

Figure 3.8: Variation of the effective electron density of the selected polymers with photon energy, due to total photon interaction.

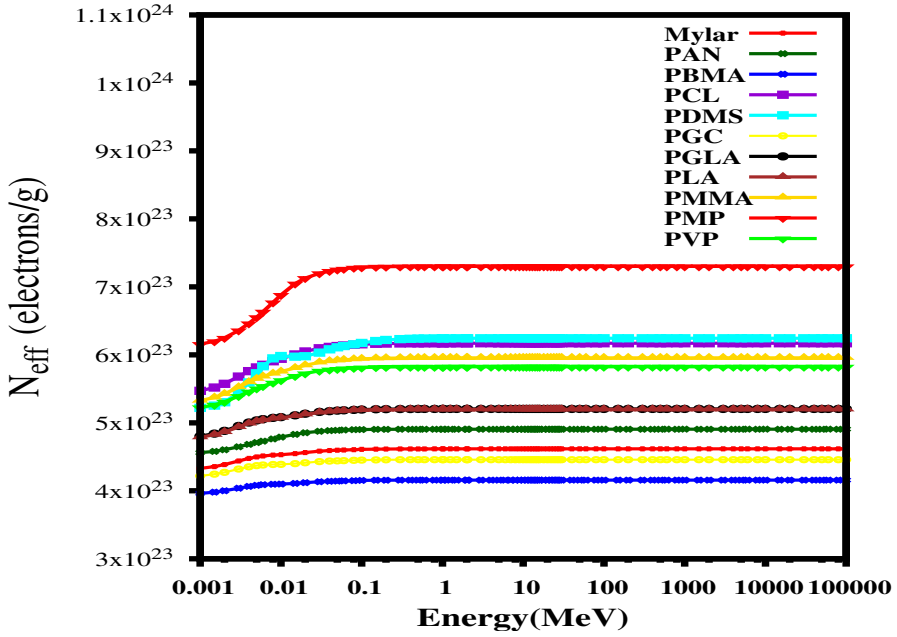

Figure 3.9: Variation of the effective electron density of the selected polymers with photon energy, due to coherent scattering.

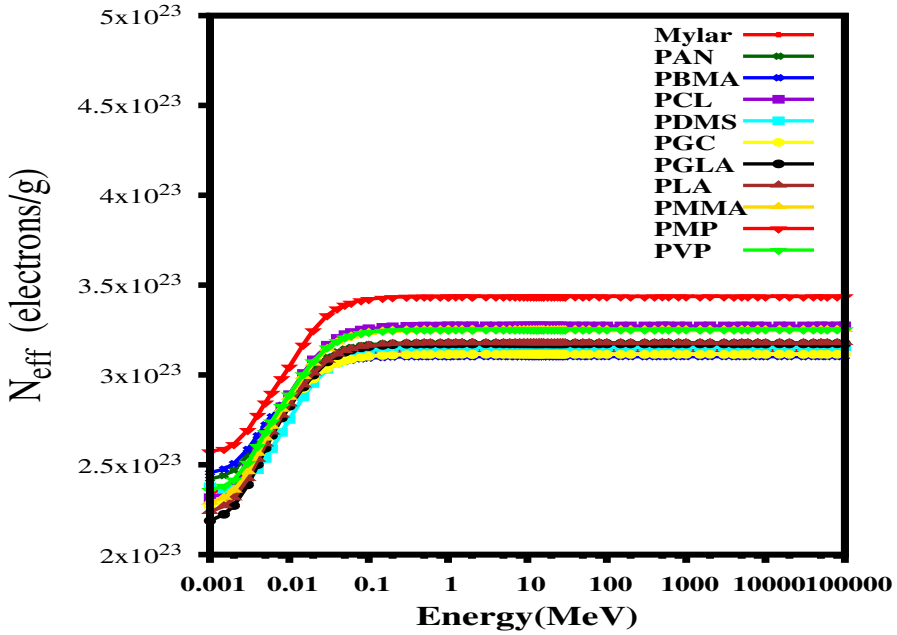

Figure 3.10: Variation of the effective electron density of the selected polymers with photon energy, due to incoherent scattering.

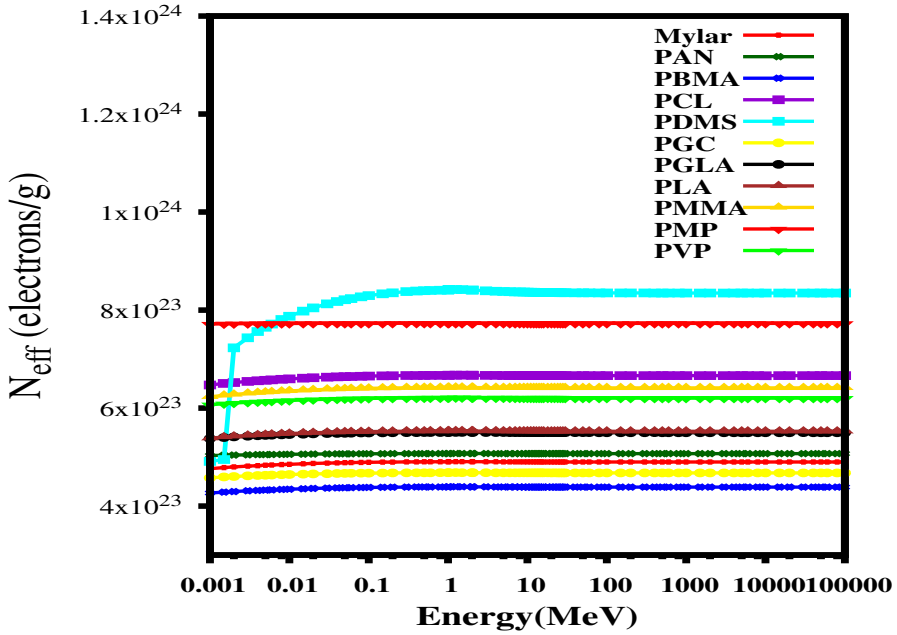

Figure 3.11: Variation of the effective electron density of the selected polymers with photon energy, due to photoelectric absorption.

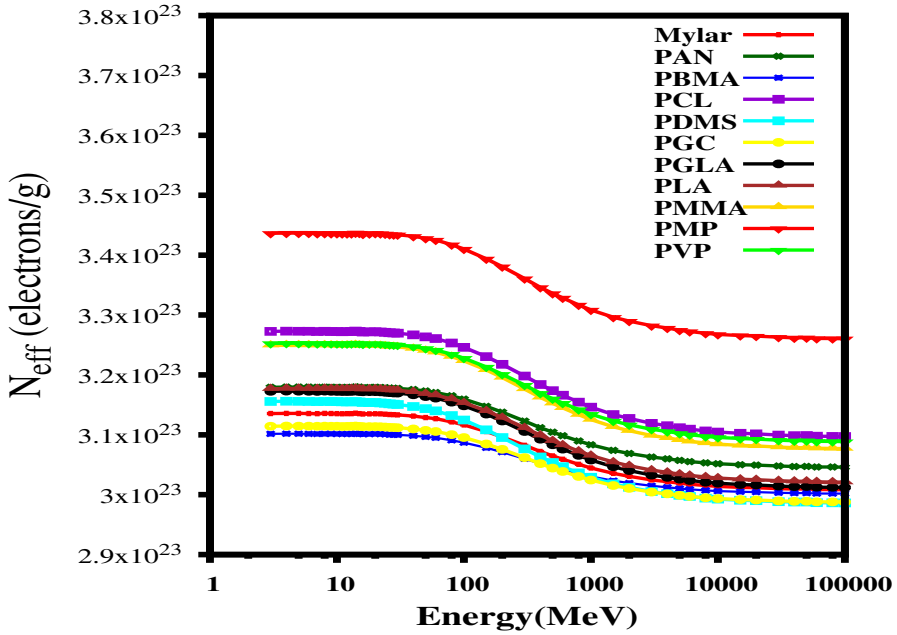

Figure 3.12: Variation of the effective electron density of the selected polymers with photon energy, due to pair production in the field of electrons.

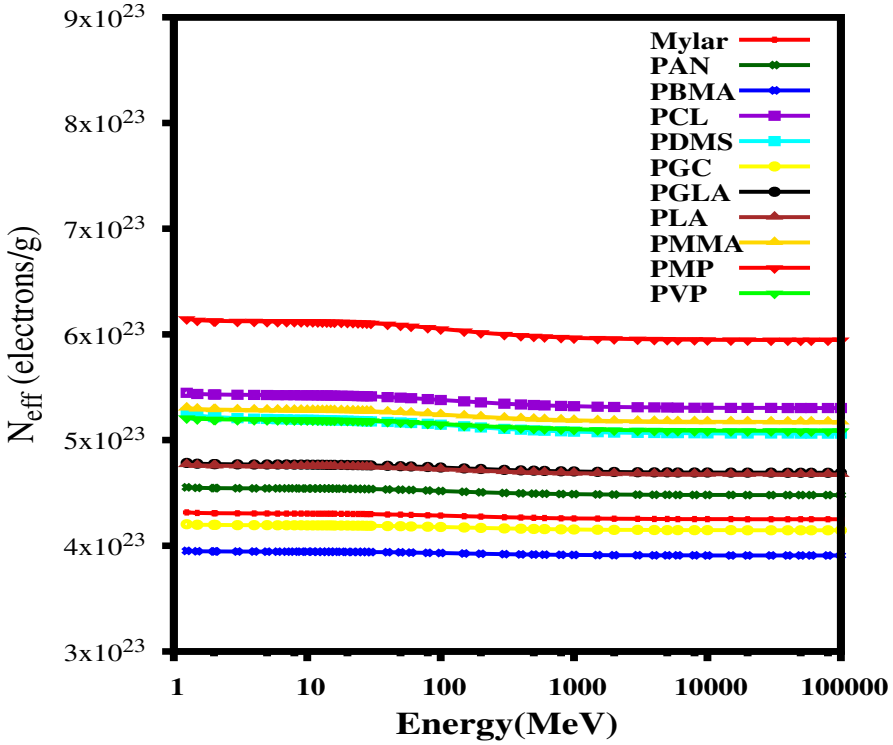

Figure 3.13: Variation of the effective electron density of the selected polymers with photon energy, due to pair production in nuclear field.

3.4.3 Mass energy-absorption coefficient

The mass energy-absorption coefficient is different from mass attenuation coefficient. The mass attenuation coefficient is the probability per unit mass that a gamma ray photon is removed from the incident beam, by taking into account all the interaction processes. But mass energy-absorption coefficient is the measure of average fractional amount of the incident photon energy transferred to the kinetic energy of the charged particles as a result of these interactions (Hubbell, 1982). Figure 3.2 shows the variation of Z_{eff} for total photon attenuation due to all the different photon interaction processes like Phtoelectric absorption, Compton scattering, Pair production etc. But, here, the mass energy-absorption coefficient of the selected polymers were de-

termined for photons in the energy range 1 keV to 20 MeV, by the mixture rule using the data for the constituent elements given by Hubbell and Seltzer (Hubbell & Seltzer, 1995) and are listed in Table 3.3. From these mass energy-absorption coefficients, the effective atomic numbers corresponding to photon energy-absorption in these materials were calculated by using a self-developed python program. The variation of the effective atomic number with the incident photon energy, corresponding to the total energy absorption in the medium, is shown in Figure 3.14.

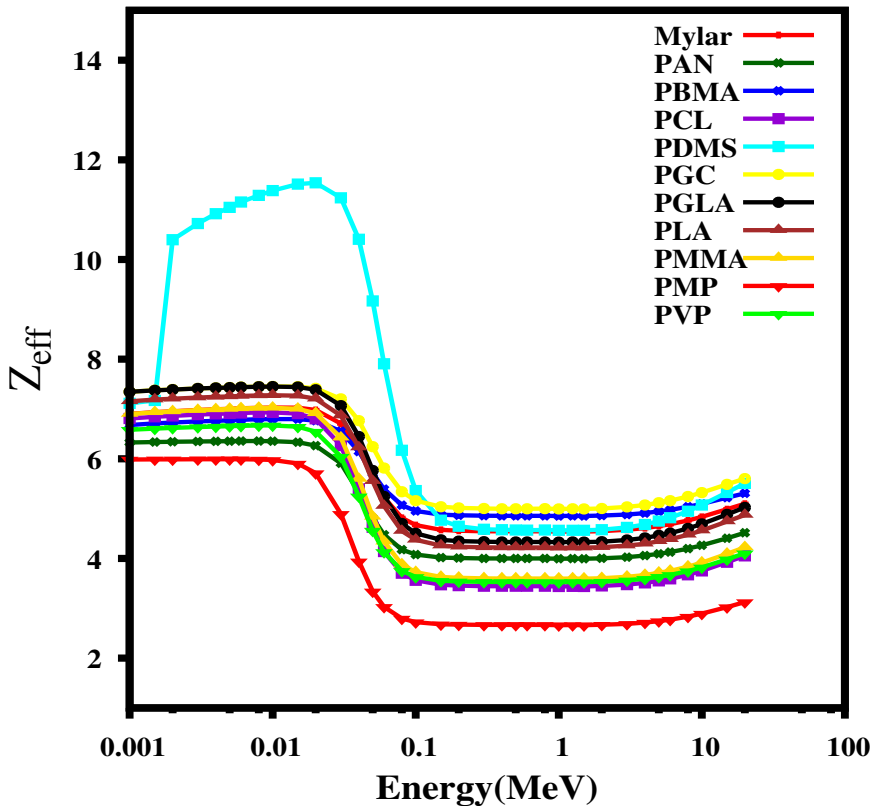

Figure 3.14: Variation of the effective atomic number of the selected polymers with photon energy, due to total energy absorption.

Table 3.3: Mass energy-absorption coefficients of the selected synthetic polymers.

Energy (MeV)	Mass energy- absorption coefficient(cm^2/g)										
	PLA	PCL	PGC	PGLA	MYLAR	PBMA	PMMA	PMP	PAN	PVP	PDMS
0.001	3140	2680	3440	3370	2900	2720	2790	1890	2370	2510	2260
0.002	458	385	507	496	419	387	402	258	330	355	882
0.003	141	117	156	153	128	117	123	76.8	99.1	107	300
0.004	59.60	49.40	66.63	64.90	34.00	49.40	51.80	31.90	41.40	45.10	136.0
0.005	30.30	25.00	33.70	33.00	27.40	25.00	26.30	16.00	20.80	22.80	72.30
0.01	3.510	2.870	3.930	3.850	3.150	2.860	3.030	1.780	2.350	2.600	9.510
0.02	0.3870	0.3160	0.4340	0.4250	0.3460	0.3130	0.3330	0.1940	0.2550	0.2840	1.1500
0.03	0.1110	0.0919	0.1230	0.1210	0.0997	0.0905	0.0964	0.0593	0.0750	0.0832	0.3300
0.04	0.0514	0.0443	0.0562	0.0555	0.0469	0.0433	0.0460	0.0320	0.0374	0.0408	0.1410
0.05	0.0331	0.0299	0.0352	0.0350	0.0308	0.0290	0.0307	0.0244	0.0263	0.0282	0.0771
0.1	0.0235	0.0237	0.0233	0.0236	0.0230	0.0226	0.0237	0.0242	0.0228	0.0234	0.0281
0.2	0.0281	0.0289	0.0276	0.0281	0.0277	0.0274	0.0287	0.0303	0.0281	0.0287	0.0284
0.3	0.0303	0.0312	0.0297	0.0303	0.0299	0.0296	0.0310	0.0328	0.0303	0.0310	0.0302
0.4	0.0311	0.0321	0.0305	0.0311	0.0307	0.0304	0.0318	0.0337	0.0312	0.0319	0.0310
0.5	0.0313	0.0323	0.0307	0.0313	0.0309	0.0306	0.0321	0.0339	0.0314	0.0321	0.0311
1	0.0295	0.0304	0.0289	0.0294	0.0291	0.0288	0.0301	0.0319	0.0295	0.0302	0.0293
2	0.0248	0.0255	0.0243	0.0247	0.0244	0.0242	0.0253	0.0268	0.0248	0.0253	0.0246
3	0.0216	0.0222	0.0213	0.0216	0.0214	0.0211	0.0221	0.0233	0.0216	0.0221	0.0216
4	0.0196	0.0201	0.0193	0.0196	0.0193	0.0191	0.0199	0.0209	0.0195	0.0199	0.0196
5	0.0181	0.0185	0.0179	0.0182	0.0179	0.0177	0.0184	0.0192	0.0180	0.0184	0.0183
6	0.0171	0.0174	0.0169	0.0171	0.0186	0.0166	0.0173	0.0179	0.0169	0.0173	0.0173
8	0.0156	0.0158	0.0155	0.0157	0.0154	0.0152	0.0158	0.0162	0.0154	0.0157	0.0163
10	0.0147	0.0149	0.0147	0.0148	0.0145	0.0143	0.0148	0.0150	0.0144	0.0147	0.0152
15	0.0135	0.0135	0.0135	0.0136	0.0133	0.0131	0.0135	0.0134	0.0131	0.0133	0.0142
20	0.0129	0.0128	0.0130	0.0131	0.0127	0.0125	0.0128	0.0126	0.0124	0.0127	0.0137

3.4.4 Kerma relative to air ($K_{poly,air}$)

The variation of kerma relative to air with photon energy (1 keV to 20 MeV) is shown in Figure 3.15. It shows a sharp decrease with photon energy from 3 keV - 4 keV and then decreases slowly with photon energy up to 40 keV. From 40 keV to 100 keV photon energy, a rapid rise in $K_{poly,air}$ value is observed and beyond that its value approaches unity and becomes independent of the energy up to 10 MeV. This is the case for all the selected polymers, except PDMS. For PDMS it shows a sharp jump due to the silicon K-edge at 1.839 keV. Thereafter, it rises with energy up to 20 keV and subsequently falls to unity at 100 keV. This plot points to the dominance of different partial interaction processes at different energy regions. The present results are similar to the results from the theoretical study of Singh et al. (Singh et al., 2014), who had reported similar type variation for kerma in tissue substitutes. In the lower energy region, photoelectric absorption is the dominant interaction process and its cross section per unit mass of the material is proportional to Z^{3-4} (Attix, 1986). Here, among the selected polymers, PMP contains hydrogen and carbon only. So its cross section per unit mass is low and hence it has a lower value for $K_{poly,air}$ in the lower energy region. In the medium energy region (100 keV to 10 MeV), the Compton scattering is the dominant interaction process and its cross section per unit mass depends on the Z/A value of the elements. For all elements, except hydrogen the Z/A value ranges from 0.4 to 0.5 and so, the Compton cross section per unit mass is independent of Z. But for hydrogen the Z/A value is 1. Here, for all polymers except PMP, the weight fraction of hydrogen is very low and so the Compton cross section per unit mass is almost the same. But, for PMP, the weight fraction of hydrogen is more, so its Compton cross section per unit mass will be higher. As a result, it shows higher value for Ka in the medium energy range. Since the Compton scattering

cross section per unit mass is almost independent of Z, it would be almost the same for all the polymers and air. So, the kerma relative to air approaches unity in Compton dominant region for all the polymers.

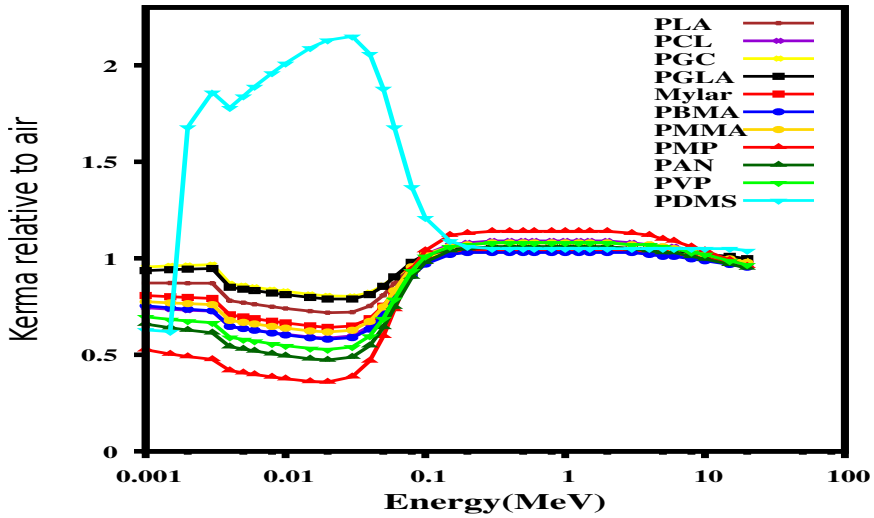

Figure 3.15: Variation of kerma relative to air of the selected synthetic polymers with photon energy.

3.4.5 Comparison of different methods

The effective atomic number of the selected polymers obtained by the direct ($Z_{eff,Direct}$), ratio of cross sections ($Z_{eff,Ratio}$) and logarithmic interpolation ($Z_{eff,LI}$) methods are listed in Table 3.4.

Also, the effective electron density of the same polymers, obtained by direct ($N_{eff,Direct}$), ratio of cross sections ($N_{eff,Ratio}$) and logarithmic interpolation ($N_{eff,LI}$) methods are listed in Table 3.5. Figures 3.16 and 3.17 show the variation of the effective atomic number and the effective electron density of polycaprolactone (PCL) with photon energy obtained by direct and interpolation methods. The mean atomic number and the effective atomic number of the selected polymers, estimated by Murty, XmuDat, and power law methods

for two different values of power (2.94, 3.5) are displayed in Table 3.6. XMuDat (Nowotny, 1998) is a program for calculating photon-interaction cross sections and absorption coefficients of elements, compounds and mixtures in the energy range from 1 keV to 50 MeV. For a given compound, XMuDat also provides a single value for the effective atomic number. Murty and power law methods provide only a single value for the effective atomic number for the entire energy range we have taken, since it is energy independent(Murty, 1965). The effective atomic numbers obtained by the method suggested by Murty are almost equal to the mean atomic number. Also, it is the same as the effective atomic number obtained by direct method in the energy range 100 keV to 10 MeV, the Compton dominant region. The values obtained from XmuDat and power law methods are very close to each other. Again, these values are close to the maximum values obtained by the direct method in the photoelectric dominant region. Hence, the effective atomic number suggested by Murty is valid in Compton dominant region and the effective atomic number obtained from XMuDat and power law methods are valid in the lower energy region where photoelectric absorption is the dominant interaction process.

From Table 3.4, it can be seen that the ratio of cross section method exactly reproduces the value of Z_{eff} as obtained by the direct method, in the entire energy range. The Polynomial interpolation method tallies with the direct method and the ratio of cross section method in the middle energy region, where Compton effect is dominant. However, in the very low (photoelectric) and high energy (pair production) regions, the values obtained by interpolation method show some deviation from the direct method. In the above two regions, the values obtained by the interpolation method are always lower than that obtained from the direct method. This is due to the nonlinear dependence of the photoelectric and pair production cross sections on the atomic number. In

the case of PDMS, due to the K-absorption edge of silicon, a large difference in the data is observed near the absorption edge.

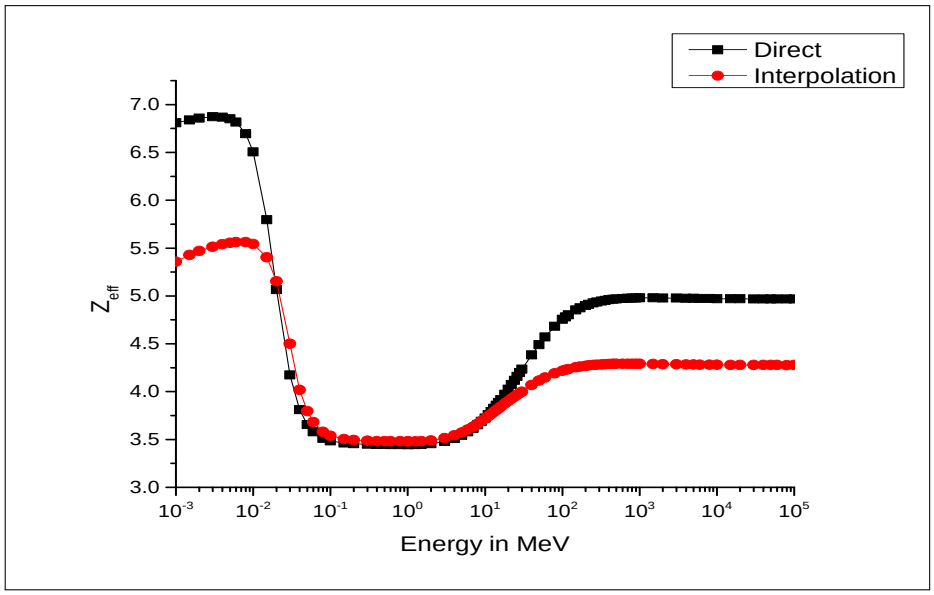

Figure 3.16: Variation of the effective atomic number with photon energy obtained by direct and interpolation methods for polycaprolactone (PCL).

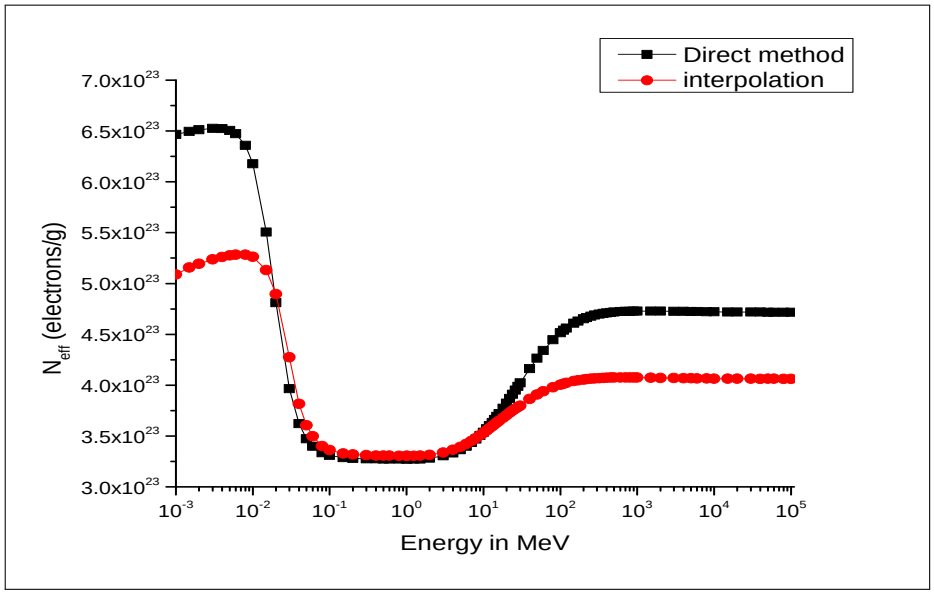

Figure 3.17: Variation of the effective electron density with photon energy obtained by direct and interpolation methods for polycaprolactone (PCL).

Table 3.4: Effective atomic number of the selected polymers by direct ($Z_{eff,Direct}$), ratio of cross sections ($Z_{eff,Ratio}$) and logarithmic interpolation ($Z_{eff,LI}$) methods.

Energy in MeV		$1x10^{-3}$	$1x10^{-2}$	$1x10^{-1}$	$1x10^{0}$	$1x10^{1}$	$1x10^{2}$	$1x10^{3}$	$1x10^{4}$	$1x10^{5}$
PLA	$Z_{eff,Direct}$	7.155	7.006	4.270	4.220	4.529	5.531	5.725	5.719	5.716
	$Z_{eff,Ratio}$	7.154	7.004	4.270	4.220	4.528	5.531	5.725	5.717	5.716
	$Z_{eff,LI}$	5.755	5.915	4.312	4.189	4.513	4.971	5.011	5.000	4.998
PCL	$Z_{eff,Direct}$	6.809	6.502	3.484	3.445	3.722	4.751	4.976	4.971	4.967
	$Z_{eff,Ratio}$	6.807	6.501	3.483	3.444	3.722	4.750	4.976	4.971	4.967
	$Z_{eff,LI}$	5.293	5.450	3.537	3.481	3.717	4.217	4.291	4.281	4.278
PGC	$Z_{eff,Direct}$	7.346	7.283	5.051	5.001	5.293	6.150	6.299	6.294	6.292
	$Z_{eff,Ratio}$	7.345	7.283	5.051	5.001	5.294	6.151	6.299	6.293	6.291
	$Z_{eff,LI}$	6.182	6.445	5.056	5.001	5.154	5.180	5.473	5.464	5.461
PGLA	$Z_{eff,Direct}$	7.344	7.199	4.388	4.334	4.660	5.709	5.908	5.902	5.898
	$Z_{eff,Ratio}$	7.344	7.197	4.388	4.335	4.660	5.710	5.909	5.901	5.898
	$Z_{eff,LI}$	5.872	6.077	4.452	4.360	4.639	5.081	5.116	5.105	5.102
PET	$Z_{eff,Direct}$	6.903	6.812	4.587	4.546	4.810	5.634	5.787	5.782	5.780
	$Z_{eff,Ratio}$	6.903	6.811	4.586	4.545	4.810	5.633	5.786	5.782	5.779
	$Z_{eff,LI}$	5.767	5.900	4.641	4.573	4.790	5.119	5.148	5.140	5.137
PBMA	$Z_{eff,Direct}$	6.802	6.629	4.890	4.857	5.074	5.725	5.841	5.837	5.835
	$Z_{eff,Ratio}$	6.680	6.627	4.888	4.857	5.074	5.722	5.841	5.835	5.834
	$Z_{eff,LI}$	5.778	5.885	4.924	4.869	5.026	5.247	5.274	5.266	5.263
PMMA	$Z_{eff,Direct}$	6.899	6.633	3.642	3.600	3.887	4.923	5.143	5.138	5.134
	$Z_{eff,Ratio}$	6.898	6.632	3.642	3.599	3.887	4.921	5.144	5.137	5.133
	$Z_{eff,LI}$	5.401	5.556	3.694	3.634	3.869	4.384	4.452	4.441	4.438
PMP	$Z_{eff,Direct}$	5.984	5.297	2.689	2.666	2.870	3.738	3.960	3.957	3.953
	$Z_{eff,Ratio}$	5.983	5.296	2.688	2.665	2.869	3.738	3.961	3.957	3.953
	$Z_{eff,LI}$	4.455	4.610	2.734	2.709	2.870	3.335	3.430	3.425	3.422
PAN	$Z_{eff,Direct}$	6.327	6.084	4.030	4.000	4.239	5.052	5.217	5.214	5.211
	$Z_{eff,Ratio}$	6.328	6.083	4.029	3.999	4.239	5.050	5.219	5.212	5.211
	$Z_{eff,LI}$	5.360	5.441	4.055	3.999	4.227	4.631	4.683	4.673	4.671
PVP	$Z_{eff,Direct}$	6.582	6.273	3.565	3.529	3.793	4.756	4.965	4.961	4.957
	$Z_{eff,Ratio}$	6.581	6.272	3.565	3.529	3.794	4.755	4.966	4.960	4.958
	$Z_{eff,LI}$	5.251	5.380	3.617	3.565	3.785	4.257	4.330	4.320	4.317
PDMS	$Z_{eff,Direct}$	7.114	11.023	4.752	4.573	5.034	6.456	6.702	6.693	6.688
	$Z_{eff,Ratio}$	7.114	11.018	4.750	4.573	5.034	6.454	6.703	6.691	6.686
	$Z_{eff,LI}$	5.471	7.841	4.846	4.600	4.970	5.416	5.456	5.447	5.444

Table 3.5: Effective electron density of the selected polymers by direct ($N_{eff,Direct}$), ratio of cross sections ($N_{eff,Ratio}$) and logarithmic interpolation ($N_{eff,LI}$) methods.

Energy in MeV		$1x10^{-3}$	$1x10^{-2}$	$1x10^{-1}$	$1x10^{0}$	$1x10^{1}$	$1x10^{2}$	$1x10^{3}$	$1x10^{4}$	$1x10^{5}$
	($x10^{23}$ electrons/g)									
PLA	$N_{eff,Direct}$	5.385	5.273	3.215	3.178	3.408	4.163	4.308	4.304	4.301
	$N_{eff,Ratio}$	5.384	5.271	3.214	3.177	3.408	4.163	4.308	4.303	4.301
	$N_{eff,LI}$	4.333	4.453	3.246	3.153	3.397	3.742	3.772	3.764	3.763
PCL	$N_{eff,Direct}$	6.471	6.179	3.311	3.273	3.537	4.515	4.729	4.724	4.720
	$N_{eff,Ratio}$	6.469	6.178	3.310	3.273	3.538	4.514	4.729	4.724	4.721
	$N_{eff,LI}$	5.036	5.185	3.365	3.312	3.536	4.012	4.082	4.073	4.070
PGC	$N_{eff,Direct}$	4.576	4.537	3.146	3.115	3.297	3.831	3.924	3.921	3.919
	$N_{eff,Ratio}$	4.575	4.536	3.146	3.115	3.298	3.832	3.924	3.920	3.919
	$N_{eff,LI}$	3.850	4.014	3.149	3.115	3.210	3.226	3.409	3.403	3.401
PGLA	$N_{eff,Direct}$	5.378	5.271	3.213	3.174	3.412	4.180	4.326	4.322	4.319
	$N_{eff,Ratio}$	5.377	5.270	3.213	3.173	3.412	4.181	4.327	4.321	4.319
	$N_{eff,LI}$	4.302	4.452	3.262	3.194	3.399	3.722	3.748	3.740	3.738
PET	$N_{eff,Direct}$	4.763	4.700	3.164	3.136	3.318	3.887	3.992	3.989	3.988
	$N_{eff,Ratio}$	4.762	4.699	3.164	3.136	3.319	3.886	3.992	3.989	3.988
	$N_{eff,LI}$	3.978	4.070	3.201	3.154	3.304	3.531	3.551	3.546	3.544
PBMA	$N_{eff,Direct}$	4.266	4.234	3.123	3.102	3.241	3.656	3.730	3.728	3.727
	$N_{eff,Ratio}$	4.266	4.233	3.122	3.102	3.241	3.655	3.731	3.727	3.726
	$N_{eff,LI}$	3.690	3.758	3.144	3.109	3.210	3.351	3.368	3.363	3.361
PMMA	$N_{eff,Direct}$	6.229	6.633	3.289	3.251	3.510	4.445	4.644	4.640	4.635
	$N_{eff,Ratio}$	6.229	6.632	3.288	3.250	3.510	4.443	4.644	4.639	4.634
	$N_{eff,LI}$	4.877	5.017	3.335	3.281	3.493	3.958	4.020	4.010	4.007
PMP	$N_{eff,Direct}$	7.714	6.828	3.467	3.437	3.699	4.819	5.105	5.101	5.096
	$N_{eff,Ratio}$	7.714	6.828	3.465	3.437	3.699	4.819	5.106	5.101	5.095
	$N_{eff,LI}$	5.745	5.945	3.525	3.493	3.701	4.300	4.423	4.417	4.413
PAN	$N_{eff,Direct}$	5.030	4.837	3.204	3.180	3.370	4.016	4.148	4.146	4.143
	$N_{eff,Ratio}$	5.031	4.836	3.203	3.179	3.370	4.015	4.149	4.144	4.143
	$N_{eff,LI}$	4.264	4.328	3.226	3.181	3.362	3.684	3.725	3.717	3.716
PVP	$N_{eff,Direct}$	6.067	5.782	3.286	3.253	3.496	4.384	4.577	4.573	4.569
	$N_{eff,Ratio}$	6.066	5.782	3.286	3.253	3.497	4.383	4.578	4.573	4.570
	$N_{eff,LI}$	4.842	4.961	3.336	3.288	3.491	3.926	3.993	3.984	3.981
PDMS	$N_{eff,Direct}$	4.912	7.610	3.281	3.157	3.476	4.457	4.627	4.621	4.618
	$N_{eff,Ratio}$	4.911	7.607	3.280	3.157	3.476	4.456	4.628	4.619	4.616
	$N_{eff,LI}$	3.778	5.415	3.347	3.177	3.432	3.740	3.768	3.762	3.760

Table 3.6: Effective atomic number of the selected polymers by different methods (Murty, XmuDat and power law)

Sample Name	<Z>	Murty	XMuDat	Power Law	
				Power:2.94	Power:3.5
PLA	4.22	4.21	6.77	6.82	6.89
PCL	3.44	3.44	6.34	6.35	6.45
PGC	5.00	4.99	7.16	7.10	7.16
PGLA	4.33	4.32	7.08	7.01	7.08
PET(Mylar)	4.55	4.54	6.71	6.64	6.71
PBMA	4.86	4.85	6.54	6.48	6.54
PMMA	3.60	3.49	6.56	6.47	6.56
PMP	2.67	2.66	5.53	5.44	5.53
PAN	4.00	3.99	6.12	6.07	6.12
PVP	3.53	3.52	6.27	6.19	6.27
PDMS	4.57	4.56	9.58	9.18	9.58

3.4.6 Comparison with experimental works

The present computed values of Z_{eff} for Mylar (4.55) and PAN (3.99) by ratio of cross section method are in very good agreement with the experimental values obtained for Mylar (4.54) and PAN (4.0) by Kacal et al. (Kaçal et al., 2019), in the same energy region (81 keV to 1333 keV). This comparative analysis shows the suitability of the present method in estimating the effective atomic number of composite materials.

3.4.7 Comparison with EpiXS

Figures 3.18 and 3.19 show the comparison of the present computed values of the effective atomic numbers and the effective electron densities of the polymer

polymethyl methacrylate (PMMA) with that obtained from EpiXS program, at different photon energies. We have compared the present calculated values of Z_{eff} and N_{eff} of the selected polymers by direct method with the data obtained from EpiXS program, which shows good agreement.

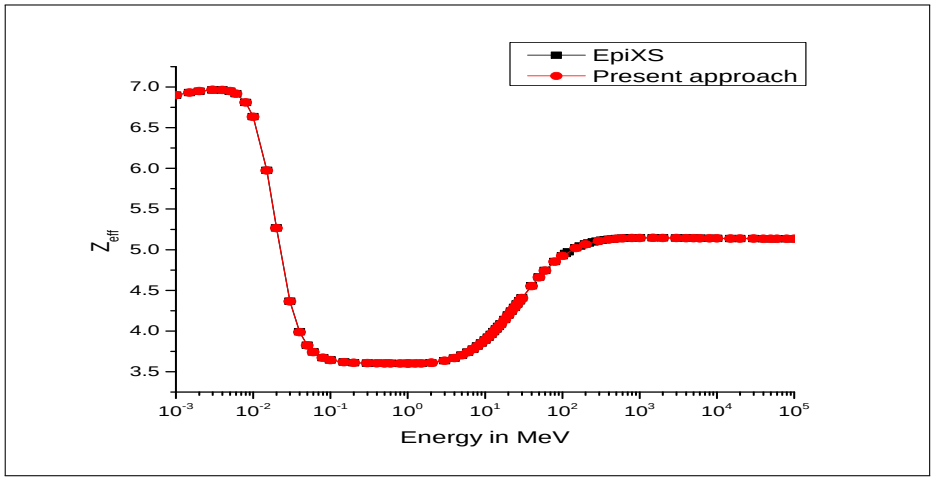

Figure 3.18: Comparison of the present computed values of the effective atomic numbers of polymethyl methacrylate (PMMA) with that obtained from EpiXS program, for different photon energies.

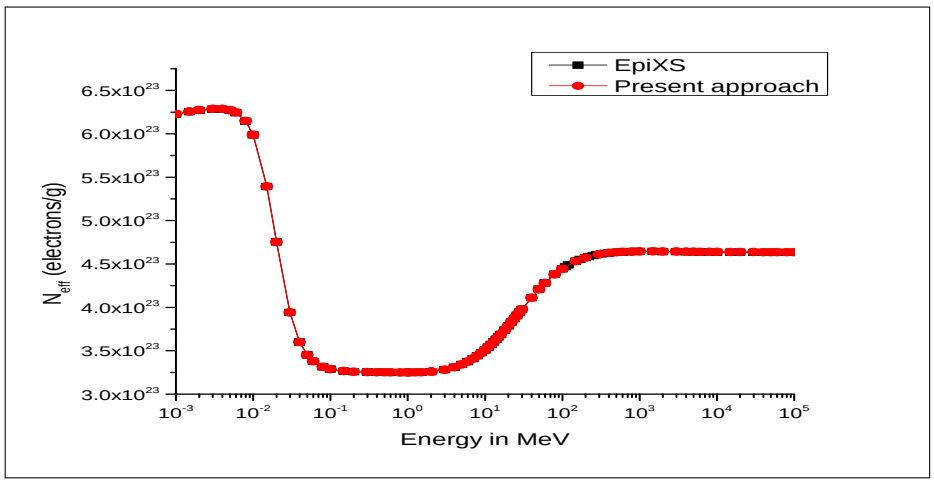

Figure 3.19: Comparison of the present computed values of the effective electron densities of polymethyl methacrylate (PMMA) with that obtained from EpiXS program, for different photon energies.

3.5 Conclusion

The mass attenuation coefficient, the effective atomic number, the effective electron density and kerma depend on photon energies and chemical composition of the polymers. The variation of these radiation interaction parameters with photon energy and chemical composition, can be attributed to the relative dominance of different partial interaction processes at different energy regions. The maximum values of Z_{eff} and N_{eff} have been observed in the low energy range, where photoelectric absorption is predominant and the minimum values of Z_{eff} and N_{eff} have been found in the intermediate energy region, where Compton scattering is dominant. In higher energy region (E>100 MeV), where pair production is predominant, the Z_{eff} has an intermediate value. For PDMS, the Z_{eff} and the N_{eff} have more than one value at 1.839 keV due to the K-absorption edge of silicon. The variation of the effective atomic number and effective electron density with chemical composition is maximum in those polymers which are composed of atoms with atomic numbers spanned over a wide range. Also, the variation of Z_{eff} and N_{eff} with chemical composition of the polymers is maximum below 100 keV due to the relative dominance of photoelectric absorption. Kerma relative to air approaches unity above 100 keV for all these polymers.

Comparison of present estimated values of the Z_{eff} with experimental results shows good agreement. Also, the present computed values of Z_{eff} and N_{eff} by direct method are in good agreement with that obtained from EpiXS program. The direct and ratio of cross section methods give almost the same results in the entire energy range considered. Direct, ratio of cross section and interpolation methods are in good agreement in the middle energy range, where Compton scattering is dominant. The values obtained in logarithmic

interpolation method in photoelectric and pair production dominant regions are always lower than that in the direct and ratio of cross section methods and this deviation is maximum in the low energy region where photoelectric absorption is dominant. The effective atomic numbers obtained by XmuDat and power law methods are almost the same. These values are close to the effective atomic numbers obtained in the photoelectric dominant region by the direct method.

Bibliography

A.Perumallu, A. N. R., & Rao, G. K. 1985, Physica., 132C, 388

Attix, F. H. 1986, Introduction to Radiological Physics and Radiation Dosimetry (Wiley, Newyork)

Berger, M., & Hubbell, J.H.and Seltzer, S. 1998, XCOM: Photon Cross Sections Database — NISTStandard Reference Database 8, Tech. rep.

Bhandal, G. S., & Singh, K. 1993, Applied radiation and isotopes, 44, 929

Cevik, U., Bacaksiz, E., Damla, N., & Çelik, A. 2008, Radiat. Meas., 43, 1437

Chandra Lingam, S., Suresh Babu, K., & Krishna Reddy, D. 1984, Indian Journal of Physics. Part A, 58, 285

El-Kateb, A. H., & Abdul-Hamid, A. S. 1991, Int. J.Rad. Appl.and Instrum. B, 42, 303

Elmahroug, Y., Tellili, B., & Souga, C. 2015, Ann. Nucl. Energy, 75, 268

Gerward, L., Guilbert, N., Jensen, K. B., & Levring, H. 2004, Radiation physics and chemistry, 71, 653

Govinda Nayak, N., Vijaya, M., & Siddappa, K. 2001, Radiat. Phys. Chem., 61, 559

Gowda, S., Krishnaveni, S., & Gowda, R. 2005, Nucl. Instrum. Methods Phys. Res., Sect. B, 239, 361

Gowda, S., Krishnaveni, S., Yashoda, T., Umesh, T. K., & Gowda, R. 2004, Pramana . J. Phys., 63, 529

Harold, E. J., & Cunningham, J. R. 1985, The Physics of Radiology (Charles.C.Thomas Publisher)

Hine, G. 1952, Phys. Rev., 85, 725

Hubbell. 2006, Radiat. Phys. Chem., 75, 614

Hubbell, J. H. 1982, The International Journal of Applied Radiation and Isotopes, 33, 1269

Hubbell, J. H., & Seltzer, S. M. 1995, Tech. rep., National Inst. of Standards and Technology-PL, Gaithersburg, MD

Hubbell, J. H. 2004, Nucl. Instrum. Methods .Phys. Res. B, 213, 1

Jackson, D. F., & Hawkes, D. J. 1981, Phys. Rep., 70, 169

Kaçal, M. R., Akman, F., & Sayyed, M. I. 2019, Nucl. Eng. Technol., 51, 818

Kiran Kumar, T., & Venkata Reddy, K. 1997, Radiat. Phys. Chem., 50, 545

Kucuk, N., Cakir, M., & Isitman, N. A. 2013, Radiat. Prot. Dosim., 153, 127

Kumar, A. 2016, Radiat. Phys. Chem., 127, 48

Kumar, S. P., & Umesh, T. 2011, Pramana, 77, 335

Maitz, M. 2015, Biosurface and Biotribology, 1, 161

Manjunathaguru, V., & Umesh, T. K. 2006, J. Phys. B: At., Mol. Opt. Phys., 39, 3969

Manohara, S., Hanagodimath, S., Thind, K., & Gerward, L. 2010, Appl. Radiat. Isot., 68, 784

Manohara, S. R., & Hanagodimath, S. M. 2007, Nucl. Instrum. Methods .Phys. Res. B, 258, 321

Manohara, S. R., Hanagodimath, S. M., & Gerward, L. 2008a, Phys. Med. Biol., 53, N377

Manohara, S. R., Hanagodimath, S. M., Thind, K. S., & Gerward, L. 2008b, Nucl. Instrum. Methods in Phys. Res.B, 266, 3906

Manohara, S. R and Hanagodimath, S. M and Gerward, L. 2009, Med. Phys., 36, 137

Motz, J. W., Olsen, H. A., & Koch, H. W. 1969, Reviews of Modern Physics, 41, 581

Mudahar, G. S., Singh, M., & Singh, G. 1991, Int. J. Radiat. Appl. Instrum. Part A, 42, 509

Murty, R. C. 1965, Nature, 207, 398

Niranjan, R. S., Rudraswamy, B., & Dhananjaya, N. 2012, Pramana J. Phys, 78, 451

Nowotny, R. 1998, "XMuDat: Photon attenuation data on PC " Tech.Rep. IAEA- NDS- 195, International atomic energy, Vienna, Tech. rep.

Olarinoye, O. 2011, Research Journal of Chemical Sciences

Parthasaradhi, K. 1968, Effective atomic numbers in compounds, Tech. rep., Andhra Univ., Waltair, India

Parthasaradhi, K., Esposito, A., & Pelliccioni, M. 1992, International journal of radiation applications and instrumentation. Part A. Applied radiation and isotopes, 43, 1481

Parthasaradhi, K., Rao, B. M., & Prasad, S. G. 1989, Medical physics, 16, 653

Prasad, S. G., Parthasaradhi, K., & Bloomer, W. 1997, Nuclear science and engineering, 126, 224

Rao, B. T., Raju, M., Narasimham, K., Parthasaradhi, K., & Rao, B. M. 1985, Medical physics, 12, 745

Revathy, J. S., Anooja, J., Krishnaveni, R. B., Gangadathan, M. P., & Varier, K. M. 2018, Pramana. J. Phys, 90, 1

Shantappa, A., & Hanagodimath, S. 2014, Indian J. Pure Appl. Phys, 88, 35

Singh, T., Kaur, P., & Singh, P. S. 2007, Journal of Radiological Protection, 27, 79

Singh, V., & Badiger, N. 2013, Nuclear Technology and Radiation Protection, 28, 137

Singh, V. P., & Badiger, N. M. 2016, Indian J. Pure Appl. Phys., 54, 333

Singh, V. P., Badiger, N. M., & Kucuk, N. 2014, Radioprotection., 49, 115

Weber, J., & Van den Berge, D. 1969, The British journal of radiology, 42, 378

White. 1978, Medical physics, 5, 467

White, D. R. 1977, Physics in Medicine & Biology, 22, 889

White, D. R. 1978, Radiat. Res., 76, 23

Chapter 4

Studies on gamma ray interaction parameters of some chemotherapy drugs, in the energy range 1 keV-100 GeV.

4.1 Introduction

In general, to treat cancer there are multimodalities, which are either sequential or concurrent. The concurrent approach of following chemotherapy and radiotherapy is known as concomitant chemoradiotherapy (CRT) or simply chemoradiotherapy (Adelstein, 2007). The key point here is the potential for synergism between the two treatment modalities - chemotherapeutic radiosensitisation. Radio-sensitation in general means the use of a drug that makes tumour cells more sensitive to radiation therapy. Even though, there are several mechanisms for radio-sensitation, chemotherapy is the most common one. It helps to reduce long-term morbidity of cancer therapy by reducing the need for radical surgery and by allowing for the use of lower radiotherapy doses

(Vokes & Weichselbaum, 1990). It is found that this procedure, in patients with locally advanced solid tumors help to overcome the radioresistance, which is the major reason for local treatment failure. It also helps to eradicate distant micrometastasis which is also a reason for systematic treatment failure.

Even though, there are different processes taking place in the cancer tissues and normal tissues during concurrent chemoradiotherapy, one of the important processes relevant here is the increased sensitivity within the radiation field as a result of the interaction of the chemotherapy drugs with radiation (Seiwert et al., 2007). Under such a situation the drug is called a sensitiser, enhancer or potentiator of the radiation. If there is no interaction or a negative interaction between the drug and the radiation, it is called protection. If there is positive sensitising effect the interaction is said to be supraadditive (synergistic).

The cancer treatment involves the tissue or cells in the organ which is affected and the medicine or drug which is administered. In addition to these, in concurrent chemotherapy, the radiation also plays a key role. So, a complete investigation of the processes involve the determination of the photon interaction parameters of the body organs and drugs. Shivaramu in 2002 carried out an extensive theoretical study of the photon interaction parameters of some selected human tissues by direct method (Shivaramu, 2002).

Many reports on the investigation of the photon interaction parameters of the medicines can be found in literature. Ferdi Akman and Mustafa Recep Kacal (Akman & Kaçal, 2018) carried out such a study on some of the selected chemotherapy drugs . We have in the present study selected some chemotherapy drugs which are administered concurrently with radiation therapy which are not subjected to the photon interaction studies so far. Eventhough, the energy range of radiotherapy is 100 keV to 18 MeV, due to scientific inter-

est and also, to study the variation of photon interaction parameters of these drugs with energy, we have carried out an extensive study in the wide range of energy from 1 keV to 100 GeV.

4.2 Materials and methodology

The purpose of chemoradiotherapy is to improve the efficacy of the treatment. The ionising radiation (photon) at a particular energy is delivered for a fixed duration so as to give a specific dose to the targeted tissue. We carry out the study for a range of photon energies including the one to which the patients are usually exposed to. We have selected five chemotherapy medicines and subjected them to the theoretical study of finding the photon interaction parameters. The molecular formula and molar masses of the selected samples are given in Table 4.1 and the elemental composition of these drugs are displayed in Table 4.2. All these samples are important in chemoradiotherapy.

Table 4.1: Molecular formula and molar masses of the chemotherapy drugs studied in the present work.

Sl. No	Sample	Molecular formula	Molecular mass
1	Hydroxyurea	$CH_4N_2O_2$	76.06
2	Trifluridine	$C_{10}H_{11}F_3N_2O_5$	296.2
3	Temozolomide	$C_6H_6N_6O_2$	194.15
4	Mitomycin C	$C_{15}H_{18}N_4O_5$	334.33
5	Trabectedin	$C_{39}H_{43}N_3O_{11}$ S	761.8

Table 4.2: Elemental composition of the selected chemotherapy drugs.

Sample	Weight fraction					
	H	C	N	O	F	S
Hydroxyurea	0.0530	0.1579	0.3683	0.4207		
Trifluridine	0.0374	0.4055	0.0946	0.2701	0.1924	
Temozolomide	0.0311	0.3712	0.4329	0.1648		
Mitomycin C	0.0543	0.5389	0.1676	0.2393		
Trabectedin	0.0568	0.6148	0.0551	0.2310		0.0421

In an earlier work, Matsuoka et al. (Matsuoka et al., 2017) studied the effects of chemoradiation treatment using trifluridine in human colorectal cancer cells in vitro. It is reported that combination chemoradiotherapy is very effective in patients with colorectal cancer which are insensitive to radiation treatment alone. No study has been so far reported on the determination of photon interaction parameters of this drug Trifluridine. Hence we have included this in our investigation.

Combined treatment with radiotherapy and adjuvant chemotherapy using temozolomide was found to be effective and offers more survival rate (Kim et al., 2017). Hence, we have selected temozolomide in our systematic study.

Another drug that we have subjected to our study is mitomycin C. In the study carried out by Marshal Flam et al. (Flam et al., 1996), it was established that the use of mitomycin C in chemoradiotherapy for anal canal cancer is more effective than the single mode of treatment. Also, mitomycin is a bioreductive alkylating agent which has the ability to increase the sensitivity of radiation

(Adelstein, 2007). Hydroxyurea is another chemotherapy drug administered to patients having cancer along with radiation therapy (Vokes et al., 2003; Haraf et al., 1992). In this and similar studies the positive role of hydroxyurea in increasing the effectiveness of radiation therapy is well established.

It is found that concurrent treatment of chemotherapy by using trabectedin and radiotherapy is very effective in controlling advanced soft tissue Sarcomas (Martin-Broto et al., 2020; Gronchi et al., 2019). Hence we have selected this drug and carried out the estimation of photon interaction parameters. It is beneficial to calculate the photon interaction parameters to determine the energy accumulation and penetration in tissues due to the interaction of cancer drugs with radiation. Chemotherapy drugs, in general help to make radiation act better by making cancer cells more sensitive to radiations. Therefore, it is reasonable to examine the interaction of chemotherapy drugs with radiations (Yorgun & Kavaz, 2019). So, the results obtained here, may give new insights into radiation treatment.

In the present study, we have used the EpiXS program for estimating the linear attenuation coefficient, mass attenuation coefficient, effective atomic number and the effective electron density of the selected samples. Here, the direct method is used to extract the effective atomic number and the effective electron density of the selected samples by using the data from EPICS-2017 data library of ENDF/B-VIII.

4.3 Results and discussion

Figures 4.1 and 4.2 show the variation of the linear attenuation coefficient and mass attenuation coefficient of the selected chemotherapy drugs with photon energy, due to total photon interaction. As in the case of polymers, here also

the linear attenuation coefficient and the mass attenuation coefficient of the selected drugs decrease rapidly with energy up to 50 keV and in the middle energy region it decreases linearly with energy. In the higher energy region, it increases slowly and remains constant. This can be explained on the basis of partial interaction processes dominant at different energy regions and on their cross section dependence on energy and on the atomic numbers of the constituent elements of the interacting medium.

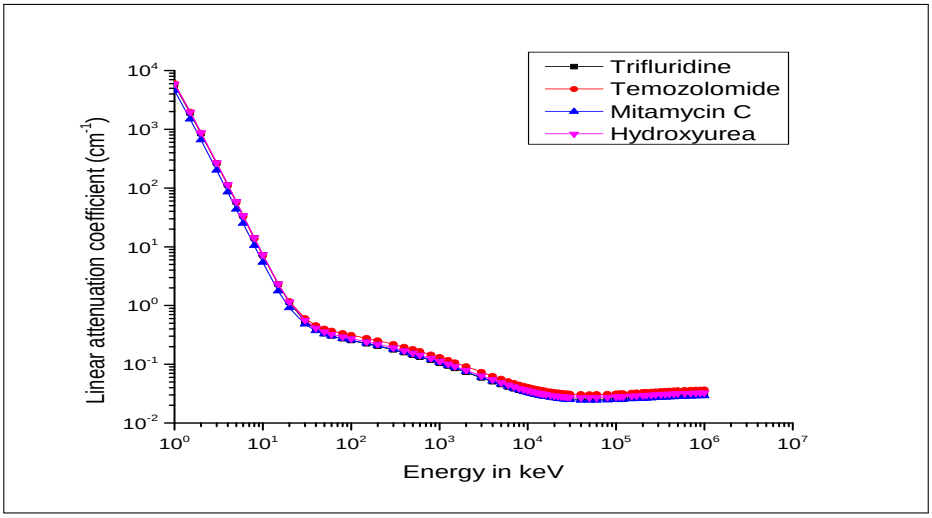

Figure 4.1: Variation of the linear attenuation coefficient of the selected chemotherapy drugs with photon energy, due to total photon interaction.

The Half-Value Layer (HVL) is the thickness of the absorber which reduces the intensity of photon beam to half of its original value. So, it is inversely related to the linear attenuation coefficient. The variation of HVL of the selected drugs with photon energy are displayed in Figure 4.3. It increases rapidly up to 100 keV; then increases comparatively slowly up to 50 MeV and thereafter it remains constant. For a given energy, the HVL is maximum for mitamycin and minimum for temozolomide. So, temozolomide shows the maximum and mitamycin shows the minimum gamma ray absorption properties.

Figures 4.4 and 4.5 show the variation of the effective atomic number and the effective electron densities of the selected chemotherapy drugs. Here, we have three energy regions.

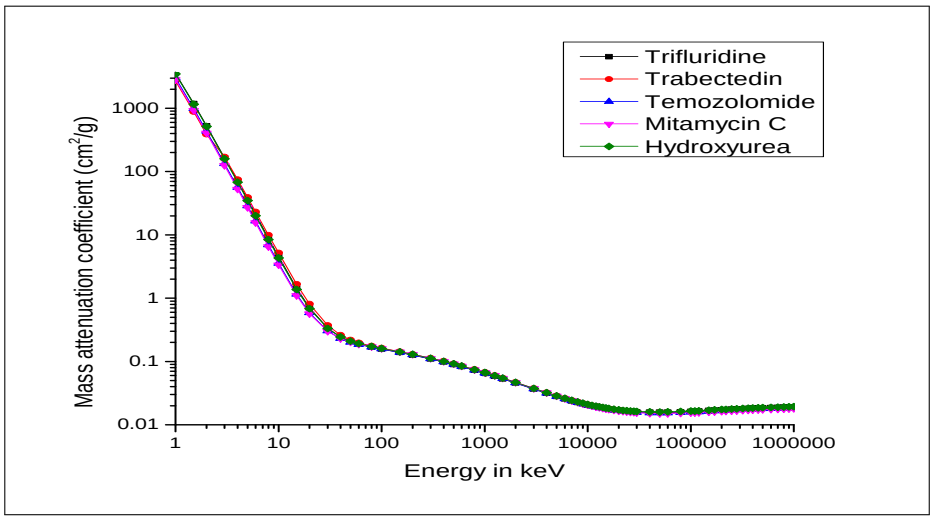

Figure 4.2: Variation of the mass attenuation coefficient of the selected chemotherapy drugs with photon energy, due to total photon interaction.

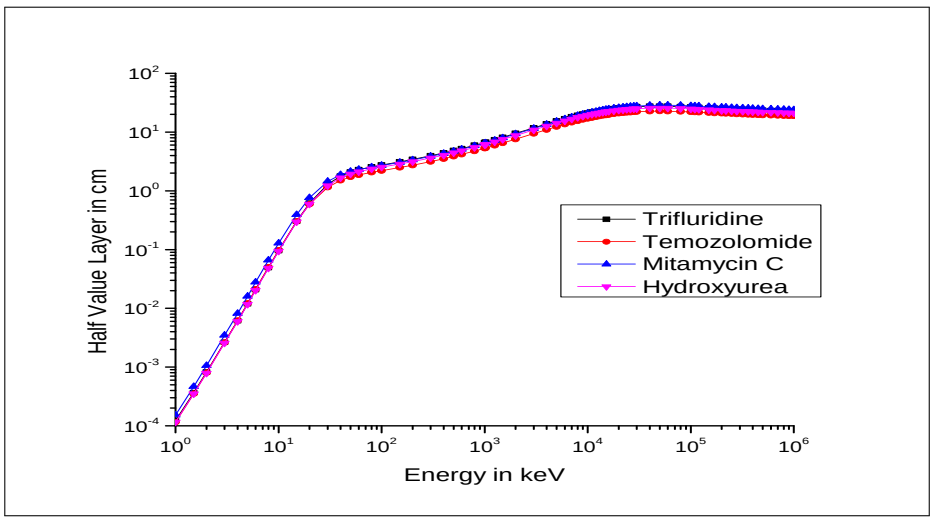

Figure 4.3: Variation of the Half -Value layer (HVL) of the selected chemotherapy drugs with photon energy, due to total photon interaction.

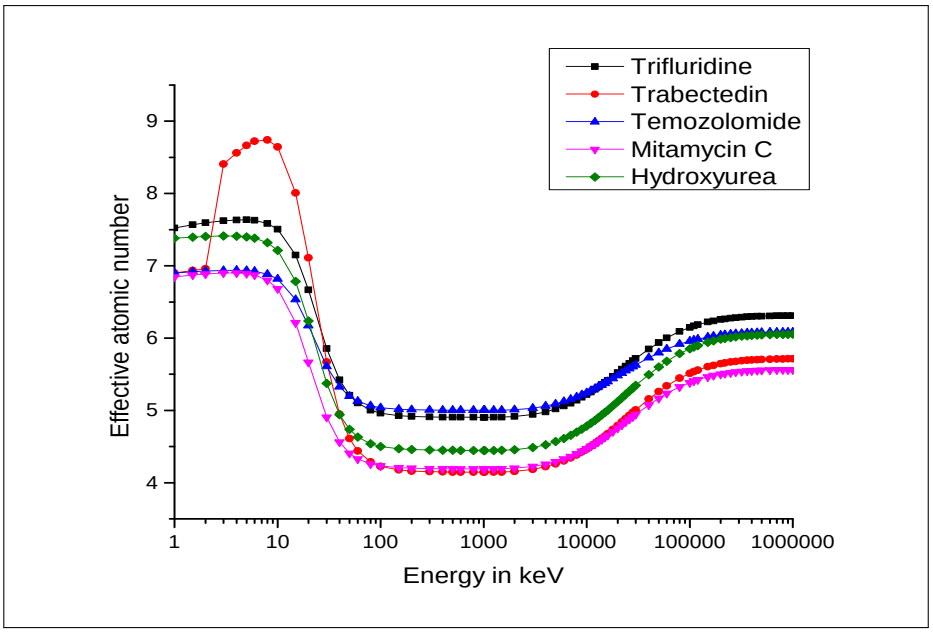

Figure 4.4: Variation of the effective atomic number of the selected chemotherapy drugs with photon energy, due to total photon interaction.

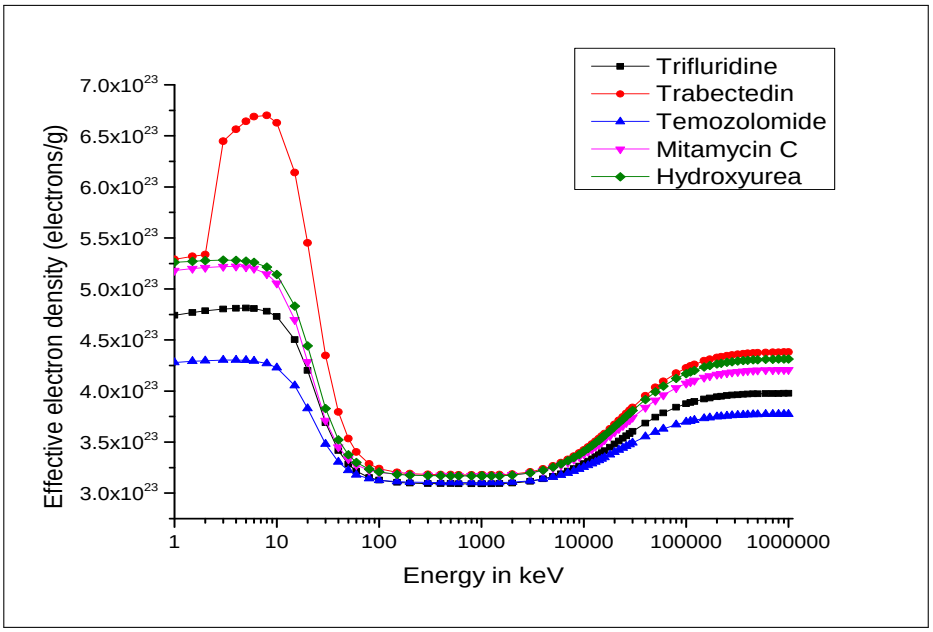

Figure 4.5: Variation of the effective electron density of the selected chemotherapy drugs with photon energy, due to total photon interaction.

In the lower energy region (0 to 10 keV), the photoelectric absorption is the dominant interaction process. In this region, trabectedin has the maximum value of Z_{eff} and mitamycin C and temozolomide have the minimum value of Z_{eff} . The effective atomic number of trabectedin shows a sharp jump at 2.472 keV due to the K-absorption edge of sulphur. In the medium energy range (100 keV to 10 MeV), where Compton scattering is dominant, temozolomide has the maximum and trabectedin and mitamycin C have the minimum values for the effective atomic number. In the higher energy region, trifluridine shows the maximum and mitamycin C shows the minimum values for the Z_{eff}. Since N_{eff} is directly related to the Z_{eff}, its variation with energy can be explained in the same way as that of Z_{eff}. N_{eff} and Z_{eff} are related by the expression $N_{eff} = \frac{N_o Z_{eff}}{<A>}$, where N_o is the Avogadro's constant and $< A >$ is the mean mass number of the drug. For each selected drug, the $< A >$ is a constant for the entire energy range. So, N_{eff} and Z_{eff} are linearly related. Hence, for a selected drug, the variation of N_{eff} with energy can be explained in the same way as that of the Z_{eff}. In Figure 4.4 and Figure 4.5 the scaling of Y-axis are different. The study shows that the radiation response characteristics of the selected chemotherapy drugs varies at different energies.

4.4 Conclusion

In concomitant or concurrent radio therapy, which is usually used to treat many cancer cases at later stages, the effect of interaction of photons with drug material is quite evident. Even though the interaction parameters of different chemotherapy drugs with photons are available, the estimation of these parameters for the drugs selected in the present study is a new investigation. It is also to be noted that these drugs are usually administered as part of the

combined chemo-and radiotherapy.

In the present study, temozolomide shows the maximum and mitamycin shows the minimum gamma ray absorption properties. For studies on treatments using electromagnetic radiation, information is required about the radiation interaction parameters like Z_{eff} and N_{eff} of substances that interact with radiation. These informations are also important in medical imaging and radiation dosimetry (Jackson & Hawkes, 1981; Vijayakumar et al., 2001). So, the estimated parameters in the present study could be useful in chemoradiotherapy (Tuğrul, 2020; Yorgun & Kavaz, 2019).

Bibliography

Adelstein, D. J. 2007, Squamous cell head and neck cancer: recent clinical progress and prospects for the future (Springer)

Akman, F., & Kaçal, M. R. 2018, Journal of Radiology and Oncology, 2, 047

Flam, M., John, M., Pajak, T. F., et al. 1996, Journal of Clinical Oncology, 14, 2527

Gronchi, A., Hindi, N., Cruz, J., et al. 2019, EClinicalMedicine, 9, 35

Haraf, D. J., Vokes, E. E., Weichselbaum, R. R., & Panje, W. R. 1992, The Laryngoscope, 102, 630

Jackson, D. F., & Hawkes, D. J. 1981, Phys. Rep., 70, 169

Kim, B. S., Seol, H. J., Nam, D.-H., et al. 2017, Cancer Research and Treatment: Official Journal of Korean Cancer Association, 49, 193

Martin-Broto, J., Hindi, N., Lopez-Pousa, A., et al. 2020, JAMA oncology, 6, 535

Matsuoka, K., Kobunai, T., Nukatsuka, M., & Takechi, T. 2017, Biochemical and biophysical research communications, 494, 249

Seiwert, T. Y., Salama, J. K., & Vokes, E. E. 2007, Nature clinical practice Oncology, 4, 86

Shivaramu, H. 2002, Med Dosim, 27, 1

Tuğrul, T. 2020, Journal of Radiation Research and Applied Sciences, 13, 758

Vijayakumar, R., Rajasekaran, L., Ramamurthy, N., et al. 2001, Radiation Physics and Chemistry, 62, 371

Vokes, E. E., & Weichselbaum, R. R. 1990, Journal of Clinical Oncology, 8, 911

Vokes, E. E., Stenson, K., Rosen, F. R., et al. 2003, Journal of Clinical Oncology, 21, 320

Yorgun, N. Y., & Kavaz, E. 2019, Results in Physics, 13, 102150

Chapter 5

Coherent scattering cross sections of some rare earth compounds at small angles below 10^o

5.1 Introduction

Accurate values of the coherent scattering cross sections of photons by materials are required in diverse fields such as radiation transport, attenuation, energy deposition, reactor shielding, industrial radiography, crystallography, plasma physics, astrophysics, medical diagnosis and imaging etc. (Kuruchu et al., 1998). It is also used extensively to obtain information on the structural properties of materials and macromolecules (Roy et al., 1999; Donativi et al., 2007). In the energy dispersive X-ray fluorescence technique using the fundamental parameter approach, the knowledge of both coherent and incoherent scattering cross sections are utilized to characterize the matrix of unknown samples (Simsek & Ertugrul, 2004). Fundamental parameter approach

is a first principles calculation method of chemical element concentration from measured X-ray fluorescence spectra using the fundamental parameters such as X-ray absorption coefficients, fluorescence yields, jump ratios, branching ratios, and the incident spectrum from the X-ray tube (Kawai et al., 2006). In condensed matter physics as well, coherent and incoherent scattering play a key role in the understanding of the excited states of many important systems (Singh, M. P and Sharma, Amandeep and Singh, Bhajan and Sandhu, B .S, 2014). Coherent scattering is one of the major interaction processes of photons having energy below 1 MeV. Delbruck scattering, nuclear resonance scattering, Thomson scattering and Rayleigh scattering are the main processes which contribute to coherent scattering. Out of these, only Rayleigh scattering from bound electrons is the sole component of coherent scattering at low photon energies (Nayak et al., 1993; K Muraleedhara Varier, 2009). In Rayleigh scattering, the incident photons are scattered from bound electrons and in this process, the atoms of the scatterer are neither excited nor ionised. The scattered photons from different parts of the atomic clouds of electrons combine in phase to give the coherent scattering. The process mainly occurs for absorbers with large atomic numbers, where the electron binding energies influence the Compton effect (Kissel et al., 1980; Kissel, 2000).

Theoretically, mainly two methods have been developed for calculating the Rayleigh scattering cross sections: numerical partial wave calculation using second order S-matrix and form factor formalism (FF). In the form factor formalism, an extended charge distribution is considered instead of a classical point charge as assumed by Thomson (Chatterjee, B K and Roy, S S, 1998). Here, in FF, two approaches are there, relativistic and non-relativistic, based on the ground state wave function used to derive the charge distribution. In 1936, Franz (Franz, 1936), suggested an electron binding energy correction to

FF and the resulting method is known as the Modified Form Factor (MFF) approach. Hubbell (Hubbell et al., 1975) has reported atomic form factors and incoherent scattering functions for elements with Z from 1 to 100. Here, the data values are obtained by following the non-relativistic form factor approach, with Hartree-Fock model for the charge distribution within the atom. Hubbell and Overbo (Hubbell & Overbo, 1979) had reported relativistic Hartree-Fock atomic form factors F(x,Z), for all the elements with Z from 1 to 100. Kahane (Kahane, 1998) had reported relativistic Dirac Hartree-Fock photon incoherent scattering functions for elements with Z from 1 to 110, using the MFF approach. Chatterjee and Roy (Chatterjee & Roy, 1998) had reported S-matrix differential elastic cross sections for 14 photon energies in the range 50 keV to 1500 keV for 55 different scattering angles. Evaluated Nuclear Reaction Database (ENDF) store nuclear data from major evaluated libraries. The new ENDF/B-VIII.0 library (Brown et al., 2018), released in 2018, fully incorporates the new IAEA standard data and results from across the US and the international nuclear science community, over the last six years. The values of the atomic cross sections included in this library have been modified in recent updates of the nuclear data files (Midhun et al., 2019). Here, in the present study, the newly recommended EPICS-2017 data, adapted in ENDF/B-VIII.0, have been used for the theoretical calculations of angle integrated coherent and incoherent scattering cross sections. In EPICS-2017, non-relativistic form factor data (coherent) and non-relativistic incoherent scattering functions of Hubbell (Hubbell et al., 1975) are included.

Many experimental investigations to determine the coherent scattering cross sections by different methods have been reported in literature (Basavaraju et al., 1994; Shahi et al., 1997; Bradley et al., 1999; Simsek & Ertugrul, 2004; Kane, 2005; Aysun Böke, 2011; Singh et al., 2012; Latha et al., 2012; Baek

et al., 2012, 2014; Aldhuhaibat et al., 2020; Akkuş, 2020). Icelli and Erzeneoglu (İçelli & Erzeneoğlu, 2002) have measured the ratio of differential scattering cross sections of coherent to Compton for 59.54 keV photons at 55^o and 115^o for Fe, Ni, Cu, Zn, Zr, Nb, Mo, Ag, Sn, Ta, Au and Pb targets, using Ge(Li) detector. They reported that the measured cross section ratio increases with increase in atomic number and are in good agreement with non-relativistic and relativistic form factor theories. Singh et al. (Singh et al., 2013) reported the coherent to incoherent scattering cross section ratio of elements in the range $6 \leq Z \leq 82$, for 145 keV incident gamma photons at scattering angles of 50^o, 70^o and 90^o. More recently, Akkuş et al. (Akkuş et al., 2019) determined the variation of coherent to Compton scattering differential cross section ratios of some lanthanides at 59.54 keV. However, experimental studies are scarce for small angles below 10^o and at low momentum transfer region, due to the difficulty in resolving the coherent scattered peak from the main peak, even by using high resolution detectors. Most of the scattering studies at small angles were done by shadow cone method (Roy et al., 1975; Kane et al., 1978; Ramanathan et al., 1979). In this method, the absolute source strength and other geometrical factors have to be measured, in addition to the scattered photon intensity. To overcome this difficulty, a new method had been suggested by Puttaswamy et al. (Puttaswamy et al., 1984), using a simple geometrical setup, earlier used for gamma ray transmission studies. This method requires only the measurement of pure transmitted beam intensity in perfect narrow beam geometry setup and with small angle scattering contributions (Vinaykumar & Umesh, 2014a,b). Based on a subsequent study, Vinaykumar and Umesh (Vinaykumar, L and Umesh, T K, 2016) have reported the angle integrated scattering cross section of 59.54 keV photons by elemental samples having atomic number in the region $13 \leq Z \leq 82$, employing this technique. But, so

far no such studies are reported for rare earth oxides in the low momentum transfer region (0-10^o). In the present study, we have determined the angle integrated total (coherent+ incoherent) scattering cross sections of oxides of rare earth elements in the lathanide series, mainly $CeO_2, Dy_2O_3, Gd_2O_3, Nd_2O_3$ and Yb_2O_3 for 59.54 keV gamma rays in the angular ranges of $0-4^o, 0-6^o, 0-8^o$ and $0-10^o$. From the total scattering cross sections, the corresponding angle integrated incoherent scattering cross sections obtained from ENDF library (based on the non-relativistic Hartree-Fock form factor method) is subtracted to obtain the angle integrated coherent scattering cross sections. The obtained angle integrated coherent scattering cross sections were compared with that determined from ENDF data. The effective atomic numbers of the selected rare earth oxides were extracted by applying the ratio of cross section method (Thulasi et al., 2021a). The variation of the angle integrated coherent scattering cross section with the effective atomic number (Hine, 1952) of the selected compounds have been studied.

Oxides of lanthanides are extensively used for many applications in scientific, technological, medical, commercial and industrial fields (Niranjan et al., 2012). Cerium oxide is used in automobile exhaust catalysis as oxygen storage material. In electronic appliances, cerium dioxide replaces silicon dioxide, because of its ability to absorb and release oxygen under oxidizing and reducing conditions. Dysprosium oxide is used in cermets as nuclear reaction control rods. Gadolinium oxide is used in making metal oxide semiconductor field effect transistors. It is also used in garnets having microwave applications, compact discs, computer memory, nuclear marine propulsion systems as a burnable poison, an emergency shut-down measure in some nuclear reactors and as intravenous radiocontrast agents to enhance images in medical magnetic resonance imaging and in positron emission tomography (Singh, M. P and

Sharma, Amandeep and Singh, Bhajan and Sandhu, B .S, 2014). Neodymium oxide is used in ceramic capacitors, colour TV tubes, colouring glasses and in vacuum deposition. Ytterbium oxide is used in the manufacture of permanent magnet materials, glass, ceramic colouring agents and laser materials. In general, oxides of lanthanides are considered as better shielding materials to the exposure of gamma radiation. In this context, the studies on the interaction parameters of these compounds in the gamma radiation environment is appropriate.

5.2 Theoretical aspects

When perfect narrow beam geometry is ensured, no scattered radiations are assumed to fall on the detector and the transmitted intensity I_1 is given by Beer-Lambert law as,

$$I_1 = I_0 e^{-\mu x} \tag{5.1}$$

where I_o is the incident beam intensity, μ is the linear attenuation coefficient, and x is the thickness of the absorber.

Now, if we allow some scattered radiations also to fall on the detector, it will reduce the value of the mass attenuation coefficient of the scatterer. Let I_2 be the intensity of transmitted plus scattered radiations, within a cone of forward acceptance angle θ^0. Then, $\Delta\mu$, the corresponding reduction in mass attenuation coefficient, can be expressed by the relation,

$$I_2 = I_0 e^{-(\mu-\Delta\mu)x} \tag{5.2}$$

From the above two equations, $\Delta\mu$, the contribution due to the scattered (coherent+incoherent) radiations is obtained as,

$$\Delta\mu = \frac{\ln\left(\frac{I_2}{I_1}\right)}{x} \tag{5.3}$$

The total scattering cross section $\Delta\sigma_{sca}$ from 0 to θ^0 in barn/molecule is then given by (Vinaykumar, L and Umesh, T K, 2016),

$$\Delta\sigma_{sca} = \left(\frac{A}{0.60225}\right)\frac{\Delta\mu}{\rho} \tag{5.4}$$

where A is the molecular weight and ρ is the density of the scatterer.

$\Delta\sigma_{sca}$ takes into account both the coherent and incoherent scattering cross sections within the angular range of 0 to θ^0, which is expressed as,

$$\Delta\sigma_{sca} = \int_o^\theta d\sigma_{coh} + \int_o^\theta d\sigma_{incoh} \tag{5.5}$$

The effective atomic numbers of the rare earth oxides are determined by the ratio of cross section method (Niranjan et al., 2012). In this method, first we deduce the atomic and electronic cross sections from the experimental mass attenuation coefficients of the compounds (μ_c) and mass attenuation coefficients of elements from XCOM data (Berger & Hubbell, 1987). The effective atomic number is then obtained from the ratio of the atomic cross section (σ_a) to the electronic cross section (σ_e).

5.3 Experimental details

In the present study, an ^{241}Am source with activity of 11.1 GBq, emitting gamma rays of energy 59.54 keV and ^{137}Cs source with activity of 0.191 GBq,

which emits gamma rays of energy 661.6 keV were used. The geometry of the experimental setup is displayed in Figure 5.1. The ^{241}Am source, in the form of a cylinder, had dimensions 10 mm x 6 mm. The ^{137}Cs source, in the form of a capsule, was sealed in an aluminium tube of 20 mm diameter and 115 mm length. The active portion of the source was 10 mm in diameter and 6 mm in length. The photon beam emitted by the source was made fine narrow by the collimators C and C1. It is further shaped using the collimators C2 and C3, having narrow holes of a few millimetres in diameter. The entire experiment was performed using the facilities provided by CARRT centre, Mangalore University, Karnataka. A NaI(Tl) detector of crystal size 76 mm x 76 mm, with an integrally - mounted photomultiplier tube (Bicron make) and a universal MCA scintiSPEC procured from Thermo Scientific, Germany, were used in this study. The schematic diagram of the detector and the associated electronics is shown in Figure 5.2. A collimator C4 of diameter 6 cm is kept in front of the detector window. The alignment of straight line geometry was ensured by optically checking, using a laser beam. A Microsoft Windows based spectroscopic application software winTMCA32 was used for the data acquisition and spectrum processing.

Rare earth oxides in powdered form, having purity $\geq 99\%$, have been used as scatterers here. From these, pellets of diameter 1 cm were prepared by using a pelletiser. Before starting the experiment, the detector was calibrated with standard gamma ray sources. First, the scatterer was placed at the position P1 so that the perfect narrow beam geometry condition has been ensured. No scattered radiations were allowed to reach the detector and pure transmitted beam intensity I_1 was measured. Subsequently, the scatterer was placed at position P2 so that the scattered radiations within a forward cone of 0-θ^0 were allowed to reach the detector along with the transmitted radiations.

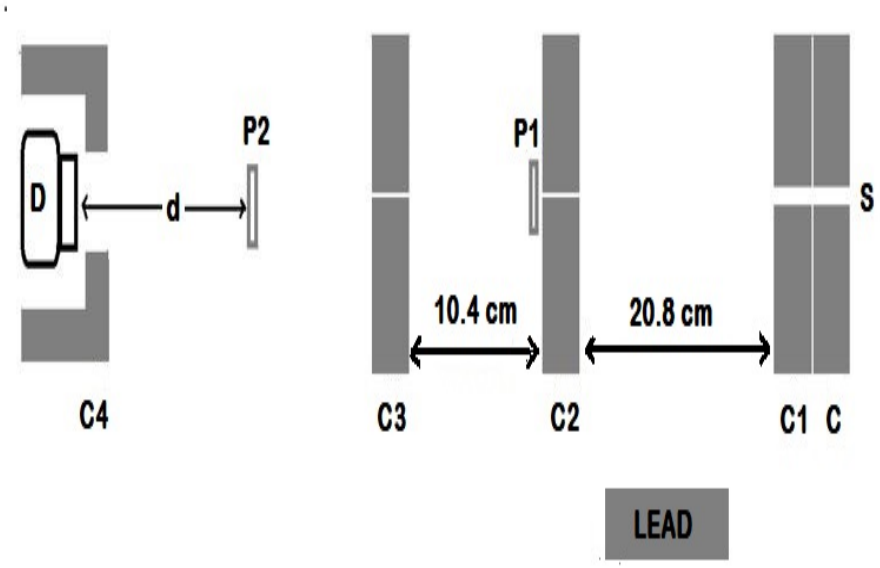

Figure 5.1: The experimental setup. S is the source, D is the NaI(Tl) detector, C, C1, C2 C3, C4 are lead collimators and P1 and P2 are scatterer positions.

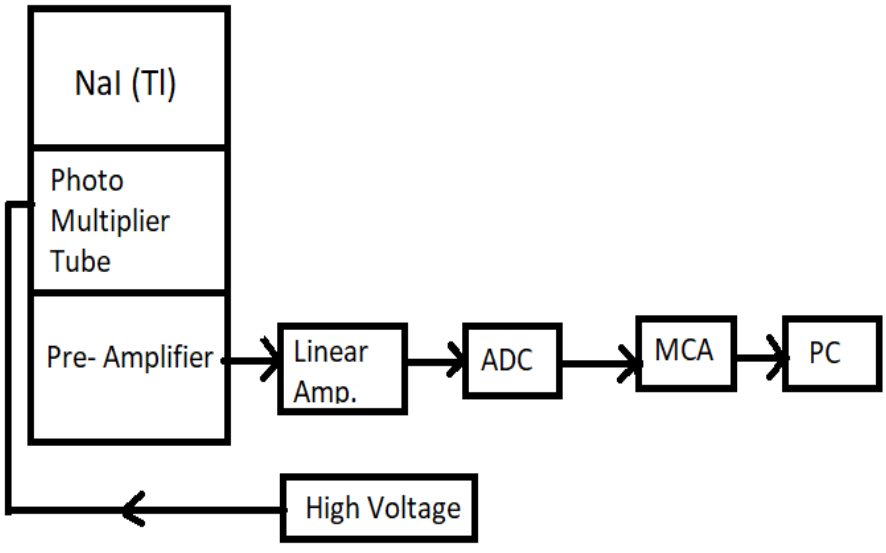

Figure 5.2: The block diagram of the detector and the associated electronics.

The corresponding intensity I_2 was determined, which contains the transmitted as well as the scattered photons within an angle θ. The angle of scattering θ was taken as the half-angle of the cone of acceptance of the detector at the scatterer. The scattering angle in terms of the distance between the detector and the scatterer d can be written as,

$$\theta = \tan^{-1}\left[\frac{3}{d(cm)}\right] \tag{5.6}$$

where 3 cm is half of the diameter of the hole size of collimator C4 kept in front of the detector.

By changing the distance d, the inscattering angle can be varied. By varying the position P2 and hence the distance d, the photon intensity I_2 (transmitted+scattered) for different angular ranges (0-4^o, 0-6^o, 0-8^o and 0-10^o) were measured. The spectra were acquired by placing each of the scatterer at the same position P1 and taking different positions for P2, in order to include the angular ranges (0-4^o, 0-6^o, 0-8^o and 0-10^o). The experiment was repeated 5 times at each position and the average value of I_2 was taken. The time for acquisition was decided in such a way that the counts under the photo peak was of the order of 10^5 - 10^6, so that the statistical error estimated in each measurement is less than 0.5% . The background counts were taken for the same interval of time by introducing a lead block of sufficient thickness in the path of the direct ray. From the background subtracted counts I_1 and I_2, the total scattering cross section $\Delta\sigma_{sca}$ for each angular range of 0-θ^0 was determined. Sample impurity error correction was not applied because samples with purity greater than 99% was used here and impurities with high atomic numbers were absent in the samples. There was a built-in provision in the MCA and the software for the dead time correction.

5.4 Calculation of angle integrated scattering cross section

In the present study, the angle integrated coherent scattering cross section was obtained by subtracting the non-relativistic Hatree-Fock (NRHF) values of the angle integrated incoherent scattering cross section from the total angle integrated cross section estimated from the experiment. Then, the estimated angle integrated coherent scattering cross sections were compared with the corresponding ENDF values. This was done for all the selected compounds. Theoretical angle integrated coherent and incoherent scattering cross sections were obtained by the numerical integration from 0 to θ^0. The integral for ENDF coherent scattering cross section is given as,

$$\sigma_{coh} = \int_o^\theta \frac{1}{2} r_o^2 (1 + \cos^2\theta) \ \left| f\left(x, z\right)\right|^2 \ d\Omega \tag{5.7}$$

where f(x,z) is the form factor.

The integral for obtaining the angle integrated incoherent (NRHF) scattering cross section is given as,

$$\sigma_{incoh} = \int_0^\theta \frac{d\sigma_{KN}(\theta)}{d\Omega} \left[S(x, Z)\right] \ d\Omega \tag{5.8}$$

where $\frac{d\sigma_{KN}(\theta)}{d\Omega}$ is the differential Klein-Nishina scattering cross section per electron, as per the well-known Klein-Nishina formula (Klein & Nishina, 1929) and S(x,Z) is the incoherent scattering cross section. $d\Omega = 2\pi \sin\theta \mathrm{d}\theta$ is the differential solid angle in steradian.

The angle integrated coherent and NRHF incoherent scattering cross sections of all the constituent elements were estimated and that for the compounds

were determined by applying the mixture rule (Jackson & Hawkes, 1981).

5.5 Results and discussion

The total scattering cross section of the selected rare earth oxides were determined experimentally in the angular ranges 0-4^o, 0-6^o, 0-8^o and 0-10^o, using 59.54 keV and 662 keV gamma rays and are presented in Tables 5.1 and 5.2, respectively.

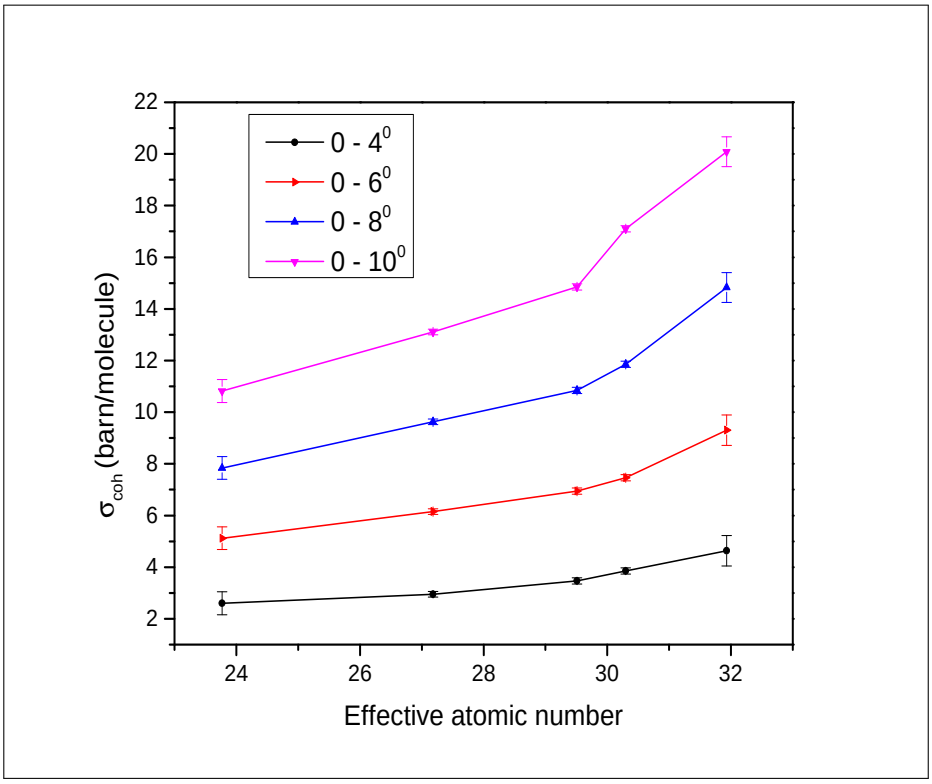

Figure 5.3: Variation of the angle integrated coherent scattering cross section with effective atomic number for 59.54 keV gamma rays.

The angle integrated incoherent and coherent scattering cross sections, for 59.54 keV and 662 keV gamma rays were estimated by the numerical integration of ENDF values and these values are also included in Table 5.1 and 5.2

respectively. The effective atomic number of the compounds were determined by the ratio of cross section method (Thulasi et al., 2021b). The experimentally determined angle integrated coherent scattering cross sections in specific angular ranges, for 59.54 keV and 662 keV have been plotted against the effective atomic number of the rare earth oxides and the variations are shown in Figures 5.3 and 5.4, respectively.

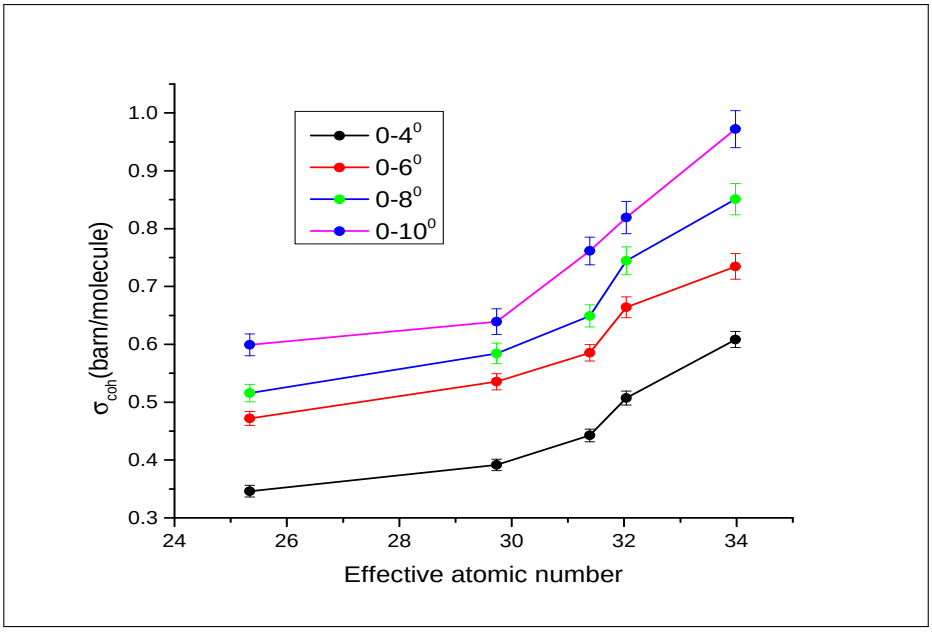

Figure 5.4: Variation of the angle integrated coherent scattering cross section with effective atomic number for 661.6 keV gamma rays

Only the statistical error in the experimental values are reported here, which are calculated using the formula (Akça & Erzeneoğlu, 2014).

$$\delta(\Delta\sigma_{sca}\ ) = K\sqrt{\left(\frac{\delta \mathrm{I}_1}{\mathrm{I}_1}\right)^2 + \left(\frac{\delta \mathrm{I}_2}{\mathrm{I}_2}\right)^2} \tag{5.9}$$

where $\mathrm{K} = \frac{1}{\rho x}\left(\frac{A}{0.60225}\right)$

Table 5.1: The angle integrated coherent scattering cross section of rare earth compounds using ^{241}Am source.

Sample	Distance d in cm	Angle in degrees	Experimental values of total scattering cross section (barn/ molecule)	Incoherent scattering cross section from ENDF (barn/ molecule)	Experimental values of coherent scattering cross section (barn/ molecule)	Coherent scattering cross section from ENDF (barn/ molecule)
CeO_2	42.9	0 - 4^o	2.61 ± 0.45	0.0058	2.60 ± 0.45	2.70
	28.54	0 - 6^o	5.14 ± 0.44	0.0201	5.12 ± 0.44	5.24
	21.35	0 – 8^o	7.89 ± 0.44	0.0471	7.84 ± 0.44	8.05
	17.01	0 - 10^o	10.91 ±0.44	0.0898	10.82 ± 0.44	10.66
Yb_2O_3	42.9	0 - 4^o	4.64 ± 0.59	0.0057	4.63 ± 0.59	4.50
	28.54	0 - 6^o	9.32 ± 0.59	0.0201	9.30 ± 0.59	9.05
	21.35	0 – 8^o	14.88 ± 0.58	0.0481	14.83 ± 0.58	14.21
	17.01	0 - 10^o	20.18 ± 0.58	0.0931	20.09 ± 0.58	19.56
Nd_2O_3	42.9	0 - 4^o	2.96 ±0.11	0.0059	2.95 ±0.11	3.09
	28.54	0 - 6^o	6.17 ± 0.11	0.0205	6.15 ±0.11	6.04
	21.35	0 – 8^o	9.68 ± 0.11	0.0482	9.63 ±0.11	9.31
	17.01	0 - 10^o	13.2 ± 0.11	0.0921	13.11 ±0.11	12.66
Dy_2O_3	42.9	0 - 4^o	3.86 ± 0.12	0.0058	3.85 ± 0.12	3.91
	28.54	0 - 6^o	7.48 ± 0.12	0.0203	7.46 ± 0.12	7.78
	21.35	0 – 8^o	11.9 ± 0.12	0.0483	11.85 ± 0.12	12.12
	17.01	0 - 10^o	17.18 ± 0.12	0.0892	17.10 ± 0.12	16.58
Gd_2O_3	42.9	0 - 4^o	3.48 ±0 .12	0.0059	3.47 ± 0.12	3.61
	28.54	0 - 6^o	6.96 ± 0.12	0.0206	6.94 ± 0.12	7.12
	21.35	0 – 8^o	10.89 ± 0.12	0.0487	10.84 ± 0.12	11.04
	17.01	0 - 10^o	14.94 ± 0.12	0.0935	14.85 ± 0.12	15.06

Table 5.2: The angle integrated coherent scattering cross section of rare earth compounds using ^{137}Cs source.

Sample	Distance d in cm	Angle in degrees	Experimental values of Total Scattering cross section (barn/molecule)	Incoherent scattering cross section ENDF (barn/ molecule)	Experimental values of Coherent scattering cross section (barn/ molecule)	Coherent scattering cross section ENDF (barn/ molecule)
CeO_2	42.9	0 - 4^o	0.3828 ± .0010	0.0367	0.3461 ± .0010	0.3647
	28.54	0 - 6^o	0.5680 ± .0012	0.0960	0.4720 ± .0012	0.4411
	21.35	0 – 8^o	0.7014 ± .0015	0.1858	0.5156 ± .0015	0.4876
	17.01	0 - 10^o	0.9060 ± .0019	0.3069	0.5991 ± .0019	0.5212
Yb_2O_3	42.9	0 - 4^o	0.6515 ± .0014	0.0432	0.6083 ± .0014	0.6296
	28.54	0 - 6^o	0.8514 ± .0020	0.1167	0.7347 ± .0020	0.7792
	21.35	0 – 8^o	1.0800 ± .0027	0.2290	0.8510 ± .0027	0.8643
	17.01	0 - 10^o	1.3530 ± .0032	0.3810	0.9720 ± 0032	0.9229
Nd_2O_3	42.9	0 - 4^o	0.4306 ± .0010	0.0390	0.3916 ± .0010	0.4168
	28.54	0 - 6^o	0.6380 ± .0014	0.1026	0.5354 ± .0014	0.5071
	21.35	0 – 8^o	0.7833 ± .0018	0.1990	0.5843 ± .0018	0.5604
	17.01	0 - 10^o	0.9685 ± .0022	0.3292	0.6393 ± .0022	0.5994
Dy_2O_3	42.9	0 - 4^o	0.5489 ± .0012	0.0417	0.5072 ± .0012	0.5337
	28.54	0 - 6^o	0.7756 ± .0018	0.1114	0.6642 ± .0018	0.6589
	21.35	0 – 8^o	0.9620 ± .0024	0.2175	0.7445 ± .0024	0.7296
	17.01	0 - 10^o	1.1800 ± .0028	0.3609	0.8191 ± .0028	0.7794
Gd_2O_3	42.9	0 - 4^o	0.4835 ± .0011	0.0409	0.4426 ± .0011	0.4923
	28.54	0 - 6^o	0.6940 ± .0014	0.1086	0.5854 ± .0014	0.6058
	21.35	0 – 8^o	0.8608 ± .0019	0.2116	0.6492 ± .0019	0.6701
	17.01	0 - 10^o	1.1120 ± .0024	0.3506	0.7614 ± .0024	0.7161

5.6 Conclusion

The angle integrated coherent scattering cross sections of the selected rare earth oxides, derived by subtracting the corresponding incoherent contributions (based on NRHF model) from the experimentally determined total scattering cross sections, in four angular ranges 0-4^o, 0-6^o, 0-8^o and 0-10^o, for 59.54 keV and 662 keV gamma rays, agree well with the respective theoretical ENDF values. Also, the angle integrated coherent scattering cross sections in specific angular ranges are found to increase with the effective atomic number of the rare earth oxides.

Bibliography

Akkuş, T. 2020, Canadian Journal of Physics, 98, 102

Akkuş, T., Uğurlu, M., & Demir, L. 2019, Results in Physics, 13, 102265

Akça, B., & Erzeneoğlu, S. Z. 2014, Science and Technology of Nuclear Installations, 2014, 1

Aldhuhaibat, M. J., Amana, M. S., Farhan, A. J., & Jubier, N. J. 2020in , IOP Publishing, 012013

Aysun Böke. 2011, Radiation Physics and Chemistry, 80, 609

Baek, W., Bug, M., & Rabus, H. 2014, Physical Review A, 89, 062716

Baek, W., Bug, M., Rabus, H., Gargioni, E., & Grosswendt, B. 2012, Physical Review A, 86, 032702

Basavaraju, G., Kane, P. P., Kissel, L. D., & Pratt, R. H. 1994, Physical Review A, 49, 3664

Berger, M. J., & Hubbell, J. H. 1987, XCOM Photon cross-sections database, Web version 1.2.National Institute of Standards and technology, Tech. rep.

Bradley, D., Gonçalves, O., & Kane, P. 1999, Radiation Physics and Chemistry, 56, 125

Brown, D., Chadwick, M., Capote, R., et al. 2018, Nuclear Data Sheets, 148, 1

Chatterjee, B. K., & Roy, S. C. 1998, J. Phys. Chem. Ref. Data, 27, 1011

Chatterjee, B K and Roy, S S. 1998, J. Phys. Chem. Ref. Data, 27, 1011

Donativi, M., Quarta, S., Cesareo, R., & Castellano, A. 2007, Nuclear Instruments and Methods in Physics Research Section B: Beam Interactions with Materials and Atoms, 264, 189

Franz, W. 1936, Z. Phys., 98, 314

Hine, P. M. 1952, Phys.Rev, 85, 725

Hubbell, J. H., & Overbo, I. 1979, J. Phys. Chem. Ref. Data., 8, 69

Hubbell, J. H., Veigele, W. J., Briggs, E. A., et al. 1975, J. Phys. Chern. Ref. Data, 4, 471

İçelli, O., & Erzeneoğlu, S. 2002, Spectrochimica Acta Part B: Atomic Spectroscopy, 57, 1317

Jackson, D. F., & Hawkes, D. J. 1981, Phys. Rep, 70, 169

K Muraleedhara Varier. 2009, Nuclear radiation detection, measurement and analysis (Narosa publishing house, NewDelhi)

Kahane, S. 1998, Atomic Data and Nuclear Data Tables, 68, 323

Kane, P. 2005, Radiation Physics and Chemistry, 74, 402

Kane, P. P., Basavaraju, G., Mahajani, J., & Priyadarsini, A. K. 1978, Nucl. Instr. and Meth., 155, 467

Kawai, J., Yamasaki, K., & Tanaka, R. 2006, Encyclopedia of Analytical Chemistry: Applications, Theory and Instrumentation, 1

Kissel, L. 2000, Radiation Physics and Chemistry, 59, 185

Kissel, L., Pratt, R., & Roy, S. 1980, Physical Review A, 22, 1970

Klein, O., & Nishina, Y. 1929, Z. Phys, 52, 853

Kuruchu, Y., Erzeneoglu, S., Durak, R., & Sahin, Y. 1998, Tr. J. of Physics, 51, 45

Latha, P., Abdullah, K. K., Unnikrishnan, M. P., Varier, K. M., & Babu, B. R. S. 2012, Phys. Scr, 85, 035303

Midhun, C. V., Musthafa, M. M., Akbar, S., et al. 2019, Nuclear Science and Engineering., 194, 207

Nayak, N. G., Balakrishna, K. M., & Siddappa, K. 1993, J. Phys. B: At. Mol. Opt. Phya., 26, 4117

Niranjan, R. S., Rudraswamy, B., & Dhananjaya, N. 2012, Pramana – J. Phys., 78, 451

Puttaswamy, K., Gowda, M., & Sanjeevaiah, B. 1984, Nuclear Instruments and Methods in Physics Research, 224, 461

Ramanathan, N., Kennett, T. J., & Prestwich, W. V. 1979, Can. J.Phys, 57, 343

Roy, S. C., Kissel, L., & Pratt, R. H. 1999, Radiation Physics and Chemistry, 56, 3

Roy, S. C., Nath, A., & Ghose, A. M. 1975, Nucl. Instr. And Meth, 131, 163

Shahi, J. S., Puri, S., Mehta, D., et al. 1997, Physical Review A, 55, 3557

Simsek, O., & Ertugrul, M. 2004, Radiation measurements, 38, 271

Singh, M., Sharma, A., Singh, B., & Sandhu, B. 2013, Radiation measurements, 59, 30

Singh, M. P., Sharma, A., Singh, B., & Sandhu, B. S. 2012, Indian journal of pure and applied physics, 50, 490

Singh, M. P and Sharma, Amandeep and Singh, Bhajan and Sandhu, B .S. 2014, Journal of Radioanalytical and Nuclear Chemistry, 302, 187

Thulasi, P. V., Antony, J., & Varier, K. M. 2021a, Radiation Physics and Chemistry, 180, 109252

Thulasi, P. V., Joseph, A., & Varier, K. M. 2021b, AIP Conference proceedings

Vinaykumar, L., & Umesh, T. 2014a, Physics Research International, 2014, 4 pages

Vinaykumar, L., & Umesh, T. K. 2014b, Eur. Phys. J. D, 68

Vinaykumar, L and Umesh, T K. 2016, Journal of Radiation Research and Applied Sciences ., 9, 35

Chapter 6

Effective atomic number studies on edible oil samples.

6.1 Introduction

In the previous chapters, we have discussed the different theoretical methods for calculating the effective atomic number of composite materials. Among the different methods for determining the effective atomic number, polynomial interpolation is the most suited one for composite materials having unknown chemical composition. Many researchers have found the effective atomic number of composite materials experimentally and theoretically (Singh & Badiger, 2016; Manjunathaguru, V and Umesh, T.K, 2006). Accounting the importance of gamma ray attenuation in food samples, in the present study, we have analysed the absorption properties of pure coconut oil, paraffin oil and a mixture of both, at different concentrations using gamma rays emitted by ^{137}Cs source. Coconut oil is a collection of fatty acids and the chemical composition and average value for weight fraction of each are given in Table 6.1 . The linear attenuation coefficients for different samples were determined using a CZT detector at 662 keV gamma ray energy. From the measured values of the mass

Table 6.1: Average chemical composition of coconut oil (Prasanth Kumar & Gopala Krishna, 2015)

Sl.No.	Component	Chemical formula	Weight fraction in percentage
1	Lauric acid	$C_{12}H_{24}O_2$	50.35
2	Myristic acid	$C_{14}H_{28}O_2$	21.18
3	Palmtic acid	$C_{16}H_{32}O_2$	9.07
4	Caprylic acid	$C_8H_{16}O_2$	7.71
5	Capric acid	$C_{10}H_{20}O_2$	5.59
6	Oleic acid	$C_{18}H_{34}O_2$	4.49
7	Linoleic acid	$O_{18}H_{32}C_2$	1.00
8	Stearic acid	$C_{18}H_{36}O_2$	0.67

attenuation coefficients, the effective atomic numbers were obtained by polynomial interpolation method, using theoretical XCOM values. The practice of adulteration of coconut oil reduces its quality and adversely affects the health of the consumers. The present study is also intended to check the feasibility of this technique to identify the adulteration of oil samples.

6.2 Experimental details

The experimental setup used for the present investigation is shown in Figure 6.1.

In the present study, ^{137}Cs source with activity 720 μCi, emitting gamma rays of energy 662 keV was made use of. Narrow beam geometry was employed so that the source, the absorber and the detector were aligned along a vertical axis and the gamma rays were well collimated. A cylindrical glass container with uniform cross section of 12.56 cm^2 was mounted between the source and the detector for holding the oil samples. The gamma rays transmitted through the absorber were analysed using a 1x1x1 cm^3 coplanar grid Cadmium Zinc

Telluride (CZT) detector, procured from Kromek Ltd. It is a unique semiconductor detector, which can be operated at room temperature. Its resolution clearly outperforms any other commercially available scintillator. The data acquisition and analysis were done through a Microsoft Windows based software, KSPECT.

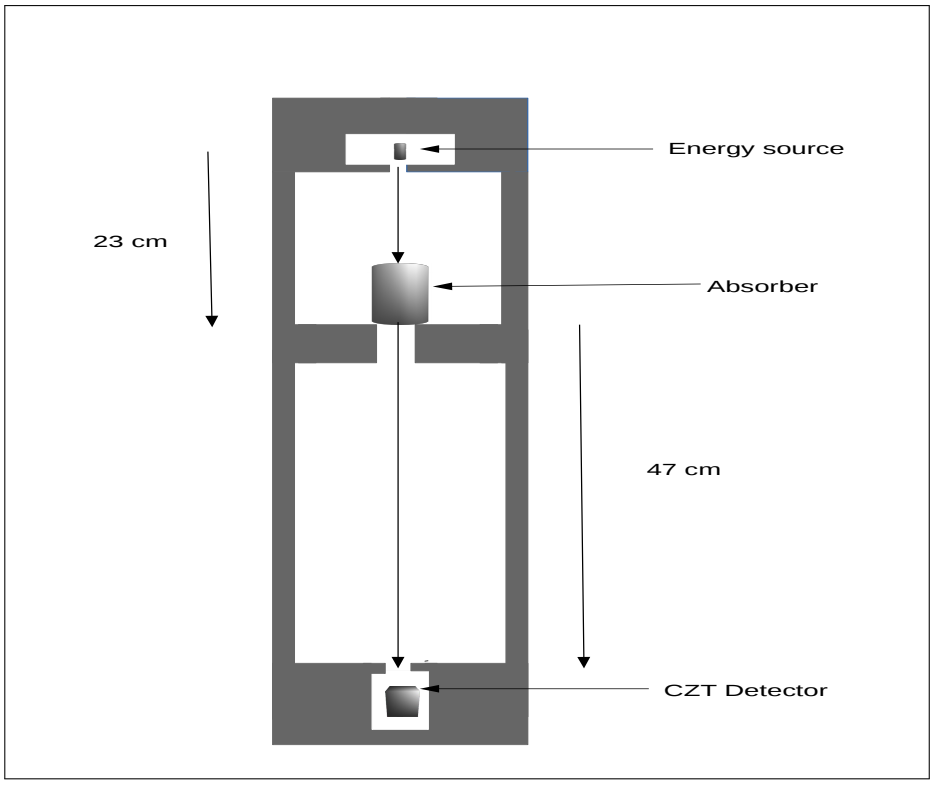

Figure 6.1: Experimental arrangement for measuring the attenuation of 662 keV gamma rays in oil samples using CZT detector.

The materials used here were pure coconut oil, paraffin oil and a mixture of both, in different proportions. Pure coconut oil was prepared at home from the extracted coconut milk. Paraffin oil was procured from the market. At first, the CZT detector was calibrated using standard gamma ray sources. The energy calibration curve is shown in Figure. 6.2. The acquisition time was set for 1000 seconds so that the statistical error is less than 2% for the

maximum thickness of the absorber. The gamma ray spectra were recorded for the same time interval for both the background and the transmitted gamma rays through the absorber (by varying the thickness). The sample height in the container was varied up to a maximum of 10.5 cm, keeping in mind the fact that the thickness must be less than the mean free path to avoid the effect of multiple scattering (Varier et al., 1986; Gopal & Sanjeevaiah, 1973). A sample spectrum from the CZT detector for ^{137}Cs alone and with coconut oil is shown in Figure. 6.3.

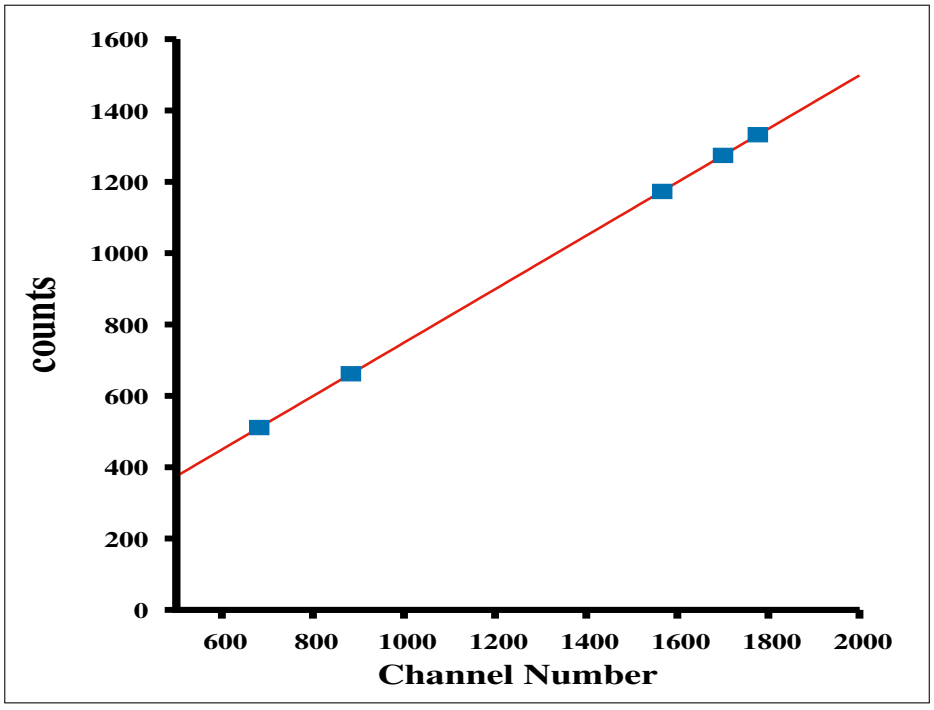

Figure 6.2: Energy calibration curve.

The area under the photopeak after subtracting the background was used to estimate the net counts. Comparing the incident (I_0) and transmitted (I) intensities of gamma rays for each absorber height, the linear attenuation coefficients were calculated. In each case, lnI was plotted against the absorber height x, and using the least square fitting, a straight line was obtained. From the

slope of this straight line, the linear attenuation coefficient was estimated. The same procedure was repeated for all the selected samples. Knowing the density of each sample, the mass attenuation coefficient were estimated from the experimentally obtained linear attenuation coefficients. The effective atomic numbers were determined by the interpolation method. The maximum uncertainty in the measured mass attenuation coefficients were found to be 1.09%. This arises mainly from the counting statistics.

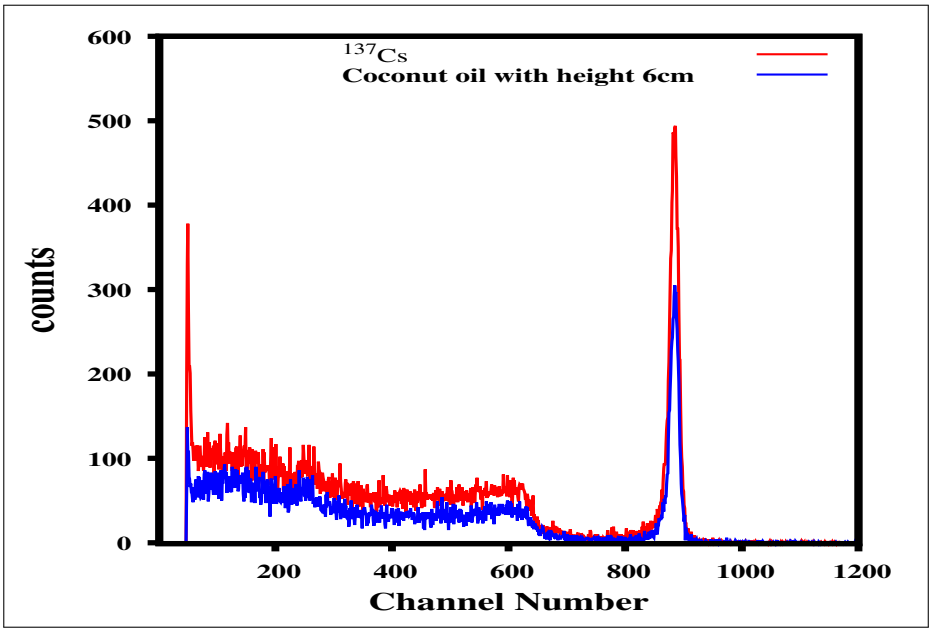

Figure 6.3: Sample spectrum from CZT detector for ^{137}Cs alone and with coconut oil for the height 6 cm.

6.3 Results and discussion

The measurements show that for each sample, the recorded count of transmitted radiation gets decreased as we increase the height of the absorber. This variation is purely exponential, which validates the gamma ray absorption law.

The plotted curve showing the variation of lnI with height of the absorber for a sample with 25% paraffin oil and 75% pure coconut oil is displayed in Figure 6.4. The same kind of straight lines were obtained for all the samples, the slope of which give the value of the linear attenuation coefficient in each case. The estimated values of the mass attenuation coefficient and the effective atomic number of the oil samples with the associated errors are presented in Table 6.2. The variation of the effective atomic number with increase in concentration of paraffin oil in pure coconut oil is displayed in Figure 6.5. Using this composition given in Table 6.1 and by applying the mixture rule, the mass attenuation coefficient of pure coconut oil was obtained as 0.0864 cm^2/g. For that, the mass attenuation coefficient of the constituent fatty acids were obtained by using the XCOM program (Berger & Hubbell, 1987).

Table 6.2: Estimated values of mass attenuation coefficient and effective atomic numbers of various oil samples.

Percentage of paraffin oil added to coconut oil	Mass att. coeff. cm^2/g	Effective atomic no.
0	0.0910 ±.0008	1.8173 ±0.0109
25	0.0926 ±.0010	1.7965 ±0.0130
50	0.0941 ±.0009	1.7769 ±0.0120
75	0.0956 ±.0008	1.7573 ±0.0109
100	0.0974 ±.0009	1.7327 ±0.0120

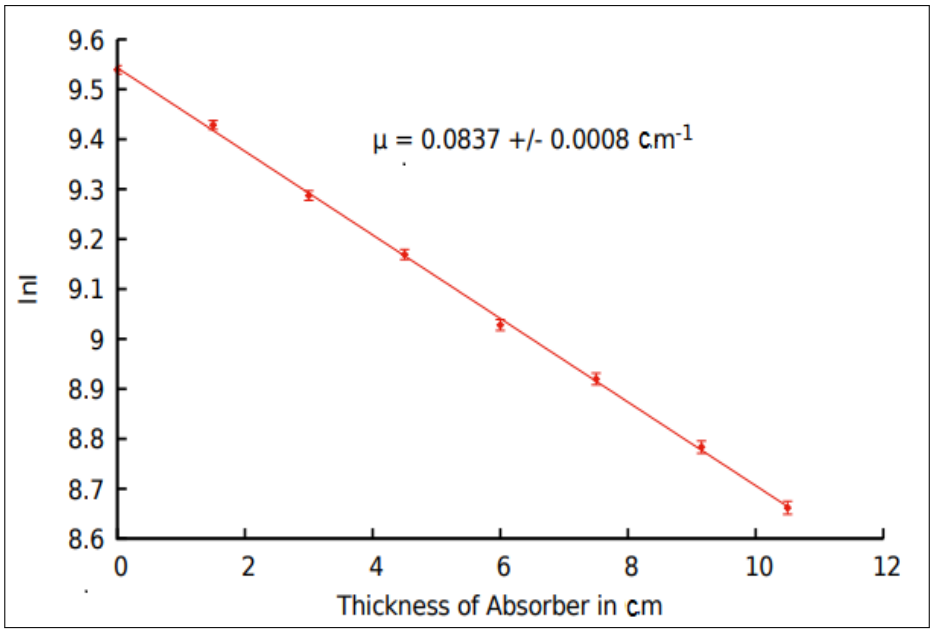

Figure 6.4: Variation of lnI with the height of the absorber oil in the beaker of the sample having 75% coconut oil and 25% paraffin.

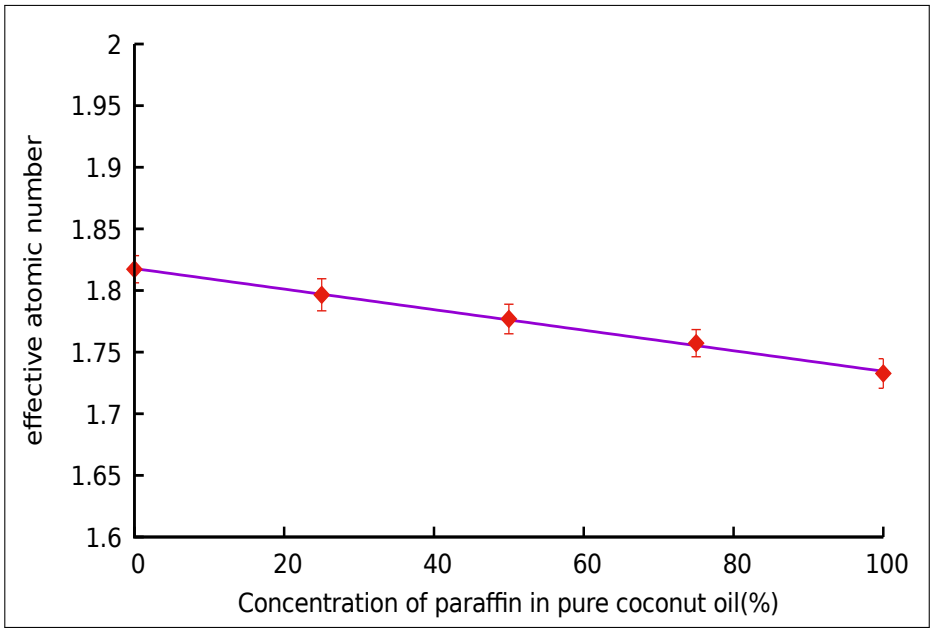

Figure 6.5: Variation of the effective atomic number with concentration of paraffin oil in pure coconut oil.

6.4 Conclusion

From the obtained results, it is clear that the values of the mass attenuation coefficient increases with increase in the amount of paraffin oil added to the coconut oil. This variation is beyond the experimental errors. Also, the effective atomic number, determined by the interpolation method, shows a linear decrease with increase in the amount of paraffin oil added to the coconut oil. The theoretically estimated value of mass attenuation coefficient of pure coconut oil (0.0864 cm^2/g) (with an average chemical composition) is in good agreement with the experimentally obtained value of the mass attenuation coefficient of pure coconut oil used here. This correlated variation of gamma ray interaction parameters with the composition of oil samples points to the suitability of using gamma ray attenuation technique, which is non-destructive (Manjunath & Kerur, 2013), for detecting the adulteration in edible oils.

Bibliography

Berger, M. J., & Hubbell, J. H. 1987, XCOM: Photon cross sections on a personal computer, Tech. rep., National Bureau of Standards, Washington, DC (USA). Center for Radiation

Gopal, S., & Sanjeevaiah, B. 1973, Nuclear Instruments and Methods, 107, 221

Manjunath, A., & Kerur, B. R. 2013, Research Journal of Pharmaceutical, Biological and Chemical Sciences, 4, 1180

Manjunathaguru, V and Umesh, T.K. 2006, Journal of Physics B: Atomic, Molecular and Optical Physics, 39, 3969

Prasanth Kumar, P. K., & Gopala Krishna, A. G. 2015, GRASAS Y ACEITES, 66, e062

Singh, V. P., & Badiger, N. M. 2016, Indian J. Pure Appl. Phys., 54, 333

Varier, K. M., Kunju, S. N., & Madhusudanan, K. 1986, Physical Review A, 33, 2378

Chapter 7

Summary and recommendations

7.1 Summary

Accurate values of gamma ray interaction parameters with matter are important in a wide variety of applications like radiation dosimetry, nuclear medicine, radiation protection, radiation therapy and power reactor shielding. Materials containing elements with high atomic number are important in radiation protection and shielding. But, materials made up of elements with low atomic number, like polymers and plastics are used as tissue equivalent substitutes and phantom materials. Several theoretical and experimental studies are reported to determine the mass attenuation coefficient, scattering cross sections, effective atomic number and effective electron density of various materials in different energy regions. The work presented in this thesis is focused on the theorectical and experimental studies for the determination of photon interaction parameters of different materials which are having applications in diverse fields. In the first part of the study, we have theoretically estimated the gamma ray interaction parameters in selected thermoplastic, biopolymer and chemotherapy drugs samples in the wide range of energies 1 keV to 100 GeV. In the subsequent experimental work, we have carried out coherent scatter-

ing cross section measurements of selected rare earth oxide samples for 59.54 keV and 662 keV gamma rays. We have also carried out some attenuation measurements in edible oil samples for 662 keV gamma ray energy.

Chapter 1 gives an introduction to different gamma ray interaction processes with matter. The general aspects of gamma ray interactions, different types of geometries like narrow beam geometry and broad beam geometry used for gamma ray attenuation studies and the databases used in the present study were also presented here.

In chapter 2, we have presented a review of the photon interaction studies carried out earlier, relevant to the present thesis work.

The effective atomic number and the effective electron density of some synthetic polymers, being used in clinical medicine, have been calculated for total and partial interaction processes, in the energy range of 1 keV to 100 GeV, using the ratio of cross section method. Mass energy-absorption coefficient, effective atomic number corresponding to gamma ray energy absorption and the kerma relative to air of these polymers have also been estimated for the photon energy range of 1 keV to 20 MeV. These parameters are found to vary with energy and chemical composition of the polymers which can be attrebuted to the relative dominance of different partial interaction processes at different energy regions. The maximum values of Z_{eff} and N_{eff} have been observed in the low energy range, where photoelectric absorption is predominant and, the minimum value of Z_{eff} and N_{eff} have been found in the intermediate energy region, where Compton scattering is dominant. In higher energy region (E>100 MeV), where pair production is predominant, the Z_{eff} has an intermediate value. For PDMS, the Z_{eff} and N_{eff} have more than one value at 1.839 keV due to the K-absorption edge of silicon. The variation of the

effective atomic number and the effective electron density with chemical composition is maximum in those polymers which are composed of atoms with atomic numbers spanned over a wide range. Also, the variation of Z_{eff} and N_{eff} with chemical composition of the polymers is maximum below 100 keV due to the relative dominance of photoelectric absorption. Kerma relative to air approaches unity above 100 keV for all these polymers. The estimated values are compared with experimental data wherever available and the comparison shows good agreement. Besides these, for total photon interaction, we have determined the Z_{eff} and N_{eff} of the selected polymers, by direct, ratio of cross section and interpolation methods, in the energy range 1 keV to 100 GeV. Also, single effective atomic number was calculated by using XMuDat, power law and by the method suggested by Murty. The effective atomic numbers obtained by different methods are compared and the suitability of different methods in various energy regions are discussed.The direct and ratio of cross section methods give almost the same results in the entire energy range considered. Direct, ratio of cross section and interpolation methods are in good agreement in the middle energy range, where Compton scattering is dominant. The values obtained in logarithmic interpolation method in photoelectric and pair production dominant regions are always lower than that in the direct and ratio of cross section methods and this deviation is maximum in the low energy region where photoelectric effect is dominant. The effective atomic numbers obtained by XmuDat and power law methods are almost the same. These values are close to the effective atomic numbers obtained in the photoelectric dominant region by the direct method. These are the contents of chapter 3.

In chapter 4 we have presented the details of the theoretical studies carried out in the the energy range of 1 keV to 100 GeV, to estimate the photon interaction parameters such as the linear attenuation coefficient, mass attenuation

coefficient, Half Value-Layer (HVL), effective atomic number and the effective electron densities of some selected chemotherapy drugs (Hydroxyurea, Trifluridine, Temozolomide, Mitomycin C, Trabectedin) which are generally used in concurrent chemoradiotherapy . The variation of these parameters with photon energy and chemical composition were studied. For a given energy, the HVL is maximum for mitamycin and minimum for temozolomide. So, temozolomide shows the maximum and mitamycin shows the minimum gamma ray absorption properties. Eventhough, the interaction parameters of different chemotherapy drugs with photons are available, the estimation of these parameters for the drugs selected in the present study is a new investigation. Also, the estimated parameters are important in dose calculations in actual treatment planning.

Chapter 5 depicts the details of the experimental investigations we have performed to determine the angle integrated total scattering cross sections of the rare earth oxides ($CeO_2, Yb_2O_3, Nd_2O_3, Dy_2O_3$ and Gd_2O_3) for 59.54 keV and 662 keV gamma rays in the angular range of ($0-4^o, 0-6^o, 0-8^o$ and $0-10^o$). From the total scattering cross sections, the corresponding angle integrated incoherent scattering cross sections obtained from ENDF library (based on the non-relativistic Hartree-Fock form factor method) is subtracted to obtain the angle integrated coherent scattering cross sections. The obtained angle integrated coherent scattering cross sections are in good agreement with that determined from ENDF data. The effective atomic numbers of the selected rare earth oxides are extracted by applying the ratio of cross section method. The angle integrated coherent scattering cross sections in specific angular ranges are found to increase with the effective atomic number of the rare earth oxides.

Chapter 6 deals with the attenuation studies carried out on edible oil samples (pure coconut oil, paraffin oil and a mixture of both in different samples) using ^{137}Cs source, emitting 662 keV gamma rays. For each sample, the effective atomic number was estimated from the experimentally obtained mass attenuation coefficients, by the interpolation method. Variation of these gamma interaction parameters with increase in concentration of paraffin oil in the pure coconut oil samples was studied. From the obtained results, it is clear that the values of mass attenuation coefficient increases with increase in the amount of paraffin oil added to the coconut oil. Also, the effective atomic number, shows a linear decrease with increase in the amount of paraffin oil added to the coconut oil. The study suggests that the gamma ray attenuation technique, which is non-destructive, can be used for detecting adulteration in edible oils.

7.2 Recommendations

The present studies on gamma ray interaction parameters of the selected polymers, chemotherapy drugs and the rare earth oxides pave way for future research as stated below.

- More experimental investigations on gamma ray interaction parameters of the polymers selected for the present study would be highly desirable. Experimental data of these polymers are not available in literature in the transition regions where the effective atomic number varies rapidly with photon energy. It would be beneficial to have experimental data in these regions for future applications.

- In the present method of estimating the effective atomic number and the effective electron densities, we have not considered the bonding effects or

any other chemical effects, when the atoms of the interacting material are in the bulk environment. To accommodate these effects, we need more experimental data at different photon energy regions, especially near the absorption edges. Such studies also necessitates more theoretical advancements.

- Chemotherapy mainly depends on the chemical properties of drugs, while radiotherapy depends on the photon interaction parameters. So, If we can correlate the chemical aspects and gamma ray interaction properties of various chemoradiotherapy drugs, it would be beneficial to develop methods which can enhance the efficacy of the treatment.

- Further extensive studies on small angle scattering by different samples by the present method can be attempted.

- In the present study of calculating the angle integrated scattering cross section of compounds, we have not included the interference effects while calculating the coherent scattering cross section. So, we feel that this effect is to be taken into account, so that it may lead to better agreement between theory and experiment.